NASA

Technical Memorandum **79690**

Topics In Astrophysical X-Ray and Gamma Ray Spectrascopy

Roger W. Bussard

NOVEMBER 1978

National Aeronautics and Space Administration

Goddard Space Flight Center
Greenbelt, Maryland 20771

TOPICS IN ASTROPHYSICAL X-RAY AND GAMMA RAY SPECTROSCOPY

by

Roger W. Bussard

Dissertation submitted to the Faculty of the Graduate School
of the University of Maryland in partial fulfillment
of the requirements for the degree of
Doctor of Philosophy
1978

Work supported by NASA Grant NGR 21-002-316

ABSTRACT

Title of thesis: Topics in Astrophysical X-ray and Gamma Ray Spectroscopy

Roger W. Bussard, Doctor of Philosophy, 1978

Thesis directed by: Doctor Reuven Ramaty

We have investigated a number of topics relating to astrophysical observations that have already been made or are currently planned of spectral features, mostly emission lines, in the X-ray and gamma ray regions of the electromagnetic spectrum. These topics include: the production of characteristic X-ray and gamma ray lines by non-thermal ions, spectral features induced by processes occurring in strong magnetic fields, and the positron annihilation line at 0.5 MeV. Although astrophysical spectroscopy in this regime is quite young, a number of conclusions can be drawn from existing observations and upper limits, and much can be learned from experiments currently under consideration.

First, we have calculated the rate of X-ray production at 6.8 keV by the 2p to 1s transition in fast hydrogen- and helium-like iron ions, following both electron capture to excited levels and collisional excitation. We used a refinement of the OBK approximation to obtain an improved charge exchange cross section. This and the corresponding ionization cross section were used to determine equilibrium charge fractions for iron ions as a function of their

energy. The effective X-ray line production cross section was found to be sharply peaked in energy at about 10 MeV/amu. Since fast ions with similar energies can also excite nuclear levels, we have calculated the ratio of selected strong gamma ray line emissivities to the X-ray line emissivity. We use these calculations to set limits on the gamma ray line intensity from the galactic center and the radio galaxy Centaurus A, and we find that these limits are generally lower than fluxes reported in the literature. In addition, the presence of interstellar dust grains can give rise to a very narrow line profile for some gamma ray lines from nuclear excitations. In a grain, a nucleus with a long lived excited state may be stopped before emitting the gamma ray. We have compiled the relevant range and energy loss relations and have then shown the results of this effect for several examples.

The intense magnetic fields (of order 10^{12} gauss) believed to exist at the surfaces of X-ray pulsars could produce observable structure in their spectra. Such fields severely quantize the motion of electrons in the transverse plane, and line emission and absorption can occur accompanying transitions between levels. We have confirmed a previous calculation of the rates for these processes, and we have calculated the cross section for electron-ion Coulomb collisions in strong fields. This cross section is significantly modified by the quantization due to the magnetic field. We have then calculated the line production rates for direct excitation by accreting material and by excitation from thermal collisions. The results are

compared with recent observations of Hercules X-1, and we find that the interpretation of the spectrum in terms of an emission line is less likely than that of an absorption feature. Future observations with higher spectral resolution should resolve the question.

Finally, we have studied the annihilation of galactic positrons in order to evaluate the probabilities of various channels of annihilation and to calculate the spectrum of the resulting radiation. The narrow width (FWHM less than 3.2 keV) of the 0.51 MeV line observed from the galactic center direction (Leventhal et al. 1978 a,b) implies that a large fraction of the positrons should annihilate in a medium of temperature less than 10^5 K and ionization fraction greater than 0.05. HII regions at the galactic center could be possible sites of annihilation.

VITA

Name: Roger Wade Bussard

Address: 8503 Greenbelt Rd., #204, Greenbelt, Md. 20770

Degree and date to be conferred: Ph.D., December, 1978

Date of birth: [redacted]

Place of birth: [redacted]

Secondary Education: Washington Irving High School, Clarksburg, W. Va.

Collegiate Institutions attended	Dates	Degree	Date
West Virginia University	1964 to 1968	B.S.	1968
University of Maryland	1972 to 1978	(Ph.D.)	(1978)

Major: Astrophysics

Publications:

"X-ray and Gamma Ray Production by Nonthermal Ions," Bussard, R. W., Ramaty, R., and Omidvar, K. 1978, Astrophysical Journal, 220, 353.

"The Excitation of Electronic Transverse Energy Levels in an Intense Magnetic Field," in Gamma Ray Spectroscopy in Astrophysics, edited by T. L. Cline and R. Ramaty, NASA Technical Memorandum 79619, page 404.

"X-ray Spectra of Hercules X-1: III. Pulse Phase Dependence in the High Energy Continuum," Praydo, S. H., Bussard, R. W., Becker, R. H., Boldt, E. A., Holt, S. S., Serlemitsos, P. J., and Swank, J. H., Astrophysical Journal, 225, 988.

"The Annihilation of Galactic Positrons," Bussard, R. W. , Ramaty, R., and Drachman, R. J., accepted for publication in Astrophysical Journal.

APPROVAL SHEET

Title of Thesis: Topics in Astrophysical X-ray and Gamma Ray Spectroscopy

Name of Candidate: Roger W. Bussard
Doctor of Philosophy, 1978

Thesis and Abstract Approved: Frank B. McDonald

Frank B. McDonald
Professor
Department of Physics and Astronomy

Date Approved: Nov. 27, 1978

DEDICATION

For their continued support and encouragement over the years, I dedicate this work to my family, especially my mother, Ms. Victoria Phillips.

ACKNOWLEDGEMENTS

I wish to thank Dr. Reuven Ramaty, my thesis advisor, for his patient guidance in this research and for critical appraisals of the manuscript. Also, I would like to thank Dr. Frank McDonald for giving me the opportunity to work in the Laboratory for High Energy Astrophysics at NASA/Goddard Space Flight Center, and Dr, Alex Dragt, the previous chairman of the Department of Physics and Astronomy at the University of Maryland.

For stimulating discussions and assistance in calculations, I gratefully acknowledge Dr. Steven Pravdo, Dr. Kazem Omidvar, Dr. Richard Drachman, and Dr. Donald Rule. And for many helpful comments I thank Dr. Elihu Boldt, Dr. Peter Serlemitsos, Dr. Barham Smith, Dr. Taeil Bai, Dr. Benzion Kozlovsky, Dr. Diana Worrall, Ms. Julia Robinson-Saba, Mr. Andrew Szymkowiak, Dr. Jean Swank, and Dr. Robert Becker.

The drafting work of Messrs. Adam Thompson, Harry Trexel, Frank Shaffer, and Larry White is greatly appreciated. And especially, I thank Ms. Barbara Pratt for her patience and good nature while typing this manuscript.

TABLE OF CONTENTS

LIST OF TABLES

LIST OF FIGURES

I. INTRODUCTION

Astrophysical information from our galaxy comes to us primarily in the form of electromagnetic radiation, from radio frequencies to high energy gamma rays. In the attempt to understand the nature of various astrophysical objects and regions and their physical processes, much can be learned from the observations in particular of spectral lines and features (broadened lines, absorption edges, cutoffs, etc.) For example, red-shifted lines in the spectra of extragalactic objects lead us to believe that the universe is expanding, since the amount of shifting is proportional to the distance to the object. Locally, lines from electronic transitions in atoms allow determination of relative elemental abundances, the spin flip line of atomic hydrogen at 21cm wavelength has been used to map neutral hydrogen in the galaxy, and the rotational transition lines of molecules give the galactic distribution of dense molecular clouds. Moreover, the simultaneous observation of two or more lines usually provides information on the physical conditions in the source, such as the density and temperature.

This work consists of a theoretical consideration of spectral features, mostly emission lines, from a very new astrophysical window, that of X-rays and soft gamma rays (about 6 keV to 6 MeV). Some of the features considered have been observed and others are possibly observable by currently planned experiments. Measurements in this spectral region must be carried out from balloons, rockets or satellites because of atmospheric absorption. The first line considered results from the electronic transition from the 2p state to the 1s state in highly ionized iron at $\sim$ 6.8 keV, the iron Kα line. Elements with higher Z, and consequently higher Kα line energies, are far less abundant than iron, and lower energy Kα line protons (from lower Z elements) will suffer much absorption, via photoionization, propagating through

the interstellar medium. The 2p state is populated follwing charge exchange and radiative recombination to excited states and the subsequent cascade, or by excitation if the ion already has one or two electrons. Since these processes occur most readily when the relative velocities of the interacting particles is about one tenth of the speed of light, Kα emission can be produced in a plasma with temperature $\sim 10^7$K, or in regions with significant fluxes of ions with energies $\sim$ 10 MeV per nucleon. In the former case, the emitting iron atom is essentially at rest, and the line profile suffers little Doppler broadening. In the latter, the iron has the velocity, $\sim$ .1c, mentioned above, leading to a line width (FWHM) $\sim$ 2.4 keV. Thus the broad 6.8 keV line is a tracer of low energy cosmic rays. Another type of line feature considered results from the excitation of nuclear levels in strong interactions by nuclei with the same energies. For example, a carbon 12 nucleus can be excited in a collision with an energetic proton, and it will subsequently deexcite by emitting a 4.44 MeV photon. Next, we consider the possibility that the strong magnetic fields associated with pulsars can give rise to line features analogous to the cyclotron lines from plasma in weaker fields. For a field strength of 10^{12} Gauss, for example, the fundamental cyclotron frequency corresponds to a photon energy of $\sim$ 11 keV. Finally, we treat the production of the 0.511 MeV line from the annihilation of positrons with electrons for various galactic sites. All these spectral features have been observed or could be observed by detector systems presently under consideration as for the Gamma Ray Observatory, for example.

A search for the Kα line of highly ionized iron was begun in the late 1960's and early 1970's by rocket born proportional counters (Holt et al. 1968 and 1969) and Bragg crystal spectrometers (Kestenbaum et al. 1971 and Griffiths 1972). Although this search was not fruitful, the iron line

eventually was observed from some weaker sources with improved, more sensitive detectors: young supernova remnants (Serlemitsos et al. 1973, Brisken 1973, Becker et al. 1976, Pravdo et al. 1976, Davison et al. 1976), collapsed stars in binary systems (Serlemitsos et al. 1975, Pravdo 1976, Pravdo et al. 1977a), and clusters of galaxies (Mitchell et al. 1977, Serlemitsos et al. 1977). Although it now appears that the line emission from young supernova remnants is consistent with that from a thermal plasma, low energy cosmic ray iron nuclei undergoing charge exchange with the ambient medium were originally proposed to explain this line (Serlemitsos et al. 1973). Nucleons with these energies also produce gamma ray lines by exciting nuclear levels and in Chapter II, we have calculated the ratio of the gamma ray line emission to the iron Kα emission produced in this way. These calculations, together with X-ray observations are used to place limits on gamma-ray line production by fast ions in various sources.

Astrophysical gamma ray spectroscopy is as young as that for X-rays. In two large solar flares of 4 and 7 August 1972, Chupp et al. (1973, 1975), using a NaI scintillation detector flown on OSO-7, reported observations of the 0.5 MeV annihilation line, the 2.2 MeV line from neutron capture on hydrogen, the 4.4 MeV line of ^{12}C and the 6.1 MeV line of ^{16}O. Lingenfelter and Ramaty (1967) had earlier made predictions of gamma ray line fluxes in solar flares, and interpretations of the observations may be found in Ramaty and Lingenfelter (1975), and Ramaty et al. (1975, 1977). More recently, a balloon flight bearing a high resolution, high purity germanium detector has observed a strong line at 510.7 $\pm$0.5 keV from the direction of the galactic center with flux $(1.21 \pm 0.22) \times 10^{-3}$ photons $cm^{-2} s^{-1}$ (Leventhal, McCallum and Stang 1978a, b). We consider the implications of this result in Chapter IV. In previous observations of the galactic center from two pioneering balloon flights in

November 1970 and November 1971, a group at Rice University, using a scintillation spectrometer, reported a marginal observation of a line at 476 $\pm$24 keV with a flux of (1.8 $\pm$0.5) x 10^{-3} photons $cm^{-2}s^{-1}$ (Johnson, Harnden, and Haymes 1972, and Johnson and Haymes 1973). Despite the low significance of the feature due to background problems, many interpretations of this emission were made, including: (i) cosmic ray excitation of interstellar ^{7}Li to its 478 keV level via $^{7}Li(p,p')^{7}Li^{*}$ (Fishman and Clayton 1972) and $^{4}He(\alpha,p)^{7}Li^{*}$ (Kozlovsky and Ramaty 1974), (ii) gravitationally redshifted positron annihilation radiation from neutron star surfaces (Ramaty, Borner, and Cohen 1973 and Guthrie and Tademaru 1973), and (iii) positronium annihilation from its triplet state via three photon decay (Leventhal 1973). Then in April of 1974, the same group, using a similar instrument but with smaller opening angle, failed to observed the above mentioned feature but saw instead a feature at 530 $\pm$11 keV with a flux of (8 $\pm$3.2)x10^{-4} photons $cm^{-2}s^{-1}$ (Haymes et al. 1975). Aside from detector problems, time variability seems the most likely interpretation of the discrepancy. We note that in all three observations, the significance of the features was $\sim 3\sigma$.

The Rice University balloon flight in 1974 gave evidence for an emission line at $\sim$ 4.5 MeV in addition to the 530 keV line from the direction of the galactic center (Haymes et al. 1975). We note that more recent observation from HEAO-1 has failed to confirm this feature, however. The $\sim$ 4.5 MeV line was also seen from the radio galaxy Centaurus A, again at about the 3σ level (Hall et al. 1976). A detailed treatment of the production of gamma ray lines by energetic particle reactions is given in Ramaty, Kozlovsky and Lingenfelter (1979); essentially all possibly observable lines are considered, and they find that the line at $\sim$ 4.4 MeV from the first excited level of ^{12}C should be the most easily detected line produced, especially for the lower resolution NaI scintillation detectors. Observations of the gamma ray lines produced

by energetic particle reactions, together with the iron line discussed above, would incicate concentrations of low energy cosmic rays, and thus perhaps provide information on the sources of the cosmic particle radiation.

Finally, we note that Jacobson et al. (1978) have reported observations of a transient event in June of 1974 which included lines at 0.413, 1.79, 2.22 and 5.95 MeV, seen by a Ge(Li) high resolution detector. An interesting interpretation of this event is given by Lingenfelter, Higdon and Ramaty (1978), in terms of gravitational redshifts.

In Chapter II the production of certain characteristic X-ray and gamma ray lines by energetic but subrelativistic ions is considered. In the first section, we have calculated x-ray production at ~ 6.8 keV by the 2p to 1s transition in fast hydrogen- and helium-like iron ions, following both electron capture to excited levels and collisional excitation. We used a refinement of the OBK approximation to obtain an improved charge exchange cross-section. This, and the corresponding ionization cross-section were used to determine equilibrium charge fractions for iron ions as functions of their energy. The effective X-ray line production cross-section was found to be sharply peaked in energy at about 8 to 12 MeV/amu. Since fast ions of similar energies can also excite nuclear levels, we have calculated the ratios of the 4.4 MeV and 0.85 MeV (the most intense nuclear line of ^{56}Fe) gamma ray line emissivities to the X-ray line emissivity. We used these calculations together with X-ray observations of the galactic center from OSO-8 and HEAO-1 to set limits on the intensity of gamma ray line emission from the galactic center and the radio galaxy Centaurus A, and we find that these limits are generally lower than those reported. In the second section of Chapter II the effect of interstellar dust grains on the width of certain gamma ray lines produced by fast ions is considered. Specifically,

for some relatively long-lived nuclear levels, the recoiling excited nucleus may be stopped in the grain before deexciting, which leads to a very narrow line profile. This problem was originally considered by Lingenfelter and Ramaty (1977); they have treated the 6.1 MeV line of ^{16}O in detail. One of the difficulties they encountered was the lack of consistent range relations through the relevant energy region ($\sim$ 1 to 100 keV/amu). In addition, since the range of the recoiling ion is of the same order as typical grain radii, straggling (statistical fluctuations in range) is expected to be important. Therefore, for the calculations presented here, we have compiled a consistent set of range and energy loss relations, taken the effect of straggling into account, and considered lines from less abundant elements. Using a Monte Carlo simulation, we have evaluated the expected strengths of these very narrow lines as functions of the grain size distribution for various energetic ion spectra. Thus possibility of obtaining information from these features with high resolution solid state gamma ray detectors is discussed.

The expectation of intense magnetic fields ($\geq 10^{12}$ gauss) at the surfaces of neutron stars gave rise to consideration of another kind of high energy spectral feature, since for such fields, the fundamental cyclotron frequency lies in the hard X-ray band. Classically, it is well known that a magnetic field will force electrons to move on a helix centered on a field line called the guiding center. As they orbit, they produce gyrosynchrotron radiation, lose energy as a result and consequently spiral inward toward the guiding center. If, however, the field is very strong, the orbits of the electrons become quantized; the gyroradius of the electron orbit and its perpendicular momentum take on discrete values. Radiative transitions between levels can occur and this process results in a quanti-

zation of the gyrosynchrotron radiation. Line emission occurs accompanying transitions from higher to lower transverse momentum levels, and upward transitions take place with absorption of resonant photons.

Several observed X-ray sources, in particular X-ray pulsars, are believed to be spinning neutron stars with the field anchored rigidly to the surface. They are powerful sources and are thought to derive their energy from the accretion of matter from a companion star. Hercules X-1 is the best studied of these objects; it shows significant spectral changes during a portion of its pulse phase (Pravdo et al. 1977b and 1978). Since in this picture the pulse phase would correspond to the angle between the line of sight and the magnetic field lines, these spectral changes are evidence for the effect of the magnetic field on photon production, absorption and scattering processes. Furthermore, there is evidence for an emission feature near 60 keV in the Her X-1 spectrum (Trumper et al. 1977 and 1978, Coe et al. 1977), which has been interpreted by these authors as a cyclotron line (see also Daugherty and Ventura 1977).

Although details of accretion flow onto rotating, highly magnetized neutron stars are unknown, if the rotation is fast enough, any plasma which falls to the surface is generally assumed to be channeled by the field into a polar cap with essentially zero pitch angle (Basko and Sunyaev 1975 and 1976, Elsner and Lamb 1976). The infalling ions lose their free fall energy by heating the atmosphere at the polar cap. The magnetic field quantizes the transverse energies of the electrons, and transitions between levels give rise to line radiation. The levels can be excited by collisions with the infalling ions or by thermal collisions with ambient ions; however, the correct cross sections for Coulomb collisions in these circumstances was not known. So in Chapter III, we have calculated these by using a

relativistically correct quantum electrodynamic treatment; then we have used them to calculate the energy loss rate for fast zero pitch angle photons. It was found that this rate is slower than that for a non-magnetized plasma, but it is not reduced as much as had been predicted (Basko and Sunyaev 1975). Including the effect of elastic proton-proton scattering, we have calculated the multiplicity of cyclotron line photons produced by an ion falling onto a highly magnetized, hot plasma, and the fraction of its energy that goes directly into line photons. We have also calculated the rate of excitation of the cyclotron levels by thermal electron-ion collisions. These results are presented in Chapter III, where we also discuss their relevance to observations of Her X-1.

Strong magnetic fields will also affect the X-ray spectra of the plasma directly, by both modifying the Compton scattering cross section (Canuto et al. 1971, and Gnedin and Sunyaev 1973) and giving rise to resonant cyclotron absorption, i.e., absorption of a photon accompanied by an excitation of the electron's transverse energy (Daugherty and Ventura 1978). An attempt has been made by Boldt et al. (1976) to explain the high energy ($\sim$ 20 keV) steepening observed for Her X-1 (Pravdo 1976) by Compton scattering off thermal electrons using the cross section of Canuto et al. (1971). However, in Chapter III, we have shown that cyclotron absorption could be important in forming this feature; specifically, we have found that the infalling ions can produce a flux of relatively high energy ($\sim$ few hundred keV) electrons streaming down the field lines toward the stellar surface. The velocities of these electrons are large enough that they can absorb photons with energies below the cyclotron energy because of the Doppler shift of the photon's frequency. The production rates of the highen energy electrons and their effect on the x-ray spectra of the pulsars is discussed in Chapter III.

In Chapter IV, we have considered the formation of the 0.511 MeV line by positron annihilation in the galaxy. As was mentioned above, a narrow, intense line has been seen from the galactic center direction at 0.5107 $\pm$0.0005 MeV (Leventhal et al. 1978a, b) with a full width at half maximum less than the detector resolution, about 3.2 keV. Since previous estimates of the line width have been larger (e.g., Stecker 1969), in Chapter IV, we have studied the annihilation of galactic positrons in order to evaluate the probabilities of various channels of annihilation and to calculate the spectrum of the resulting radiation. These channels include positronium formation by charge exchange with neutral atoms and by radiative recombination with free electrons and direct annihilation with either bound or free electrons. In a nearly neutral gas, charge exchange will occur before most of the positrons can thermalize; otherwise they thermalize before annihilating. We have calculated the fraction which annihilate in flight (before thermalization) as a function of the ionization fraction of the medium by a Monte Carlo simulation, and we have evaluated the dependence on gas temperature of the annihilation rates for the various processes mentioned above for those which thermalize. Then, we have calculated the annihilation radiation spectrum for all these cases.

We find that the narrow width of the 0.511 MeV line observed from the Galactic Center implies that a large fraction of positrons should annihilate in a medium of temperature less than 10^5K and ionization fraction greater than 0.05. Since most of the matter in the galactic center region is expected to be in neutral molecular clouds, it is difficult to reconcile the narrow line observation with diffuse positron production unless they are unable to penetrate the clouds. Another possibility is that the positron source is localized very near to the galactic center itself, in

which case the HII regions at the nucleus are possible sites of annihilation. If future observations confirm the small angular extent of the source of this radiation a massive collapsed object at the galactic center is suggested.

Chapter V is a summary of the preceding topics, with a discussion of possible future investigations, both theoretical and experimental. Searches for the characteristic iron X-ray line and nuclear gamma ray lines will provide constraints on cosmic ray origin theories. High resolution spectroscopy can be useful in several ways. Nuclear lines from interstellar dust could be distinguished, depending on the size distribution of grains. Physical processes in the intense magnetic fields of binary X-ray pulsars can be determined by such detectors made sensitive to as low as $\sim$30 keV. And high resolution spectroscopy at 0.5 MeV can provide information on sites of positron annihilation.

II. X-RAY AND GAMMA RAY LINE PRODUCTION BY NONTHERMAL IONS

a) Introduction

A flux of fast subrelativistic ions in a medium can produce line emission in both the X-ray and the γ-ray regions. This chapter is concerned with the production of the lines of the 2p to 1s transitions in hydrogen- and helium-like iron ions (at ~ 6.8 keV), and with the comparison of these lines with the strong γ-ray line at 4.44 MeV resulting from the nuclear deexcitation of ^{12}C. The 2p to 1s transitions in more abundant species such as C, N ,nd O give rise to less energetic X-ray photons, which subsequently suffer interstellar absorption.

The X-ray calculations presented in this chapter are of the same nature as those of Pravdo and Boldt (1975) who have treated X-ray line production from energetic oxygen nuclei in the interstellar medium. Watson (1976) has calculated the multiplicities of X-rays produced by fast iron and oxygen nuclei interacting with ambient hydrogen, but as we shall show, interstellar oxygen and iron, and not hydrogen, are the main contributors to electron capture by fast iron ions. By using improved cross sections for charge exchange and excitation, we have carried out a detailed calculation of X-ray line production from fast ions moving through an ambient medium with solar system abundances.

Astrophysical γ-ray line production has been investigated by Ramaty, Kozlovsky and Lingenfelter (1975) and Ramaty, Kozlovsky and Suri (1977) for solar flares, and by Meneguzzi and Reeves (1975), Lingenfelter and Ramaty (1977), and Ramaty, Kozlovsky and Lingenfelter (1979) for the interstellar medium. By combining these results with the calculated X-ray line emission, we evaluate ratios of the X-ray and γ-ray line intensities. These can be used to set limits on the expected γ-ray line emission from

various source regions for which X-ray observations are available. As was mentioned in Chapter II, iron line emission has been observed from young supernova remnants and clusters of galaxies (Virgo, Coma, and Perseus), but this emission has a narrow width, consistent with production in a thermal plasma with a nearly solar abundance of iron. A broadened iron feature has been seen from collapsed stars in binary systems, but the broadening is most likely due to rotational bulk motions, since charge exchange by the accreting matter is not efficient enough to provide the observed line luminosity. So, only upper limits are available at the present time on the intensity of the $\sim$ 6.8 keV line from nonthermal particles.

b) X-ray Production

1) Charge Exchange, Excitation and Ionization Cross Sections

We consider energetic (about 1 to 300 MeV/amu) Fe ions moving through an ambient medium with solar abundances (Cameron 1973, except for the abundance of He for which we use the results of Brown and Lockman 1976). The 2p to 1s transitions in such ions having one or two bound electrons give rise to Kα X-rays at 6.9 and 6.7 keV, respectively. Because of Doppler broadening, however, these 2 lines merge into a broad feature centered at about 6.8 keV. For bare nuclei, the 2p state can be populated by charge exchange with ambient atoms; for ions having one electron, the 2p state can be populated by charge exchange or excitation; and for ions having 2 electrons, the 2p to 1s transition can only occur following excitation.

The method for calculating the charge exchange cross sections for bare Fe nuclei, a refinement of the Oppenheimer, Brinkman, and Kramers (OBK) approximation, is described in Bussard, Ramaty and Omidvar (1978). The OBK method is a Born approximation which treats target electrons as distinguishable (Oppenheimer 1928, Brinkman and Kramers 1930). Nikolaev

(1967) has developed an empirical factor which brings the OBK cross sections into agreement with existing data; we have applied this correction to the case of iron projectiles. The results at five energies, tabulated by the species of target atom, are shown in Table II-1. The three rows for each target element give the capture cross sections to any state which subsequently deexcites to the 1s, 2p and 2s levels, respectively.

The charge exchange cross sections which lead to electrons in the 2p level are shown in Figure II-1 as functions of the temperature of the ambient medium for the 5 energies given in Table 1. At low temperatures ($< 5 \times 10^5$ K) these cross sections are the same as those given in Table 1. The cross sections decrease with increasing temperature because the target atoms lose some of their orbital electrons. We have estimated the temperature dependence shown by folding together the contribution of the partial cross sections for charge exchange from each electronic orbital and the ionization fractions at a given temperature. For these partial cross sections we used the calculations described in Bussard, Ramaty and Omidvar (1978), while the ionization fractions are from J. C. Raymond (private communication 1977). The results indicate that the cross sections are fairly constant up to a gas temperature of a few hundred thousand degrees, but fall off rapidly with increasing temperature. It should be noted that the temperature dependences shown in Figure II-1 might require some modification since the partial cross sections were obtained for neutral targets. In subsequent calculations, however, we only use the cross section at low temperatures where the targets which are the major contributors to charge exchange are mostly neutral. This cross section is shown as a function of energy by the dotted line in Figure II-2.

The cross section for excitation of a hydrogen-like ion from the 1s to the 2p configuration is given by:

$$\sigma_{exc}(E) = \frac{2^{18}\, Z_m^2\, \pi A_o^2}{\left(\frac{m_e}{m_p}\frac{E}{I_H}\right)^2} \int_{t_{min}}^{\infty} \frac{dt}{t^3}\left[1 - \frac{16\, Z^3}{(4Z_m^2 + t^2)^2}\right]\left[\frac{3t}{Z}\left(\frac{4t^4}{Z^4}+9\right)^{-3}\right]^2 \qquad (II\text{-}1)$$

(Bates 1962). Here Z_m is the atomic number of the gas atom causing excitation, A_o is the Bohr radius (.529Å), and Z is the charge, in units of the electron charge, of the ion being excited. Also, m_e and m_p are the electron and proton masses, respectively, E is the kinetic energy per nucleon of the projectile, and I_H is the ionization potential of hydrogen (13.6 eV). The lower limit on the integral, t_{min}, is given by

$$t_{min} = \frac{\Delta E}{2}\left(\frac{m_p}{m_e I_H E}\right)^{1/2}\left(1 + \frac{m_p}{4M}\frac{\Delta E}{E}\right) \qquad (II\text{-}2)$$

where ΔE is the difference in energy between the two levels, and M is the reduced mass for the encounter.

The ionization cross section of iron ions in collisions with ambient neutral hydrogen were taken from Watson (1976), but since he considered a gas consisting only of hydrogen, we have scaled his cross sections to account for the effects of helium. There are two contributions to these cross sections: one in which the target atom is not itself excited, called the elastic part, and an inelastic part, which includes the sum over all possible excitations of the target (e.g. Rule 1977). For iron projectiles on hydrogen and helium, each part contributes almost equally, but the elastic part scales as the target charge squared, while the inelastic part varies linearly with the target charge. Also we compared the calculations of Rule (1977) with the Watson (1976) cross section for ionization of the hydrogen-like iron and found good agreement.

Since the energy required to ionize the iron projectiles is so large compared to the target ionization potentials, the ionizing collisions take place at very small impact parameters. Thus, electronic

screening of the target nuclei is not very important, and these same results should apply to an ionized medium. In fact, Rule (1977) calculated the ionization cross sections for both cases, and found differences of $\leq 10\%$ for the energies under consideration.

2) Effective X-ray Production Cross Sections

The effective X-ray production cross sections were obtained by folding the cross sections for capture and excitation with the appropriate charge fractions:

$$\begin{aligned} \sigma_c(2p) &= f_0\,\sigma_c^{(0)}(2p) + f_1\,\sigma_c^{(1)}(2p) \\ \sigma_{exc} &= f_1\,\sigma_{exc}^{(1)} + f_2\,\sigma_{exc}^{(2)} \\ \sigma_c(2s) &= \tfrac{3}{4}\,f_1\,\sigma_c^{(1)}(2s) \end{aligned} \qquad \text{(II-3)}$$

where σ_c (2p) is the effective cross section for X-ray production following the capture of an electron which cascades through the 2p to 1s levels, $\sigma_c^{(n)}$ (2p or 2s) is the cross section for the capture of an electron into the 2p or 2s level, either directly or following a cascade, by an ion which already has n electrons, σ_{exc} is the X-ray production cross section following excitation, and $\sigma_{exc}^{(n)}$ is the cross section for excitation of an ion with n electrons. The cross sections $\sigma_c^{(n)}$ are obtained by multiplying the cross sections given in Table 1 by $(Z_{eff}/26)^5$, where Z_{eff} is the bare charge corrected for electronic screening. The screening effect was taken from Burns (1964) for all the cross sections considered. The 2s term represents the magnetic dipole transition, which occurs more rapidly than two photon emission only in the triplet state of the helium-like ion. On the average, this state is populated 3 times more often than the singlet state, giving rise to the factor 3/4. The f_n are the charge fractions or the fractions of all ions with n electrons.

The charge fractions satisfy the equation:

$$\frac{\partial f_n}{\partial t} + \frac{\partial}{\partial E}\left(f_n \frac{dE}{dt}\right) = n_H v \left(f_{n-1}\sigma_c^{(n-1)} - f_n \sigma_I^{(n)} + f_{n+1}\sigma_I^{(n+1)} - f_n \sigma_c^{(n)}\right) \qquad (II-4)$$

where the subscript I refers to ionization, n_H is the hydrogen density, v the projectile velocity, and $\frac{dE}{dt}$ is the time rate of energy loss. In a steady state situation and if the energy losses are slow compared to charge exchange and ionization collisions, equation II-4 reduces to

$$f_n \sigma_c^{(n)} = f_{n+1} \sigma_I^{(n+1)} \qquad (II-5)$$

For this equation to be valid, the time between collisions represented by terms on the right side of equation II-4 should be much shorter than the energy loss time of the ions. Since the charge exchange collisions manifest themselves in X-ray production, we expect that this condition will be satisfied when the X-ray multiplicity, defined by

$$N = \frac{n_H}{\rho} \int_0^E dE' \quad \frac{\sigma_x(E')}{\frac{dE'}{dX}} \qquad (II-6)$$

is much larger than unity. Here ρ is the gas mass density, $\sigma_x = \sigma_c(2p) + \sigma_{exc} + \sigma_c(2s)$ is the total 6.8 keV X-ray production cross-section from equation II-3, dE/dX is the energy per amu lost per g cm^{-2} of matter traversed, and E is some energy at which the ions are essentially bare. In evaluating equation II-6 we assume that the Fe ion is in charge equilibrium at all energies. The energy loss rate dE/dX in a neutral medium was taken from the tabulations of Barkas and Berger (1964) and Northcliffe and Schilling (1970), for a gas composed of H and He with 8.5% He by number. The effective charge for the Fe ions was taken from Northcliffe and Schilling (1970). The losses of fast ions in an ionized medium were calculated by using

$$\frac{dE}{dX} = \frac{2\pi Z^2 e^4}{\rho E} n_e \ln\left(\frac{m_e^3 v^4}{\pi \hbar^2 n_e e^2}\right) \qquad (II-7)$$

Ginsburg and Syrovatskii (1964), where e and m are the electron charge and

mass, Ze the ion charge, v is the velocity of the ion, and n_e is the electron density, taken equal to the hydrogen density.

Table II-2 shows the multiplicity of $\sim$ 6.8 keV X-rays as evaluated from equation II-6 for several values of E. For a neutral medium, the multiplicity is high enough that equation II-5 should be a good approximation. However, in an ionized medium the multiplicity is low, and hence equation II-5 may not be a good approximation. An exception is the case of continuous acceleration where another term is added to equation II-4 to cancel the effects of the energy losses. But even if such acceleration is not present, we would still expect about one X-ray photon per each energetic iron ion. Since the multiplicity for the ionized case in Table 2 is already close to unity, we do not expect that the use of equation II-5 will lead to any substantial error, even in this case.

Figure II-3 shows the charge fractions as functions of the projectile kinetic energy per nucleon, calculated by using equation II-5. It shows that on the average, the iron nuclei are bare above $\sim$ 40 MeV/amu, that they have picked up one electron by $\sim$ 11 MeV/amu, that they have two electrons by $\sim$ 10 MeV/amu. Below about 6 MeV/amu, the average iron ion has 3 or more electrons. When this happens, the outer electron usually takes the energy from collisions, so the Kα transition occurs rarely from ions with 3 or more electrons.

The charge fractions shown in Figure II-3 were then used to weight the cross-sections discussed in section IIa, according to equations II-3. The results are shown in Figure II-2 as the solid lines. Both curves show the same energy dependence, and excitation is seen to be the dominant mechanism for X-ray line production. Both cross-sections are fairly sharply peaked in energy at around 10 MeV/amu. Because of the sharpness of the peak,

we estimate the width of the broad 6.8 keV feature to be $\simeq$ 2.4 keV. Also, observation of this line will give the amount of iron with energy from approximately 5 to 20 MeV/amu in the source. This number is about 10^{-44} $M_\odot$ of iron per photon per sec produced, for a hydrogen density of 1 cm^{-3}, and varies little with the assumed spectrum of ions ($\pm \sim 50\%$ over the spectra considered in this chapter).

c) Results

We have integrated the X-ray production cross-sections shown in Figure II-2 over a variety of spectra of fast ions. The abundances of these ions were extrapolated from measurements at $\geq$ 300 MeV/amu (e.g. Meyer, Ramaty, and Webber 1974), H: He: C: N: O: Fe = 1: .1: 5.6×10^{-3}: 2.8×10^{-3}: 5.4×10^{-3}: 5×10^{-4}, and taken to be independent of energy. The spectra used for all species are power laws in kinetic energy per amu with a low energy cutoff, E_c:

$$n(E) \propto \begin{cases} E^{-s} & \text{for } E > E_c \\ \text{constant} & \text{for } E \leq E_c \end{cases} \qquad (II-8)$$

where n(E) is the number density of ions per interval of kinetic energy/amu. We have also set n(E) equal to zero for E>300 MeV. As mentioned above the gas abundances used were taken from Cameron (1973), with the exception of He (Brown and Lockman 1976). They are given in Table II-1.

The solid curves in Figure II-4 show the 6.8 keV line emissivity per H atom for an energy content of 1 eV cm^{-3} in fast ions from 1 to 300 MeV/amu. It can be seen that the spectra which maximize X-ray production have breaks at around 10 MeV/amu and fall off rapidly above that energy. This is a result of the sharp maximum in the X-ray production cross section at around 10 MeV/amu, shown in Figure II-2. Because of evidence that a galactic gradient of heavy abundances exists, we have also repeated these calculations for the same fast ion fluxes in a medium with these abundances

increased by about a factor of 5, as Ramaty, Kozlovsky and Lingenfelter (1979) have assumed for the 5kpc ambient medium based on the radial gradients found by Peimbert et al. (1978) for N and O. These abundances are given in parenthesis in table II-1. The results are shown by the dotted lines in Figure II-4. The overall X-ray production is not affected much; however, due to the enhanced possibility for charge exchange, the production is shifted slightly to emphasize higher energy particles.

Figure II-5 shows the ratio of 6.8 keV photons produced to the energy deposited in the gas by the fast ions, assuming local abundances. Here, the X-ray line emission is maximized with respect to energy deposited when the spectrum has a break at about 15 MeV/amu. The curves are shown for both a neutral and an ionized gas. They have the same shapes for both types of medium, but since energy is lost faster in a plasma owing to collective long range interactions (emission of plasma waves) the curves are displaced downward in an ionized gas.

In addition to the X-ray lines of iron, ions in the energy range under consideration will cause nuclear reactions, with subsequent γ-ray line emission. Meneguzzi and Reeves (1975) and Ramaty, Kozlovsky and Lingenfelter (1975) have shown that in these reactions the strongest line is at 4.44 MeV from the first excited nuclear level of ^{12}C. This line has two components. One is narrow, resulting from nuclei in the ambient gas excited by fast H and He, and the other is broad, from the excitation of the fast nuclei by ambient H and He. Since we are assuming different relative abundances of heavy nuclei in the gas and the fast particles, these two components have equal intensities, and hence are treated separately in the present work. For the calculation of both the narrow and broad 4.44 MeV line intensities, we use the cross section compiled by Ramaty, Kozlovsky

and Suri (1977). In addition, we also include the broad component of the 0.85 MeV line of ^{56}Fe, since this line intensity scales directly with the amount of fast iron which produce the broad $\sim$ 6.8 keV X-ray line.

In Figure II-6, we show ratios of γ-ray to X-ray line emissivities, $q_\gamma/q(6.8)$, calculated for the equilibrium case, for the two components of the carbon-line and the broad component of the iron γ-ray line. In addition to the effects of direct excitation of carbon by hydrogen and helium, we have also included the contribution of spallation of nitrogen and oxygen to the excited carbon nucleus. The X-ray production scales directly with the relative abundance of iron in the fast ions, but varies in a more complicated way with the relative abundances of heavy nuclei in the gas, primarily iron and oxygen. On the other hand, the broad component of γ-radiation scales with the relative abundance of fast C, N and O ions, and the narrow component scales with the gas abundances of these nuclei. Thus, the ratio of γ-ray to X-ray yields depends somewhat on the relative abundances of medium and heavy nuclei. For example, by increasing the abundances of C and heavier nuclei in both the gas and fast particles by a factor of 10, the 4.44-MeV γ-ray intensity also increases by a factor of 10, but the $\sim$ 6.8 keV X-rays increase by about a factor of 20 at most, and hence $q_\gamma/q(6.8)$ remains constant or decreases somewhat, up to a factor of 2.

Figure II-6 shows that there is less than an order of magnitude of variation of $q_\gamma/q(6.8)$ with the various spectra assumed for the fast ions, except for those which flatten at $\geq$ 50 MeV/amu. The flatter spectra favor γ-ray emission because the cross sections for nuclear excitation drop off much more slowly at high energies than does the X-ray production cross section. This trend is also reflected in the fact that lower spectral indices favor γ-ray emission. Since we have assumed a high energy cutoff at 300 MeV/amu,

we do not take into account γ-ray emission from π° decay produced by particles at higher energies.

d) Applications to the Galactic Center, Cen A, and Cas A

We now apply the results of the previous section to examine the consistency of the reported γ-ray data from the galactic center region and the radio galaxy Centaurus A (Haymes et al. 1975, Hall et al. 1976) with upper limits on the nonthermal 6.8 keV line from these sources (Kellogg et al. 1971, R. Mushotzky, private communication 1977). We also set limits on the flux of energetic particles in the supernova remnant Cassiopeia A by using upper limits on the broad X-ray line emission from this source (P. J. Serlemitsos, private communication).

Haymes et al. (1975) have claimed to see a feature at around 4.6 MeV from the direction of the galactic center which they attributed to the 4.44 MeV line of ^{12}C. The opening angle of the γ-ray detector used was 13° (FWHM). From the observations of Kellogg et al. (1971) of the X-ray sources GCX at the galactic center, we take the measured flux of 1.1×10^{-2} photons $cm^{-2} s^{-1}$ in a 2.4 keV band centered at 6.8 keV as an upper limit on the intensity of the broad iron Kα line from GCX. Using this upper limit, we have set upper limits on both the broad and narrow γ-ray lines produced by fast ions in GCX. Under the most favorable conditions for γ-ray production considered ($s = 1.2$, $E_c = 100$ MeV/amu, see Figure 6) the upper limits on the narrow and broad components are 3.2×10^{-5} and 3.3×10^{-4} photons $cm^{-2} s^{-1}$, respectively. Haymes et al. (1975) give an intensity of $(9.5 \pm 2.7) \times 10^{-4}$ photons $cm^{-2} s^{-1}$ with a width of several hundred keV, so they could have been observing the broad component. In this case, our upper limit is a factor of three below their observation. Since the opening angle of the γ-ray detector is larger than the angle subtended by GCX, Worrall et al.

(1978) have examined data from the Goddard Cosmic X-Ray Spectroscopy Experiment on board OSO-8 to obtain the X-ray flux from an area of 20°x20° centered on GCX. They find the upper limit to a broad 6.8 keV feature is 0.13 photons $cm^{-2}s^{-1}$, which implies after scaling to 13°x13°, upper limits of $8x10^{-3}$ $8x10^{-4}$ photons $cm^{-2}s^{-1}$ to the broad and narrow γ-ray components, respectively. It should be noted the region is source confused, and efforts are presently under way to eliminate problems from discrete sources. Thus the observation of Haymes et al. (1975), provided they indeed represent the broad γ-ray component and their source is larger than GCX, is not inconsistent with the upper limits set by the X-ray data. However, as we shall now discuss the energy density in energetic particles required to account for the γ-ray data under the constraints of the X-ray upper limits is much larger than the limits set by the distribution of gas perpendicular to the plane in the galactic center region.

The energy density in fast ions required to produce a $\sim$ 6.8 keV X-ray flux corresponding to the gamma ray observation for s = 1.2 and E_c = 100 MeV/amu, of $4.8x10^{-2}$ photons $cm^{-2}s^{-1}$ is, from Figure II-4, $4x10^{11}/M_H$ eV cm^{-3}, where M_H is the mass of hydrogen in the source, in solar masses. Scoville, Solomon, and Jefferts (1974) and Mezger (1974) have estimated that the amount of gas in the nuclear region is some 10^7 to 10^8 $M_\odot$, and so, the above γ-ray flux requires several keV cm^{-3} in fast ions. This energy density is 2 orders of magnitude larger than that required to maintain the z distribution of gas at the galactic center (Sanders and Wrixon 1973). We could lower this energy density in a manner similar to that suggested by Ramaty, Kozlovsky and Lingenfelter (1979). They proposed that the abundances of C and heavier nuclei relative to H in both the ambient gas and energetic particles could be larger than solar and cosmic ray abundances. Also, we

can assume spectral parameters for the energetic particles which maximize the γ-ray line emission with respect to energy content ($s \geq 3$, $E_c \simeq 15$ MeV/amu). However, both these assumptions lower $q_\gamma/q(6.8)$. As can be seen from Figure II-6, for s = 3 and E_c = 15 MeV/amu, $q_\gamma/q(6.8)$ is lower by about an order of magnitude than for s = 1.2 and E_c = 100 MeV/amu. Furthermore, since q(6.8) depends on the relative abundances of the heavy nuclei in both the gas and the energetic particles, while q_γ depends on these relative abundances in only one component, an increase of heavy nuclei abundances decreases $q_\gamma/q(6.8)$. Therefore, we conclude that it is difficult to lower substantially the energy density required to produce the γ-ray flux observed by Haymes et al. (1975) without leading to conflict with the X-ray data. The only exceptions could arise if the source region is so hot that the charge exchange and X-ray production are suppressed, or that it is opaque to the X-rays but not to the gamma rays.

We note, from Figure II-5, that to produce a 6.8 keV X-ray flux of 4.8×10^{-2} photons $cm^{-2}sec^{-1}$, the energy deposited in a neutral gas by the energetic particles with spectrum s = 1.2 and E_c = 100 MeV is about 4×10^{42} erg/sec. This energy release is large, but still of the same order as the observed far infrared luminosity of the galactic center (Hoffman, Frederick, and Emergy, 1971). The energy deposited in an ionized gas is larger by a factor of 5 than that in a neutral gas.

If, nonetheless, we use the spectral parameters s = 3 and E_c = 15 MeV/amu, we find that the observed upper limit on the broad 6.8 keV line from a 13°x13° region implies, from Figure II-6, upper limits of 1.4×10^{-5} and 2.8×10^{-4} photons $cm^{-2}s^{-1}$ on the narrow and broad 4.44-MeV line intensities. For these fluxes the energy density in fast ions is, from Figure II-4, only $7.4\times10^{9}/M_H$, a factor of 50 less than that required to

account for the observations of Haymes et al. (1975) under the other assumed spectrum.

One interesting possibility for explaining the incompatibility of the gamma ray observation with the X-ray upper limits and gas distribution is time variability. In September 1977, observations of the galactic center from the HEAO-1 A4 experiment, a scintillation detector with opening angle $\sim 20°$, have provided an upper limit of 5.7×10^{-4} photons $cm^{-2}s^{-1}$ in a 700 keV band centered on 4.4 MeV (J. Matteson, private communication, 1978). If we accept both measurements, then the galactic center source must vary on a time scale of a few years. Since this would imply a fairly localized source, we are tempted to suggest accretion onto a massive black hole as the source, as has been suggested to explain the time variability of Centaurus A (Fabian et al. 1976). Lingenfelter, Higdon and Ramaty (1978) have treated the γ-ray line production in the accreting gas. Ions falling into the disk have little or no time to cool, and predicted temperatures are favorable for nuclear interactions. This interpretation, however, has the disadvantage that the temperatures are high enough to suppress X-ray production by charge exchange.

In addition to the galactic center, γ-radiation was also detected from Centaurus A (Hall et al., 1976). They claimed a feature at 4.5 MeV, most likely less broad than ~ 150 keV, at a confidence level of 3.3σ, with a line flux of $(9.9 \pm 3.0) \times 10^{-4}$ photons $cm^{-2}s^{-1}$. We examined the X-ray spectrum of Cen A around 6.8 keV (R. Mushotsky, private communication), and placed an upper limit of 8.1×10^{-3} photons $cm^{-2}s^{-1}$ on the broad Fe Kα flux. Again, using the most favorable spectrum for γ-ray production, we obtained upper limits of 2.5×10^{-5} and 2.6×10^{-4} photons $cm^{-2}s^{-1}$ to the narrow and broad 4.44 MeV components, respectively. Thus, the upper limit on the narrow component is a factor of 40 below the observation. Because of the quoted width

of the $\sim$ 4.5 MeV feature from Cen A, it is unlikely that this feature is the broad 4.44 MeV line.

Since supernovae or supernova remnants are candidates for sites of particle acceleration, we examined the spectrum of Cas A, a young supernova remnant. Because of a narrow thermal line at 6.7 keV (Pravdo et al. 1976), we used for an upper limit on flux in a broad line the flux above continuum at 4.85 keV (P. J. Serlemitsos, private communication 1977). This was fit to a gaussian centered at 6.8 keV and a full width at half maximum of 2.4 keV and gave an upper limit of 7×10^{-3} photons $cm^{-2} s^{-1}$ in the broad line. At an assumed distance of 3 kpc, we obtain for the mass of Fe in the energy range 5 to 20 MeV/amu, as discussed in section b2, $< 0.1/n_H \, M_\odot$, where n_H is the atomic hydrogen density at the source. From Figure II-6, we can set upper limits on the broad and narrow components of the 4.44 MeV ^{12}C line of 2.8×10^{-4} and 2.7×10^{-5} photons $cm^{-2} s^{-1}$, respectively. Presently planned γ-ray experiments could detect such fluxes, and thus we expect to obtain even more meaningful limits on the fluxes of energetic ions in supernova remnants from these experiments.

e) The Effect of Interstellar Dust on Gamma Ray Line Shapes

There is mounting evidence that significant fractions of the interstellar heavy nuclei are condensed out of the gas phase in dust grains with linear dimensions distributed around a few tenths of a micron. When these nuclei are excited by fast protons or alpha particles, they attain recoil velocities from around one keV per amu for ^{56}Fe to several tens of keV per amu for CNO nuclei. In the gas phase, the nuclei are not decelerated; the recoil velocity is the velocity at which the gamma ray is emitted and consequently is responsible for Doppler broadening of the line. However, in grains, nuclei excited to states with long enough lifetimes have a chance

to be significantly slowed or even stopped before emitting the gamma ray, which leads to a much narrower line profile than produced in the gas.

To investigate the importance of this effect quantitatively, we have compiled the energy loss and range relations for ^{12}C, ^{16}O, ^{20}Ne, ^{24}Mg, ^{28}Si, and ^{56}Fe with energies from 10^{-3} to 1 MeV/amu slowing down in water. For a recoil energy E_r greater than 12.5 keV/amu, these quantities are taken directly from the tables of Northcliffe and Schilling (1970). At lower energies, we have used the tabulated values of Winterbon (1975), using the scaling laws given there to apply his results to our nuclei and target material. Where overlaps occurred in the results from the two sources, differences were found to be less than about 10%. Another effect we had to consider was that of range straggling, or statistical fluctuations about the mean range. This quantity was obtained from the tables of Brice (1975), and the ratio of the variation in range to the mean range was found to be essentially the same for all nuclei considered. The rate of energy loss, dE/dX, the mean rectilinear stopping range, $\langle X(E_r)\rangle$, and the square of the ratio of the fluctuation in X due to straggling to X, $(\Delta X/X)^2$ are shown in Figure II-7 for ^{16}O, ^{24}Mg and ^{56}Fe nuclei slowing down in water assuming that the grains are predominantly ice. These quantities, however, are not strongly dependent on the assumed grain composition. For a density of 1.5g cm^{-3}, nuclei with recoil velocities as mentioned above slow down in less than about 7×10^{-13} sec over distances less than $\sim 10^{-4}$ cm. By comparing with the mean lives listed in Table II-3, (from Ramaty, Kozlovsky, and Lingenfelter 1978) and the expected sizes of interstellar grains, it is evident (Lingenfelter and Ramaty 1977) that many lines could have significant very narrow components.

Ramaty, Kozlovsky and Lingenfelter (1979) have performed an extensive, detailed calculation of the gamma ray line shapes resulting from nuclear excitation by energetic particles, using a Monte Carlo simulation which takes into account the reaction kinematics, excitation of the fast ions as well as the ambient gas nuclei, and excitation following spallation reactions, for various ion spectra parametrized by power law indices and break energies as in equation II-8. In this calculation, a large number of interactions are considered; the interacting particles and the energy of the nonthermal ion are chosen according to the cross sections for the interactions, the abundances of the particles and the energy spectrum of the fast ions. After the interaction, the recoil angle is determined from nuclear data, and the recoil energy can then be determined (in two-body reactions) by kinematics. We have added to this calculation the possibility that some of the heavy gas nuclei may be concentrated in dust grains. The nuclei considered are those listed in Table II-3 with mean lives longer than 10^{-13} seconds.

In our calculations we consider spherical grains having an exponential size distribution and containing half of the interstellar C, N, O, Ne and S and all of the Al, Mg, Si, Ca, and Fe. For such grains, the probability that a nuclear interaction takes place in a grain of radius between a and a+da is

$$P(a)\,da = a^3 e^{-a/a_o}\,da \,/\,(6a_o^4) \qquad (II\text{-}9)$$

where a_o is the characteristic grain radius. We assume that the energetic particle flux is isotropic, and that the matter density and composition are constant throughout the grain. Then if an interaction producing a recoil with energy E_r occurs in a grain, we evaluate the grain radius from equation II-9, and the position of the interaction in the grain and the recoil angle

at random. From these parameters, we can then determine the distance r the recoiling nucleus must travel to reach the edge of the grain. It is of interest to note that the distribution of r in spherical grains can be obtained analytically. If the distance from the center of the grain to the interaction is x, then the probability normalized to 1 that x lies in dx is given by

$$P(x)\,dx = 3x^2 dx / a^3 \qquad (II-10)$$

If we then construct a radius vector through x, the distribution in recoil angle θ about this line is assumed isotropic, or

$$P(\cos\theta)\,d(\cos\theta) = \frac{1}{2}\,d(\cos\theta) \qquad (II-11)$$

The cosine law gives r in terms of a, x and cosθ as

$$a^2 = r^2 + x^2 - 2xr\cos\theta \qquad (II-12)$$

Then the probability of occurrence of r is given by integrating over x. Equation II-12 implies a minimum value of x exists for a given r,

$$x_{min} = |a-r| \qquad (II-13)$$

Then the desired distribution in r is obtained:

$$P(r)\,dr = \int_{x_{min}}^{a} dx\; P(x)\; P(\cos\theta)\; \left|\frac{d(\cos\theta)}{dr}\right| dr \qquad (II-14)$$

After substituting for x_{min}, P(x) and P(cosθ), and evaluating d(cosθ)/dr from equation II-12, we obtain

$$P(r) = \int_{|a-r|}^{a} dx\; \frac{3x^2}{2a^3}\; \frac{r^2+a^2-x^2}{2xr^2} = \frac{3}{16a^3}\left(4a^2 - r^2\right) \qquad (II-15)$$

This distribution was given in Ramaty, Kozlovsky and Lingenfelter (1978).

Once a value for r is determined, we find the stopping range X for the excited recoiling nucleus by assuming a Gaussian distribution with mean $\langle X(E_r)\rangle$ and standard deviation ΔX as shown in Fig. II-7, and a lifetime t_ℓ from an exponential distribution with mean life given in Table II-3. If the nucleus stops in the grain (r>X), E_r' the energy of the recoiling

nucleus at the time it deexcites, is evaluated from

$$\int_{E_r'}^{E_r} \frac{dE}{\rho v \frac{dE}{dx}} = t_\ell \qquad (II-16)$$

where ρ is the density and v the recoil velocity; this case includes the possibility that $E_r' = 0$, i.e. the nucleus stops before it deexcites. Equation (19) is also used when $r < X$, provided that the nucleus deexcites before it reaches the grain edge, i.e. when

$$\int_{E_r^{edge}}^{E_r} \frac{dE}{\rho v \frac{dE}{dx}} > t_\ell \qquad (II-17)$$

Here E_r^{edge}, the energy of the nucleus at the edge, is obtained by solving

$$\left\langle X(E_r^{edge}) \right\rangle = \left\langle X(E_r) \right\rangle - r \qquad (II-18)$$

If condition II-17 is not satisfied, then $E_r' = E_r^{edge}$, i.e. the nucleus leaves the grain in an excited state and deexcites later in the interstellar medium where its energy remains essentially E_r^{edge}. The resultant gamma ray energy is determined by the velocity corresponding to E_r', and the angle between the velocity and the emitted photon, assumed isotropic in the nucleus' rest frame.

The effect of the grains on gamma ray line profiles and the dependence of these shapes on the characteristic grain radius are shown in Figures II-8 through II-11. These figures result from the calculations of Ramaty, Kozlovsky, and Lingenfelter (1978) for an ion spectrum with a differential kinetic energy spectral index of 3, assuming solar composition for the fast ions and the ambient gas. Figure II-8 results from the absence of grains; figures II-9, II-10, and II-11 show the effect of including spherical grains with radii distributed exponentially about characteristic radii of 0.1μ, 0.3μ and 0.5μ, respectively. The case with $a_o = 0.1\mu$ shows very minimal differences from the spectrum with no grains. However, as the characteristic radius increases, there are noticeable enhancements in the

very narrow components of the lines at 0.847 and 1.238 MeV from ^{56}Fe, at 1.369 MeV from ^{24}Mg, and at 1.779 MeV from ^{28}Si, as well as in a number of lower intensity lines. But the most dramatic and probably easiest to observe effect occurs for the 6.129 MeV line of ^{16}O. These figures show that simultaneous observations of a number of these lines with very narrow components would then yield information on the size distribution and compositions of the grains.

f) Conclusions

Using detailed cross sections for charge exchange, ionization, and excitation, we have calculated the production rate of Kα X-rays from subrelativistic iron ions. After assuming a set of abundances and energy spectra for these ions, we presented X-ray line production rates for both a given energy density and a given energy deposition rate of the energetic particles. Then, we compared these results with the rate of γ-ray production from the first excited levels of ^{12}C and ^{56}Fe. In section d, these calculations were applied to the galactic center, Cen A, and Cas A. For the galactic center, the reported observation of the 4.44 MeV line (Haymes et al. 1975) are not inconsistent with upper limits on the broad 6.8 keV line. However, this consistency with the X-ray data implies that the energy density in fast ions required to produce the observed gamma rays is several keV cm^{-3}. If we accept these results, however, recent observations from HEAO 1 imply time variability exists. In the case of Cen A, Hall et al. (1976) reported a feature at ~ 4.5 MeV with a width of ≤ 150 keV. The intensity of this feature is a factor of 40 larger than the upper limit on a narrow ^{12}C line set by the X-ray data. We note, however, that the constraints on gamma-ray line intensities imposed by upper limits on broad 6.8 keV emission do not apply to sources that are either hotter than a million degrees or opaque

to the 6.8 keV photons. Thus, the future detection either of nuclear γ-ray line emission or of a broad 6.8 keV x-ray line, or both, could give very valuable information on the existence of fast ions in the interstellar medium and on the physical conditions that lead to the production of these particles. In addition, observations of certain γ-ray lines by high resolution detectors could provide some constraints on the composition and size distributions of interstellar grains. We have shown the dependence of these profiles on the grain size distribution in Figs. II-8 through II-11.

III. CYCLOTRON FEATURES IN INTENSE MAGNETIC FIELDS

a) Introduction

Pulsars with periods in the range from tens of milliseconds to seconds are believed to be spinning neutron stars with strong magnetic fields rigidly anchored to their surfaces. These values of the rotation period are obtained from the conservation of angular momentum during the collapse of a main sequence star to a neutron star (with radius ~ 10 km). By assuming magnetic flux is frozen into the collapsing plasma, the strength of the magnetic field is estimated to be $\sim 10^{12}$G. Pulsations arise from the confinement of the radiating plasma by the magnetic field. Fields of this strength alter considerably the interactions of electrons with both radiation and ions, primarily by quantizing the allowed electron energies from motion transverse to the field. Radiative transitions between energy levels give rise to cyclotron line emission and absorption, and the Coulomb scattering process becomes highly modified because of the restricted recoil of the electron. The line processes have been treated in detail by Daugherty and Ventura, (1977 and 1978); the Compton scattering cross section for low energy photons ($\omega \ll eB/(m_e c)$) was calculated by Canuto, Lodenquai and Ruderman (1971). Resonances in the non-relativistic Coulomb electron-ion collision frequency were discovered by Ventura (1973). Current X-ray observations, however, require more refined calculations of the collisional cross sections. In this chapter, we have calculated an effective scattering cross section for line photons and the Coulomb cross section for electron-ion collisions, treating the electrons relativistically.

The motivation for the type of calculations carried out in this chapter is based on a model for a specific type of X-ray pulsar, a highly magnetized star in a binary system with a less evolved companion.

X-ray pulsars in binary systems derive their energy from the accretion of matter from the nearby companion. The matter is accelerated by the gravitational field of the neutron star, and it is believed to be channeled by the field onto a magnetic polar cap with zero pitch angle. There it releases a significant amount of its infall energy by heating the atmosphere to temperatures at which electrons begin to become relativistic; for example, the effective electron temperature of Hercules X-1, the best studied binary X-ray pulsar, is greater than 20 keV (Pravdo et al. 1977b). Evidence has been presented for an emission line feature at about 60 keV (Trümper et al. 1977 and 1978, Coe et al. 1977); the electrons involved in producing such a feature are mildly relativistic. Thus in this chapter we have considered cyclotron line production by electron-ion collisions and the cross section involved in effectively scattering the line photons in a relativistically exact treatment.

In section b, we discuss the quantization of electron orbits in strong fields, and show that under the conditions expected at the polar caps of X-ray pulsars, electrons will likely spend most of their time in the magnetic ground state, corresponding to zero pitch angle. Then, using a fully relativistic quantum electrodynamic (QED) approach, we calculate the electron-ion Coulomb cross section and the absorption cross sections and emission rates for cyclotron photons. In section c, the Coulomb cross sections are used to calculate the energy loss rate of the infalling protons. This rate, together with the rate of elastic nuclear proton-proton collisions, is then used to calculate the number of line photons an infalling proton can be expected to produce, directly or indirectly. We also calculate the thermal line production coefficient as a function of the one-dimensional temperature for a gas in which the electrons are in the ground state. In addition, we find that the infalling protons can create a flux of

super-thermal electrons streaming down the field lines toward the surface. Section d consists of an application of our results to the data from Hercules X-1. In particular, we consider the possible observation of the cyclotron emission line mentioned above and present a more likely alternative interpretation in terms of an absorption feature. Finally, in section e, we summarize our results and indicate the need for further observations with better energy resolution to distinguish between the models. In addition, we propose a more quantitive and comprehensive calculation to determine the expected radiation from the whole class of binary X-ray pulsars.

b) Physical Processes in Intense Magnetic Fields

The Dirac equation for the spinors ψ representing electrons in an external static and homogeneous magnetic field is, in units where $\hbar = c = 1$,

$$(\gamma^\mu \pi_\mu - m_e)\,\psi(x) = 0 \qquad \mu = 1 \text{ to } 4 \qquad \text{(III-1)}$$

where m_e is the electron mass, γ^μ are the Dirac matrices, and

$$\pi_\mu = i\,\frac{\partial}{\partial x^\mu} + e A_\mu(x) \qquad \text{(III-2)}$$

$$A_0 = 0 \qquad \vec{A} = \tfrac{1}{2}\,\vec{B} \times \vec{x} \qquad \text{(III-3)}$$

The eigenvalues of total energy W are given by

$$W^2 = p^2 + m_e^2\left(1 + \frac{2B}{B_q}\,j\right) \qquad j = 0, 1, 2 \ldots \qquad \text{(III-4)}$$

where p is the electron momentum parallel to the field, c is the speed of light, m_e is the mass of the electron, and in cgs units,

$$B_q = \frac{m_e^2 c^3}{e\hbar} = 4.413 \times 10^{13} \text{ gauss.} \qquad \text{(III-5)}$$

The corresponding spinors for a particular positive energy state, assuming B lies in the z-direction, are

$$\psi(x) = \frac{(\gamma^\mu \pi_\mu + m_e)}{[2L\,W(W+m_e)]^{1/2}}\, f_{j-s-\frac{1}{2},q}(\vec{x}_\perp)\, e^{-iWt + ipz}\, u_s, \quad q = 0, 1, 2 \ldots \qquad \text{(III-6)}$$

where L is the normalization length, $\vec{x}_\perp$ is the projection of the position vector into a plane perpendicular to the field, s is the spin of the electron,

and

$$u_{+\frac{1}{2}} = \begin{pmatrix} 1 \\ 0 \\ 0 \\ 0 \end{pmatrix}, \qquad u_{-\frac{1}{2}} = \begin{pmatrix} 0 \\ 1 \\ 0 \\ 0 \end{pmatrix} \qquad \text{(III-7)}$$

The quantum number j labels the angular momentum parallel to the field from the contributions of spin and orbit around the guiding center, while q gives the distance from the guiding center to the z-axis of the chosen coordinate system. The functions $f_{nq}(\vec{x}_\perp)$ are defined most conveniently by the ladder operators:

$$\pi^\pm = \frac{1}{\sqrt{2}}(\pi^x \pm i\pi^y)$$
$$X^\pm = \frac{1}{\sqrt{2}}(x \pm iy) \pm \frac{i}{eB}\pi^\pm ; \qquad \text{(III-8)}$$

then

$$\pi^\pm f_{nq}(\vec{x}_\perp) = \left[eB\left(n + \tfrac{1}{2} \pm \tfrac{1}{2}\right)\right]^{\frac{1}{2}} f_{n\pm1,q}(\vec{x}_\perp) \qquad \text{(III-9)}$$

and

$$X^\pm f_{nq}(\vec{x}_\perp) = \left[\frac{q + \frac{1}{2} \mp \frac{1}{2}}{eB}\right]^{\frac{1}{2}} f_{n,q\mp1} \qquad \text{(III-10)}$$

together with

$$f_{00}(\vec{x}_\perp) = \left(\frac{eB}{2\pi}\right)^{\frac{1}{2}} e^{-\frac{eB}{4}\vec{x}_\perp^2} \qquad \text{(III-11)}$$

define the functions completely. The π operators correspond to the canonical momentum of the electron and the X operators to the coordinates of the guiding center. There are two contributions to the transverse energy quantum number j, expressed by setting

$$j = n + s + \tfrac{1}{2}, \qquad n = 0, 1, 2\ldots, \qquad s = \pm\tfrac{1}{2} \qquad \text{(III-12)}$$

Then n refers to the Landau level, the state of the orbital motion of the electron about its guiding center, and s is the contribution of spin to the magnetic moment. Note that only s = -1/2 is permitted for the ground state.

In a magnetic field, radiation can be emitted and absorbed

accompanying transitions between transverse energy levels. Under normal astrophysical conditions, particle energies are much larger than the energy level separation, and the particles consequently have large parallel momenta and high quantum numbers. This leads to a classical approximation, and while the radiation is still quantized, the large parallel momenta Doppler shift the emitted photons into a continuous synchrotron spectrum. However, even for mildly relativistic electrons ($\gamma \leq 1.1$) in fields greater than 10^{12} gauss, the quantum nature of the radiation must be taken into account. Discrete cyclotron line emission rates and absorption cross sections have been calculated for intense fields by Daugherty and Ventura (1977 and 1978). We have repeated these calculations in the representation above, which is somewhat different from theirs. The QED matrix element for a transition is given by

$$S_{fi} = ie \int d^4x \, \overline{\psi_f(x)} \, \vec{\gamma} \cdot \vec{A}_1(x) \, \psi_i(x) \qquad \text{(III-13)}$$

where the subscripts f and i refer to final and initial states and $\vec{A}_1(x)$ is the photon vector potential, given by

$$\vec{A}_1(x) = \left(\frac{2\pi}{\omega V}\right)^{1/2} \hat{\varepsilon} \, e^{\pm i(\omega t - \vec{k}\cdot\vec{x})} \qquad \begin{cases} - \text{ for absorption} \\ + \text{ for emission} \end{cases} \qquad \text{(III-14)}$$

where ω and k are the photon frequency and wave-vector, ε is the polarization vector, and V is the normalization volume. The bar over ψ_f indicates the Pauli adjoint of the spinor, $\psi_f^{\dagger}\gamma^0$.

We have confirmed the results of Daugherty and Ventura (1977 and 1978) for the absorption cross sections and emission rates using the ladder-operator representation in cylindrical coordinates. For example, the cross section for an electron in the ground state to absorb a fundamental cyclotron photon is given here in the center of parallel momentum frame, where the

sum of the parallel momenta of the photon and electron yanishes:

$$\sigma_a(\omega,\theta) = \frac{\pi^2 e^2 c}{\omega} \frac{\delta(W_i' + \hbar\omega - W_i)\, e^{-\xi}}{W_i (W_i + m_e c^2)(W_i' + m_e c^2)} \left(m_e^2 c^4 + 2W_i' \hbar\omega \cos^2\theta + 2\hbar^2\omega^2\cos^2\theta\right)^{-1/2}$$

$$\left\{ \delta_{s_f, -\frac{1}{2}}\, 2m_e^2 c^4 \frac{B}{B_q} \left(\left[(W_i + m_e c^2)\xi + (W_i' + m_e c^2) \right]^2 \cos^2\theta\, \varepsilon_o^2 + (W_i' + m_e c^2)^2 \varepsilon_x^2 \right) \right.$$

$$\left. + \delta_{s_f, \frac{1}{2}}\, \hbar^2\omega^2 \left[(W_i' + m_e c^2 + \hbar\omega\cos^2\theta)^2 \varepsilon_o^2 + (W_i + m_e c^2)^2 \cos^2\theta\, \varepsilon_x^2 \right] \right\} \qquad (III-15)$$

where θ is the angle of propagation of the photon and ω its frequency, and

$$W_i = m_e c^2 \left(1 + \frac{2B}{B_q}\right)^{1/2} \qquad (III-16)$$

$$W_i' = \left(m_e^2 c^4 + \hbar^2\omega^2\cos^2\theta\right)^{1/2} \qquad (III-17)$$

$$\xi = \frac{\hbar^2\omega^2 \sin^2\theta}{2m_e c^2} \cdot \frac{B_q}{B} \qquad (III-18)$$

ε_o and ε_x are the polarization amplitudes in the ordinary (wave's electric field parallel to B) and extraordinary modes, respectively. As we shall now discuss, this cross section is of particular importance for intense magnetic fields, since it will determine the opacity in the line feature.

In a strong field, mildly relativistic electrons will spend most of their time in the ground state, unless the densities are very high. To see this, Figure III-1 shows the lifetime τ_1 of the first excited state as a function of field strength for electrons with no parallel velocity. This was calculated by numerically integrating over all photon transitions to the ground state, according to

$$\tau_1 = \left(\int d^3k\, R_{01}(\vec{k}) \right)^{-1} \qquad (III-19)$$

where $R_{01}(\vec{k})d^3k$ is the rate per electron of photon emission into d^3k centered about $\vec{k}$ and is calculated in the appendix. As mentioned before, there are two possible spin orientations for the excited states; the lifetime of each is shown separately in the figure. As can be seen, for low enough densities, collisional excitation times will be much longer than radiative lifetimes. We will return to this after calculating the collisional cross sections.

In a Coulomb collision, the momentum transfer prefers to occur perpendicular to the relative velocity. For energetic protons with small pitch angle colliding with an electron in the ground state of an intense field, the transfer of energy to the electronic plasma is inhibited (Basko and Sunyaev 1975). However, under energetically favorable conditions, the proton can transfer transverse momentum to the electron by excitation of the quantum levels. In addition, head-on or knock-on collisions can occur, in which the electrons are not excited, but are reflected along their field line. We have calculated the cross sections for these processes as a function of the electron energy in the proton's rest frame by a single photon exchange approximation. The matrix element is given by

$$S_{fi} = -ie \int d^4x \; \bar{\psi}_f(x) \; \gamma^c A_o^{(c)}(x) \; \psi_i(x) \qquad (III-20)$$

where $A_o^{(c)}(x)$ is the Coulomb potential due to the ion charge. After a Fourier decomposition of this potential as outlined in the appendix, we find the cross section σ_j for excitation of the jth state from the ground state in a Coulomb collision with an ion of charge Ze with zero pitch angle is given in the ion's rest frame by (in cgs units)

$$\sigma_j(p) = \frac{\pi B_q}{2B} \frac{Z^2 r_e^2}{c^2(W+m_e c^2)^2} \frac{1}{j!} \sum_{\pm} |p\, p'_{\pm}|^{-1} \left\{ \delta_{s',-\frac{1}{2}} \left[2W(W+m_e c^2) + p(p'_{\pm}-p)c^2 \right]^2 \right.$$
$$\left. + \delta_{s',\frac{1}{2}} \, 2j \, \frac{B}{B_q} \, m_e^2 c^4 p^2 c^2 \right\} \varepsilon_j\left(\frac{B_q}{2B}, \frac{(p'_{\pm}-p)^2}{m_e^2 c^2} \right), \qquad (III-21)$$

where r_e is the classical electron radius, 2.82×10^{-13} cm, p and p' are the initial and final momenta to the field respectively, of the electron, E is the electron kinetic energy, and s' is its final spin. There are two possible values of the final momentum, given by $p'_{\pm} = \pm \sqrt{p^2 - 2m_e^2 c^2 \, B/B_q \, j}$, and these are summed over in equation (3). Finally the ε_j are defined by

$$\varepsilon_j(x) = \int_x^\infty \frac{dt}{t^2} \, e^{(x-t)} (t-x)^j \qquad (III-22)$$

The first three are given here in terms of the exponential integral:

$$\mathcal{E}_0(x) = \frac{1}{x} - e^x E_1(x)$$
$$\mathcal{E}_1(x) = e^x (1+x) E_1(x) - 1 \qquad \text{(III-23)}$$
$$\mathcal{E}_2(x) = 1 + x - x(2+x) e^x E_1(x)$$

The j=o cross section refers to a knock-on collision, where the parallel momentum of the electron changes sign (in the ion's rest frame), but no transverse excitation occurs. Higher j values refer to collisions in which the electron is excited to the j level. These results are shown in Figure III-2 for 2 magnetic field strengths, 10^{12}G and 6×10^{12}G. Because of a breakdown in the approximation, the cross sections become infinite at the thresholds of excitation. However, the bandwidth of the breakdown is small, so we have arbitrarily smoothed these infinities. The approximation breaks down because p', the final momentum, becomes small, and the particles are near each other for a long enough time to exchange more than one virtual photon. These infinities are the resonances discovered by Ventura (1973). As in the non-magnetized case, bound states are even possible.

From Figure III-2, we see that above its threshold, the excitation to $j = 1$ dominates all others, and $\sigma_1(p)$ is roughly inversely proportional to B. Thus we can compare the lifetime of the first excited state from Figure III-1 to the collision time using Figure III-2 to find the density at which electrons may be in an excited state for a significant time. Explicity the critical density n_{ex} is

$$n_{ex} = (\sigma_1 v \tau_1)^{-1} \simeq 5\times10^{25} \text{ cm}^{-3} \text{ for } B=10^{12}\text{G}, v=10^{10}\text{cm s}^{-1}, \qquad \text{(III-24)}$$

and n_{ex} increases for increasing B roughly as B^3. The X-ray emitting regions in binary pulsars are expected to be much less dense than n_{ex} for $B \geq 10^{12}$G.

Under conditions where the electrons occupy the ground state, the opacity in the cyclotron line is determined from the cross section given

in equation III-15. Since this cross section is much larger than that for Compton scattering, the possibility arises of a source region optically thick to line photons but not to the surrounding continuum. Since Compton scattering is the most important factor in radiative transfer outside the line process, a line feature will appear in this case. The width of the line can be roughly determined by finding the photon frequency and angle ranges where the optical depth exceeds unity. The optical depth is given by

$$\tau_B(\omega,\theta) = n_e \int d\ell \int dp\ f_e(p)\ \sigma_a(\omega^*,\theta^*) \qquad (III-25)$$

where $d\ell$ is the line of sight increment, $f_e(p)$ is the electron parallel momentum distribution function, and σ_a is given by equation III-15. The asterisk denotes the center of parallel momentum frame. If we assume that the electron spectrum is uniform throughout the source, the δ-function in equation III-15 allows us to evaluate the momentum integral to obtain

$$\tau_B(\omega,\theta) = N_e \sum_{\pm} f_e(p_\pm)\ S(\omega^*,\theta^*)\ \frac{W_1}{\omega}\ \frac{W_\pm}{|W_\pm \cos\theta - p_\pm|} \qquad (III-26)$$

where N_e is the column density of electrons in the source, $p_\pm$ and $W_\pm$ are the momenta and total energy which satisfy the line resonance condition, given below, and $S(\omega^*, \theta^*)$ is the right hand side of equation III-15 without the δ-function. $W_\pm$ and $p_\pm$ are solved for from

$$W_\pm - p_\pm \cos\theta = \frac{1}{2\omega}\left(2m_e^2 \frac{B}{B_q} - \omega^2 \sin^2\theta\right) \qquad (III-27)$$

which yields:

$$p_\pm = \frac{1}{\sin^2\theta}\left[RHS \cos\theta \pm \left(RHS^2 - m_e^2 \sin^2\theta\right)^{1/2}\right] \qquad (III-28)$$

where RHS is the right hand side of equation III-27. We note an important feature: there exists an angular dependent upper bound $\omega_{max}(\theta)$ on the line energy where the quantity under the square root in equation III-28 becomes negative. This limit is given by

$$\omega_{max}^2(\theta) \sin^2\theta = 2m_e^2\left[1 + \frac{B}{B_q} - \left(1 + \frac{2B}{B_q}\right)^{1/2}\right] \qquad (III-29)$$

To undertake a study of the radiative transfer of the line photons, we note that for $n \ll n_{ex}$, an electron which is excited by absorbing a line photon will deexcite radiatively before anything can happen to change its momentum. Thus, the process is effectively a scattering of the line photon. The scattering cross section is the product of the absorption cross section and the probability of emission into a given final angle, or in cgs units,

$$\frac{d\sigma(\omega,\theta)}{d(\cos\theta')} = \frac{\pi^2 e^4}{4\hbar}\frac{\omega'}{\omega}\;\frac{\delta(W_i+\hbar\omega-W_1)\,e^{-(s+s')}\,(m_e^2c^4+2W_i\hbar\omega\cos^2\theta)^{-1/2}}{W_1^2\,(W_i+m_ec^2)^2\,(W_1+m_ec^2-\hbar\omega)^2\,(W_1+m_ec^2-\hbar\omega')^2\,(W_1-\hbar\omega'\sin^2\theta')}$$

$$\left\{\left(\frac{2B}{B_q}\right)^2 m_e^2c^4\,\tau_1(s=\tfrac{1}{2})\left[\left((W_1+m_ec^2)s+(W_1+m_ec^2-\hbar\omega)\right)^2\cos^2\theta\,\mathcal{E}_o^2+(W_1+m_ec^2-\hbar\omega)^2\,\mathcal{E}_x^2\right]\right.$$

$$\cdot\left[\left((W_1+m_ec^2)s'+(W_1+m_ec^2-\hbar\omega')\right)^2\cos^2\theta'\,\mathcal{E}_o'^2+(W_1+m_ec^2-\hbar\omega')^2\,\mathcal{E}_x'^2\right]+$$

$$\hbar^4\omega^2\omega'^2\,\tau_1(s=\tfrac{1}{2})\left[(W_1+m_ec^2-\hbar\omega\sin^2\theta)^2\,\mathcal{E}_o^2+(W_1+m_ec^2)^2\cos^2\theta\,\mathcal{E}_x^2\right]$$

$$\left.\cdot\left[(W_1+m_ec^2-\hbar\omega'\sin^2\theta')^2\,\mathcal{E}_o'^2+(W_1+m_ec^2)^2\sin^2\theta'\,\mathcal{E}_x'^2\right]\right\}, \qquad \text{(III-30)}$$

where everything is as defined for equation III-15, and the primes indicate the emitted photon. The τ_1's are shown in Figure III-1. We note the symmetry between final and initial photons. The emitted photon has the energy

$$\hbar\omega' = \frac{1}{\sin^2\theta'}\left[W_1 - m_ec^2\left(1+\frac{2B}{B_q}\cos^2\theta'\right)^{1/2}\right]. \qquad \text{(III-31)}$$

Solving the expression in the argument of the δ-function in (III-30) for ω gives the same equation with the primes removed.

c) Line Production by Collisional Excitation

Using the results of the previous section for the Coulomb cross sections σ_j in an intense magnetic field, we have calculated the energy loss rate per unit matter traversed for a proton with zero pitch angle by Coulomb processes:

$$\frac{dE}{dX} = \frac{1}{m_p v}\sum_{j=0}^{\infty}\int_{-\infty}^{\infty} dp\; f_e(p)\; v_{rel}(E,p)\,\sigma_j(E,p)\,\Delta E_j(E,p), \qquad \text{(III-32)}$$

where m_p is the proton mass, v is the proton velocity, p is the electron parallel momentum, f_e is the electron distribution function in p, v_{rel} is the relative velocity between the particles in an encounter, and ΔE_j is the energy lost in the collision. We assume a relativistic one dimensional thermal distribution of electrons, so that $f_e(p)$ is given by

$$f_e(p) = \left[2m_e K_1\left(\frac{m_e}{T}\right)\right]^{-1} \exp\left[-(p^2+m_e^2)^{1/2}/T\right] \qquad (III-33)$$

where $K_1(x)$ is the modified Bessel function (Abramowitz and Stegun 1965) and and T is the temperature in units of energy. The results are shown in Figure III-3 for four temperatures and a field strength of 6×10^{12}G. For comparison the energy loss rate in a non-magnetized gas of temperature 35 keV is shown by the dashed line (Book and Ali 1975) and in a field of 10^{12}G with temperature 15 keV by the dash-dotted line. For T = 0, there is a sharp discontinuity at the threshold for excitation, but this disappears when the electrons take on a thermal distribution, and for the higher field strength at T = 35 keV, dE/dx is relatively constant in energy.

Figure III-4 shows the Coulomb mean ranges for the temperatures discussed above and a field strength of 6×10^{12}G. As Basko and Sunyaev (1975) pointed out, for high enough energies elastic proton-proton nuclear scattering has a mean free path smaller than the Coulomb range ($X_{p-p,elas} \sim 50$ gm/cm^2). In an elastic scattering, the proton is deflected from zero pitch angle, and then the energy can be given up rapidly to ambient electrons, via the excitation of plasma waves parallel to the field, for example. Thus, the equation for the energetic zero pitch angle proton distribution function in a steady state atmosphere can be written

$$\frac{\partial \Phi}{\partial X} - \frac{\partial}{\partial E}\left(\Phi \frac{dE}{dX}\right) = -\frac{\sigma_{pp}(E)}{m_p}\Phi(E,X) \qquad (III-34)$$

where E is the proton energy, X the amount of matter traversed (in gm/cm^2 for example), Φ is the differential (in energy) flux of protons, and σ_{pp} is the

cross section for a nuclear collision with an ambient proton, taken from the compilation of Barashenkov and Maltsev (1961). The solution to this equation with the boundary condition that injection occurs at the top of the atmosphere, (X=0) with flux $\varphi_0 \delta(E-E_0)$ is

$$\Phi(E,X) = \frac{\varphi_0}{\frac{dE}{dx}} \exp\left[-\int_E^{E_0} \frac{dE' \sigma_{pp}(E')}{m_p \frac{dE'}{dx}}\right] \cdot \delta\left(X - \int_E^{E_0} \frac{dE'}{\frac{dE'}{dx}}\right) \qquad \text{(III-35)}$$

To evaluate the line productivity of the protons in a one dimensional thermal gas, we have integrated the flux given by equation (III-35) with the cross sections for knock-on and excitation collisions. The production rates at a depth X of electrons in quantum level j with momentum p in dp is given by

$$q_j(p,X) = n_e \int dp' f_e(p') \int_0^{E_0} dE\, \Phi(E,X) \frac{v_{rel}(p',E)}{v(E)} \sigma_j(p'^*) \delta(p - p_\pm(p',E)) \qquad \text{(III-36)}$$

where n_e is the electron number density $\Phi(E,X)$ is the proton flux given by equation III-35, $v_{rel}(E,p')$ is the relative velocity between the particles; $v(E)$ is the velocity of the ion, p'^* is the incident momentum in the ion rest frame, and the momentum in the delta function is obtained from the conservation equations:

$$\begin{aligned} p'^* &= \gamma(p' + \beta W'), \qquad W'^* = \gamma(W' + \beta p') \\ p_\pm^* &= \pm (p'^{*2} - 2eBj)^{1/2}, \qquad W^* = W'^* \\ p_\pm &= \gamma(p_\pm^* - \beta W^*) \\ \gamma &= 1. + \frac{E}{m_p}, \qquad \beta = \left(1 - \frac{1}{\gamma^2}\right)^{1/2} \end{aligned} \qquad \text{(III-37)}$$

where the *'s refer to the ion's rest frame. The total column density production rate is found by integrating along dz, the path of the infalling ions:

$$\dot{N}_{e,j}(p) = \int dz\, q_j(p,X) = \frac{1}{\rho} \int_0^\infty dX\, q_j(p,X) \qquad \text{(III-38)}$$

The resulting expression for this quantity, after taking the delta functions into account, is

$$\dot{N}_{e,j}(p) = \frac{n_e}{\rho} \varphi_0 \int_0^{E_0} dE \sum_\pm f_e(p_\pm') \left|\frac{\partial p}{\partial p'}\right|^{-1}_{p_\pm'} \sigma_j(p_\pm'^*) \frac{v_{rel}(p_\pm', E)}{v(E)} \exp\left(-\int_E^{E_0} \frac{\sigma_{pp}(E')\, dE'}{m_p \frac{dE'}{dx}}\right) \qquad \text{(III-39)}$$

The excitation of an electron to the jth level was assumed to yield j line photons since the electrons tend to deexcite in single step transitions (Canuto 1977, Daugherty and Ventura 1977). A knock-on (j=0) was assumed to produce as many line photons as was energically possible, by Coulomb collisions with ambient ions. It is important to note that here we neglect energy losses of the knock-ons to continuum photons by resonant absorption (Pravdo et al. 1978) which results in the conversion of these photons to line photons; this process is discussed below. The results for the multiplicity of line photons produced under these assumptions are shown for the four temperatures with $B = 6 \times 10^{12}$ G in Figure III-5a, and Figure III-5b shows the fraction of the proton's energy put into line photons as a function of the injection energy. For Figure III-5b, we assume a line photon has an average energy equal to the energy of the 1st excited state with $p = 0$.

In order to investigate the production of cyclotron line photons by the high energy tail of a one dimensional thermal electron distribution in collisions with ambient protons, we have integrated the cross section for the excitation of the first excited state with such a distribution function. The resulting line production rate per unit gas density squared, α_1, is given by

$$\alpha_1(T) = \int dp \; f_e(p) \, \sigma_1(p) \, v(p). \qquad \text{(III-40)}$$

The results for temperatures of 1 to 100 keV are shown in Figure III-6, for field values of 10^{12} and 6×10^{12} Gauss. As can be seen, the line production coefficient α_1 rises quite rapidly as kT approaches $eB/(m_e c)$ and flattens somewhat at higher temperatures.

As noted above, these results apply to line production by electron-ion collisions alone. However, a photon with energy below the

cyclotron energy can collide with a fast ($\beta \sim 0.6$ to 0.8) knock-on electron and be absorbed as a cyclotron photon because of the Doppler shift. When the electron deexcites, the photon tends to be emitted preferentially into the electron's forward hemisphere, or downward toward the star's surface. The importance of this effect may be twofold: reemission at angles around 90° leads to an increase in line photons, and the absorption results in a depletion of the continuum below the line energy, which could make a line appear more intense relative to continuum radiation. It is difficult to be quantitative about this effect because although the production rate of knock-on can now be calculated, their momentum spectrum depends also on the energy loss rate to the radiation, the spectrum of which is unknown. It is, however, interesting to note that if the field strength is as high as implied by the data of Trümper et al (1977 and 1978), $\sim 6 \times 10^{12}$ gauss, then the knock-on process is the dominant one for producing line photons under the previous assumptions (neglect of radiation). So if now we assume that the knock-ons lose all their energy by converting $\sim$ 30 keV photons to $\sim$ 60 keV photons instead of losing 60 keV per photon produced, then the multiplicity is only increased by at most a factor of 2. The knock-on production rates are strongly dependent on the field strength because of the threshold effect; at lower field values, relatively more direct excitations than knock-ons occur.

d) Application to Hercules X-1

The results of the calculations in the preceding section of the fractional energy lost by infalling protons to line photons may be compared with recent possible observations of a line feature in the spectrum of Hercules X-1 at around 60 keV (Trümper et al. 1977 and 1978, Coe et al. 1977). Assuming that the line is directly produced by the infalling ions and the rest of the ions' energy goes into continuum radiation, the calculations

leading to Figure III-5 will apply if radiative transfer in the source or outside does not convert continuum photons into line photons or vice versa. There are two observed components of continuum radiation, hard (2 to 20 keV) and soft (.1 to 1 keV) X-rays, with roughly comparable luminosities of 1 to 2×10^{37} ergs s^{-1} (Giacconi et al. 1973, Schulman et al. 1975, Catura and Acton 1975), while the observed line luminosity is $\sim 2\times10^{35}$ ergs s^{-1}. The infalling protons are generally assumed to power both continuum components, so at most, only 1/2 to 1 percent of the energy comes out in the line. Since the effective hard X-ray temperature is $\geq$ 20 keV (Pravdo et al. 1977b), we see from Figure III-5b that this fraction is consistent with infall proton energies of 140 MeV to 180 MeV. However, we still must investigate the effect of radiative transfer, in the source and outside.

To ascertain whether radiative transfer is important, we need to estimate the electron density in the source. From Figure III-4, we see that the range of accreting matter is at least of order 10 gm cm^{-2}, corresponding to $\sim 6\times10^{24}$ $e^- cm^{-2}$. The reported width of the line feature is 12 keV (FWHM), and this places an upper limit on the linear dimension of the source parallel to the field, since the line energy varies as field strength. The upper limit is obtained from assuming $B \propto R^{-3}$ as for a dipole field:

$$L \lesssim \frac{1}{3} R \frac{\Delta B}{B} \simeq \frac{1}{3} R \frac{\Delta\omega}{\omega} = 7\times10^{4}\,cm \cdot \left(\frac{R}{10\,km.}\right) \qquad \text{(III-41)}$$

where R is the neutron star radius. Thus the lower limit on the average electron density in the source is given by

$$n_e \simeq \frac{N_e}{L} \gtrsim 10^{20}\,cm^{-3} \left(\frac{R}{10\,km}\right)^{-1} \qquad \text{(III-42)}$$

From equations III-25 and III-15, then, we estimate the opacity to be

$$\tau_B \sim \frac{\pi^2 e^2 \hbar c}{(2\pi m_e c^2 T)^{1/2} m_e c^2} n_e \Delta L \simeq \frac{\Delta L}{50\,cm} \cdot \left(\frac{R}{10km}\right)^{-1} \left(\frac{T}{35\,keV}\right)^{-1/2} \qquad \text{(III-43)}$$

This implies that if the line of sight covers 50cm or more of the source, radiative transfer will be important.

The preceding considerations apply if the infalling protons directly excite the line. If, however, the protons simply thermalize without yielding appreciable line emission, the problem becomes that of calculating a thermal production coefficient. Applying the results of such a calculation shown in Fig. III-6 to the observation of Trumper et al. (1977 and 1978), we obtain the product of the density squared and the volume V of the source region

$$n^2 V = 2 \times 10^{56} \ cm^{-3} \qquad (III-44)$$

for a temperature of 35 keV and field strength of 6×10^{12}G. As before, we can set an upper limit on the volume, and thus a lower limit on the density, by assuming that the transverse area occupied by the accreting matter is at most $\pi \cdot (0.1R)^2$, or

$$A \lesssim 3 \times 10^{10} cm^2 \left(\frac{R}{10 km} \right)^2 \qquad (III-45)$$

This limit, together with that expressed by III-38, implies

$$n \gtrsim 3 \times 10^{20} cm^{-3} \left(\frac{R}{10 km} \right)^{-3} \qquad (III-46)$$

implying that transfer is important in this case, also. Therefore, an optically thin treatment of this radiation, as in Daugherty and Ventura (1977) is not likely to relate directly to observations.

We have considered the problem of line transfer in a rudimentary way, by calculating the opacity at a given angle and frequency for a thermal gas of electrons. The motivation for this is the following: where the opacity is large, photons are trapped in the source and must diffuse out, and at the surface, the intensity radiating outward approaches approximately its blackbody value. Therefore, where $\tau(\omega,\theta) \gtrsim 1$, we assume the line rises out of the continuum. The upper limit to the width of the line reported by Trumper et al. (1977 and 1978) is 12 keV; as mentioned above, the field

implied is $\sim 6 \times 10^{12}$G, and in addition, they show evidence that this feature is produced in a gas with temperature $\sim$ 35 keV. So for these conditions and four values of electron column density, we have estimated the width of a cyclotron line feature for several viewing angles and column densities by finding the frequencies where $\tau = 1$. Since Doppler shifting by the motion of the electrons is responsible for most of the smearing of the opacity, we expect the line to be narrowest at 90° to the field lines (and electron motion) and to broaden as the angle departs from this. Another factor which is important is the maximum frequency allowed, given by equation III-29, especially near 90°, where it is responsible for the high energy drop in line opacity.

The results for the line width are shown in Table III-1, for viewing angles from 10° to 90°, and electron column densities 10^{22}, 10^{23}, 10^{24}, and 10^{25} cm^{-2}. As can be seen, for an electron temperature of 35 keV, this calculation cannot reproduce the width of the observed feature. The column density can't be much lower than $10^{22} cm^{-2}$ because of the estimates of lower limits on the density expressed in equations III-39 and III-43. Thus to be consistent with the observation, we are forced to assume a lower electron temperature. As mentioned before, lower energy measurements have placed the temperature greater than 20 keV; so we have shown the line width results for this value also. Here we find that the reported width can be reproduced if the viewing angle is restricted to be very close to 90° and if the column density is the very minimum allowed. We note that the same conclusion about the viewing angle has been arrived at classically (Meszaros 1978). We also point out that the line of sight through the 20 keV source must be less than 100 cm, at most.

There is an additional problem with the interpretation of the observation as a cyclotron line feature because of its pulse phase dependence.

The 1.24 second pulse period shows about a factor of 4 increase in 2 to 20 keV X-rays over about 30% of its phase (Pravdo 1976). Because of the sudden rise and fall of the intensity pulse, the most likely explanation is occultation by a corotating cloud of gas which is presumably responsible for the soft X-ray flux mentioned above. The luminosity and temperature of this soft source imply that it has linear extent of around 10^8cm, which places it well above the surface of the star. A likely candidate is a corotating Alfvén shell, plasma concentrated in the region where the magnetic field begins to dominate the inflow (McCray and Lamb 1976, Basko and Sunyaev 1976). The observations of Trumper et al. (1977 and 1978) together with the analysis of Kendziorra et al (1978) imply that the line is pulsed in phase with the 2 to 20 keV X-rays. Since we have shown that observation of the line at angles smaller than $\sim 85°$ will contribute significant broadening (see Table III-1), this implies that the pulse is a very narrow fan beam. If this were the case, then the Alfven shell would have to suddenly thin at an angle close to 90° to the polar field lines, the opposite of what has been proposed (McCray and Lamb 1976, Basko and Sunyaev 1976). Thus we conclude that this interpretation is unlikely.

A more likely interpretation of the "feature" at 60 keV which is still consistent with the data is that it is simply residual continuum radiation with an accompanying absorption dip at lower energies. The absorption would be due to the magnetic field, but the assignment of a field strength may not be straightforward because of Doppler shifts. No such shift would result if the absorbing electrons were cold, but because of the high field strength required, they must be located in or near the source; consequently, they are bathed in X-rays and should approach an equilibrium temperature. In this case, they become part of the blackbody, and no

absorption will appear. The knock-ons discussed in the preceding section are a possible solution to this problem. These electrons stream down the field lines with $\beta \sim 0.6$ to 0.8, and can consequently absorb upward moving photons below the cyclotron frequency to as low as 20 keV. Since they are mildly relativistic, they preferentially reemit a line photon in their forward direction, i.e. downward. If the column density of knock-ons is such that the absorption depth doesn't exceed unity, then re-emission into the backward hemisphere will be not important. Consequently, a depletion of photons below the cyclotron frequency results, appearing as an absorption dip, but the field strength is not readily obtainable until the electron spectrum is known.

This picture predicts a certain behavior of the absorption feature with pulse phase. In particular, as the line of sight comes closer to the polar field lines, the energy at which absorption begins should become lower, and the variation in energy should become smoother. In a recent paper (Pravdo et al. 1978), we assumed an arbitrary high energy electron distribution, and directly compared data from the cosmic X-ray experiment on OSO-8 with these predictions. As discussed there, the fit was acceptable over the region of the spectral pulse, and the best fit angles generally performed $\sim 20°$ excursion in a region around 40°. As opposed to the line emission interpretation, however, here the spectral pulse (which may only be loosely correlated with the intensity pulse probably formed by the Alfvén shell) defines a pencil beam (or cone). The best fit field strength was coincidentally consistent with the emission measurements, $\sim 6 \times 10^{12}$G. However, the cyclotron photon energies here are too broad to form a well-defined line feature.

e) Summary and Discussion

The strong magnetic fields ($\geq 10^{12}$G) believed to exist at the

surfaces of neutron stars can strongly modify the interactions of electrons with ions and radiation. We have considered the effects of such modifications on the X-ray spectra of the pulsars in binary systems which derive their luminosity from an accretion from their companions. The effect of the intense field is to quantize the allowed electron momenta transverse to the field lines. Radiative transitions between levels give rise to cyclotron emission and absorption, and since transverse momentum transfer from an ion to an electron must occur in discrete quanta, the Coulomb cross section becomes a knock-on cross section and a series of excitation cross sections. We have shown that electrons in the polar caps should almost always be found in their ground state and have then calculated the cross sections for these processes treating the electrons relativistically.

Since Hercules X-1 is the best studied of these binary X-ray pulsars and shows a possible line feature, we have used the above cross sections in an attempt to understand the physical conditions in the polar cap of this source. Data from 2 to $\sim$ 20 keV imply that the effective electron temperature in the source is greater than 20 keV. To produce the observed line feature with such a narrow width, we find that the temperature cannot be higher than 20 keV, the angle between our line of sight and the polar cap field lines must lie within 10° of 90° during the entire high intensity part of the pulse, and the linear extent of the source along the line of sight must be less than 100cm. Since these requirements are quite stringent, we have attempted an alternate explanation of the data. Due to the limited resolution of scintillation detectors, the observation could not distinguish between an emission line and an absorption dip at lower energies, although the authors preferred to stress the former interpretation. The absorption dip could be more likely, however, because of the ability of the ions to produce a high

parallel momentum population of knock-ons, which would absorb upward moving continuum photons and reemit them preferentially downward. This interpretation has the added feature that it provides an acceptable fit to the observed steepening at $\sim$ 20 keV.

An observation of this source with high resolution detectors would discriminate between these possibilities. We note that some clarification should be forthcoming from a recent point at Her X-1 by the HEAO-1 A2 experiment. In addition, there are several other objects in this category and presumably we are seeing them at different ranges of viewing angles. High resolution spectroscopy of many of them can probably be used to gain a comprehensive understanding of the physical processes occurring in the strong magnetic fields of these objects.

IV. THE ANNIHILATION OF GALACTIC POSITRONS

a) Introduction

Since positrons from outside the heliosphere have been observed at energies from about 200 MeV to 10 GeV, and a gamma ray line at 0.51 MeV has been observed from the galactic center direction, it is reasonable to expect that there may be a significant number of positrons annihilating in the galaxy. The primary sources of these positrons are the decay of π^+ mesons, β^+ decay of radioactive nuclei and perhaps the strong electric and magnetic fields of pulsars. The π^+ mesons are created in energetic particle collisions; the threshold in a proton-proton collision is $\sim$ 290 MeV if one proton is at rest. Most of the time, this meson decays into a μ^+ and its neutrino; the μ^+ then decays into a positron. Positrons produced in this way by galactic cosmic rays probably account for a significant fraction, if not all, of those observed at earth. The radioactive nuclei which decay by positron emission can be formed in nuclear reactions involving protons and alpha particles on C, N, and O, as tabulated by Ramaty, Kozlovsky, and Lingenfelter (1975). These reactions are expected to occur in regions with large fluxes of low energy cosmic rays, which may be concentrated around supernova remnants. Also, heavier β^+ decay nuclei with long lifetimes can be formed in the explosive nucleosynthesis associated with supernovae and novae. In either case, supernova remnants are a likely site of positron concentrations. The two production modes can possibly be distinguished, since low energy cosmic rays produce a strong 4.443 MeV line, while explosive nucleosynthesis produces ^{26}Al in supernovae and ^{22}Na in novae. The ^{26}Al decays to ^{26}Mg and the ^{22}Na to ^{22}Ne excited states, and they deexcite by emitting gamma rays at 1.809 and 1.275 MeV, respectively. If any of these lines were observed accompanying the 0.511 MeV line, the production mode of

the positrons could probably be determined. Finally, pulsars have been suggested as a positron source (Sturrock 1971). In their intense magnetic fields, gamma rays of energy greater than 1.022 MeV will quickly produce e^+-e^- pairs, and if a strong electric field is present, the positrons can be accelerated away from the pulsar before annihilating. All these sources produce relativistic positrons.

Leventhal, McCallum and Stang (1978a, b) have recently reported observation of positron annihilation radiation from the Galactic Center using a balloon borne germanium detector. The observed line is at 510.7 $\pm$0.5 keV, and its full width at half maximum (FWHM) is less than 3.2 keV. The total flux in the line was $(1.22 \pm 0.22) \times 10^{-3}$ photons $cm^{-2} s^{-1}$. There is also some evidence for the three-photon continuum from triplet positronium annihilation. The 0.511 MeV line was previously seen from the solar flares of 1972, August 4 and 7 (Chupp, Forrest and Suri 1975), but because the lower energy resolution of the NaI detector used, only an upper limit of about 40 keV could be set on the line width from this observation.

Depending on the temperature and density of the ambient medium, positrons and electrons can either annihilate directly or form positronium. The importance of positronium formation in the interstellar medium was pointed out by Steigman (1968), by Stecker (1969), and by Leventhal (1973), and positron annihilation in solar flares, both direct and via positronium, has been treated by Crannell et al. (1976). Positronium can form either in the singlet state which annihilates into two 0.511 MeV photons, or in the triplet state which decays by 3 photon annihilation.

Positronium is formed by both radiative recombination with free electrons and charge exchange with neutral hydrogen (atomic or molecular). Charge exchange with heavier ions is much less important than these processes (Crannell et al. 1976). Once formed in a particular spin state, positronium

in the interstellar medium annihilates from the same state, because the lifetimes of both singlet and triplet positronium (10^{-10} sec, and 10^{-7} sec, respectively) are much shorter than typical collision times with interstellar gas.

Except for ultrarelativistic positrons, the probability for annihilation in flight is negligible until the positrons slow down to energies of the order of several hundred eV. (Ultrarelativistic positrons have a small probability $\sim 10\%$, for annihilating in flight, but these annihilations produce only a broad continuum which in general cannot be observed above other continua.) The purpose of the present paper is to investigate the annihilation process at energies below a few hundred eV. At these energies positrons either form positronium in flight or thermalize. The importance of free electrons in thermalizing positrons was first pointed out by Crannell et al. (1976).

In Section b we discuss the energy loss processes of positrons in a partially ionized medium, and the charge exchange cross section with neutral hydrogen; in Section c we calculate, using a Monte Carlo simulation, the probability of positronium formation in flight in a partially ionized gas as a function of temperature, density and degree of ionization; in Section d we present the rates of direct annihilation and positronium formation of thermal positrons as a function of the temperature; in Section e we calculate line shapes resulting from positronium formation in flight and after thermalization; in Section f we discuss the implications of the observed line width on the site of positron annihilation in the Galaxy and the consistency of the flux in the line with various positron production modes; and we summarize our results in Section g.

b) Energy Losses and Charge Exchange of Positrons

When a positron is injected into a partially ionized medium, it loses energy to the ionized component by exciting plasma waves and to the neutral component by the excitation and ionization of hydrogen atoms and molecules. The energy loss rate in the plasma, measured in eV/cm, is given by (Book and Ali 1975)

$$\frac{dE}{dl} = 1.3 \times 10^{-13}\, n_e \left[M\left(\frac{E}{kT}\right) - M'\left(\frac{E}{kT}\right) \right] \frac{\ln \Lambda}{E} \qquad (IV-1)$$

where E is the positron energy in eV, n_e is the electron density in cm^{-3}, T is the temperature of the electrons in the plasma,

$$M\left(\frac{E}{kT}\right) = \frac{2}{\sqrt{\pi}} \int_0^{\frac{E}{kT}} dx\, x^{1/2} e^{-x} \qquad (IV-2)$$

$$\Lambda = \left(\frac{kT}{4\pi n_e e^2}\right)^{1/2} \cdot \left[\max\left(\frac{2e^2}{m_e u^2}, \frac{\hbar}{m_e u} \right) \right]^{-1} \qquad (IV-3)$$

$$u = \left(\frac{2E}{m_e}\right)^{1/2} - \left(\frac{8\,kT}{\pi m_e}\right)^{1/2} \qquad (IV-4)$$

and M' is the derivative of M with respect to its argument.

Unlike the energy loss process in a plasma, which is essentially continuous, in a neutral medium the positron loses a significant fraction of its energy whenever it excites or ionizes an atom or molecule. The cross sections for ionizing atomic hydrogen and exciting its 2p level from the ground state by electrons are shown by solid lines in Figure IV-1 (Kieffer 1969). The cross sections for exciting other levels are small in comparison to that for the 2p level (Kieffer 1969, Moiseiwitsch and Smith 1978), and are not expected to contribute significantly to the energy loss. We assume that the cross sections of these processes for positrons are the same as for electrons. Also shown by a solid line in Figure IV-1 is the cross section for positronium formation by charge exchange with atomic hydrogen. This cross section was calculated by Drachman, Omidvar and McGuire (1978) for positronium formation in the ground state. The inclusion of the excited states may increase this cross section.

The dashed line in Figure IV-1 are positron cross sections in molecular hydrogen. The total cross section is from laboratory measurements made by Kauppila et al. (1977). (Similar measurements by Coleman, Griffith, and Heyland (1974) give somewhat lower values). The ionization cross-section is from the compilation of Keiffer and Dunn (1966) for electrons in molecular H. For the charge exchange cross section above 50 eV, we use the calculation of Sural and Mukherjee (1970). This cross section would also be significantly larger if the excited states make an important contribution. Below the ionization and excitation thresholds we have estimated the charge exchange cross section by subtracting from the total the positron elastic scattering cross section of Hara (1974). We then connected the low energy values with those above 50 eV as shown in Figure IV-1. We assume that above the excitation threshold, the difference between the total cross section and the sum of those of ionization and charge exchange is the excitation and dissociation cross section of molecular hydrogen by positrons. We wish to note that except for the total, the cross sections in molecular H are quite uncertain and we call for further studies to determine their values.

In atomic hydrogen, the energy lost in an excitation collision is 10.2 eV. For ionization, the mean energy of the ejected electron is 1/4 of its binding energy, and the distribution of the ejected electron velocities can be approximated by a Gaussian with standard deviation $0.382\ \alpha c$ ($\alpha = 1/137$) (Omidvar 1965). In molecular hydrogen we assume an energy loss of 12 eV in an excitation and dissociation collision (Herzberg 1950) and we take the same distribution of the ejected electrons as in atomic hydrogen except for the different binding energy.

c) Positronium Formation in Flight

We consider a positron of energy E_o injected into a partially ionized hydrogen gas of temperature T and ionization fraction $X = n_e/(n_e+n_H)$,

where n_e and n_H are the electron and neutral hydrogen densities. If the temperature of the ambient medium is of order 10^5K or larger, the positrons will thermalize before forming positronium. If, however, the temperature is lower, then some fraction of the positrons form positronium in flight by charge exchange with neutral hydrogen. To evaluate this fraction, we have performed a Monte Carlo simulation in atomic hydrogen with ionization fraction X and $T < 10^5$K. Slowing down of positrons in molecular hydrogen is treated separately below.

We then allow the positron to lose energy continuously to the ionized component until it makes an inelastic collision with a hydrogen atom. The energy, E_1, at which this collision takes place is determined from

$$R = \exp\left[- \int_{E_1}^{E_0} \frac{\bar{n}_H \sigma \, dE}{\frac{dE}{d\ell}} \right] \qquad (IV-5)$$

where R is a uniformly distributed random number, $dE/d\ell$ is given by equations (IV-1) through (IV-4), and σ is the sum of the ionization, excitation and charge exchange cross sections in atomic hydrogen shown in Figure IV-1. The probability that any one of these processes occurs at E_1 is proportional to its cross section at this energy. If positronium is formed, we remove the positron from the calculation because positronium in both the singlet and triplet states is expected to annihilate in a time much shorter than its collision time in the interstellar medium. In an excitation or ionization collision on the other hand, the positron loses energy as discussed in Section b. After an excitation or ionization we repeat the process specified by equation (IV-5) with a new value for E_o given by the difference between E_1 and the energy lost in the collision, and we continue this procedure until either positronium is formed or the energy falls below the positronium formation threshold.

The fraction of positrons which form positronium in flight before thermalizing, f_{ps}, is shown in Figure IV-2 as a function of X for two cases: $n_e = 0.1 cm^{-3}$, T = 8000K and $n_e = 5 \times 10^{13} cm^{-3}$, $T = 1.16 \times 10^4 K$. The parameters of the first case could be representative of the warm component of the interstellar medium (McKee and Ostriker 1977), while those of the second case are essentially the same as the values considered by Crannell et al. (1976) for solar flares. The fraction of positrons forming positronium in flight increases with decreasing ionization fraction; for the interstellar case and $X < 0.05$ more than half the positrons form positronium before they thermalize. If $n_e = 0$, about 95% of the positrons form positronium in flight. We also see that f_{ps} increases with increasing electron density because of the reduction of the energy loss rate to the plasma due to the reduction of the Coulomb logarithm, whose argument is given in equation (IV-3). We have calculated f_{ps} for temperatures other than shown in Figure IV-2, and we find that it varies by less than 20% for $T < 6 \times 10^4 K$. For higher temperatures, f_{ps} is expected to be small in any case because of the absence of neutral hydrogen.

We have compared the results of Figure 2 with the calculations of Crannell et al. (1976) and we find that for X = 0.5, our f_{ps} is smaller by about a factor of 2 than theirs (see Figure 4 in Crannell et al. 1976). This results from an erroneous factor of 2 in the Fokker-Planck equation that was used by them to treat the slowing down of positrons in a partially ionized plasma (G. Joyce, private communication 1978). For X = 0.09, the discrepancy is much smaller because in this case, energy loss to the plasma is less important relative to charge exchange. We wish to note that for low values of X, the effect of the neutrals on the energy loss becomes important; for example, for X = 0.09, neglecting the neutrals would increase

f_{ps} by about 20%.

We do not expect molecular hydrogen in a phase of the interstellar medium with high temperatures and high ionization fraction. For molecular hydrogen, therefore, we only evaluate f_{ps} for $n_e = 0$. Using the same Monte Carlo simulation as for atomic hydrogen and the cross sections of Figure IV-1, we obtain $f_{ps} = 0.93$. This value is slightly lower than f_{ps} in atomic hydrogen at $n_e = 0$ because of the higher threshold for positronium formation in the molecular case. We note that the possible increase of the charge exchange cross sections due to the inclusion of the excited states would increase f_{ps} for both atomic and molecular hydrogen.

d) The Fate of Thermal Positrons

Having evaluated the fraction of positrons that form positronium in flight, we now consider the fate of those positrons which thermalize before annihilation. Thermal positrons will eventually form positronium or annihilate directly, and both these processes can occur with either bound or free electrons. Positronium formation with free electrons is radiative recombination. Radiative recombination and direct annihilation rates with free electrons were calculated by Crannell et al. (1976); we have extended these calculations to lower temperatures, and the results are shown in Figure IV-3. The direct annihilation rates with atomic electrons were obtained by Bhatia, Drachman and Temkin (1977) from a detailed quantum-mechanical scattering treatment. Their thermally averaged annihilation rates are also shown in Figure 3. The rate of positronium formation due to radiative recombination includes the contributions of the excited states (Seaton 1959).

The rate of charge exchange of thermal positrons with residual neutral hydrogen can be calculated by assuming that the positrons are in

thermal equilibrium with the ambient medium. This is justified because even though annihilation and positronium formation tend to modify the positron distribution, the rate of reestablishing thermal equilibrium is much faster than the sum of the rates of all annihilation processes. Therefore, the rate of charge exchange of thermal positrons can be written as

$$R_{ce}/n_H = \int_{6.8eV}^{\infty} n_{MB}(E)\,\sigma_{ce}(E)\,v(E)\,dE \qquad (IV-6)$$

where n_{MB} is the Maxwell-Boltzmann distribution, and σ_{ce} is the charge exchange cross section with atomic hydrogen shown in Figure IV-1. We have evaluated equation IV-6, and the results are shown in Figure IV-3. As can be seen, this rate is a very strong function of temperature, but even at its maximum, it is lower than the thermalization rate (Spitzer 1962).

From Figure IV-3 we see that for temperatures greater than 10^6K, the dominant annihilation process is direct annihilation with free electrons. At lower temperatures, radiative recombination becomes more important than direct annihilation, but depending on the amount of residual neutral hydrogen present, charge exchange may in fact be the most important process. For example, at $T = 10^5$K, the rate of charge exchange is greater than that of radiative recombination if $n_H/n_e > 5\times10^{-6}$. Since for temperatures less than 10^5K, we expect larger neutral hydrogen concentrations, charge exchange should be the dominant process down to temperatures around 10^4K. At 8000 K, $R_{ce}/n_H = R_{rr}/n_e$, so that if, for example, the medium is half ionized (e.g. the warm ionized component of the interstellar medium, McKee and Ostriker 1977), the rates of charge exchange and radiative recombination are about equal. At lower temperatures, radiative recombination should remain the dominant process as long as there is an appreciable concentration of free electrons. However if n_e/n_H becomes small, a large fraction of the positrons form positronium in flight, as can be seen from Figure IV-2.

From Figure III-3 we also see that there is a finite probability for direct annihilation even when positronium formation is the dominant process. For example, at T = 8000K and $n_e = n_H$, about 7% of the positrons will annihilate directly (mostly with free electrons).

e) The Energy Spectrum of Positron Annihilation Radiation

In this section, we evaluate the energy spectrum of positron annihilation radiation resulting from annihilation in a cold neutral and a partially ionized medium. We first consider the cold neutral medium where the radiation is produced by positrons forming positronium in flight and by positrons annihilating directly with bound electrons. Using the Monte Carlo simulation described in Section c, we calculate the photon spectrum resulting from positronium formation in molecular and atomic hydrogen with $n_e = 0$. The probabilities for forming positronium in the singlet or triplet state are 0.25 and 0.75, respectively. Annihilation from the singlet state produces two photons of 0.511 MeV in the rest frame of the positronium. In the frame of the galaxy, the energy of a photon from such an annihilation is

$$\mathcal{E}_\gamma = \mathcal{E}_0 \frac{1-\beta\cos\theta^*}{(1-\beta^2)^{1/2}} \qquad (IV-7)$$

where $\epsilon = 0.511$ MeV, β is the velocity of the positronium, and θ^* is the angle between the positronium velocity and the photon direction of the positronium rest frame. We assume that the photon direction is isotropic in this frame. Annihilation from the triplet state produces three photons whose energies can also be obtained from equation (IV-7) provided that ϵ_0 is replaced by ϵ^* which is chosen according to the distribution given by Ore and Powell (1949). The results for positronium formation are shown in panels a and b of Figure IV-4, and as can be seen there is little difference between the line shapes for the atomic and molecular cases. The full width at half maximum for both these cases is about 6.5 keV.

For direct annihilation with atoms or molecules, the line shape is determined by the momentum distribution of the bound electron modified to account for the fact that the positron cannot approach the nucleus too closely. For the positron-hydrogen atom system, this momentum distribution was accurately calculated by Humberston and Wallace (1972), and from it the gamma-ray line shape is easily obtained. The FWHM is only 2.6 keV, considerably less than that from positronium formation in flight. For the positron-hydrogen molecule system, there exists an experimental determination of the momentum distribution (Briscoe, Choi and Stewart 1968), and a FWHM of 3.2 keV can be extracted from their work; however, since their measurement was done in liquid H_2, it is expected to be slightly too wide. The reason for this is discussed by Humberston (1974) in the case of liquid helium. The scaling of his results to molecular hydrogen results in an expected FWHM of only 3 keV; consequently we have reduced the energy scale of the work of Briscoe et al. (1968) by a factor of 3/3.2.

Panels c and d of Figure IV-4 show the spectrum of positron annihilation radiation in a cold neutral medium. The direct annihilation spectra were integrated over 1 keV intervals and added to the positronium formation histograms shown in panels a and b. Although only 6.5% and 5.5% of the positrons in molecular and atomic hydrogen, respectively, fall below the Ps formation threshold (from the Monte Carlo simulation described above), their contribution is enhanced because direct annihilation always yields two gamma-rays, while Ps decay yields three photons 75% of the time. As can be seen in Figure IV-4, the FWHM of the 0.511 MeV line in cold neutral hydrogen is about 5 keV. If, however, the inclusion of excited states increases significantly the charge exchange cross section, then fewer positrons fall below the Ps formation threshold. In this case, the line

width is closer to the value (6.5 keV) determined for positronium formation in flight. The effect of the three photon annihilation is manifest in a slight asymmetry in the line shape and a low energy tail.

In the case of annihilation in a partially ionized medium ($X > 0.05$), most of the positrons thermalize rather than charge exchange in flight. As discussed in the previous section, thermal positrons will directly annihilate and radiatively recombine with free electrons, and if the gas is warm enough, they form positronium by charge exchange with residual neutral hydrogen. The shape of the 0.511 MeV line from both singlet positronium annihilation following radiative recombination and direct annihilation with free electrons is expected to be a Gaussian of FWHM $\simeq$ 0.011 (keV) $(T(K))^{1/2}$ (Crannell et al. 1976). For example, if $T = 10^4$K, the width is 1.1 keV.

The photon spectra, $q(\varepsilon_\gamma)$, resulting from charge exchange of thermal positrons was calculated as follows: For annihilation from the singlet state

$$q(\varepsilon_\gamma) = \int_{E_1}^{\infty} \frac{n_{HB}(E)\,\sigma_{ce}(E)\,v\,dE}{[(E-6.8eV)(E-6.8eV+4\varepsilon_0)]^{1/2}} \qquad (IV-8)$$

where $E_1 = (\varepsilon_\gamma - \varepsilon_0)^2/\varepsilon_\gamma + 6.8$ eV, while for the triplet,

$$q(\varepsilon_\gamma) = \int_{E_2}^{\infty} dE \; \frac{n_{HB}(E)\,\sigma_{ce}(E)\,v\,d}{[(E-6.8eV)(E-6.8eV+4\varepsilon_0)]^{1/2}} \int_{x_1}^{x_2} dx \; \frac{P_t(x)}{x} \qquad (IV-9)$$

where

$$E_2 = \begin{cases} E_1 \text{ for } \varepsilon_\gamma > \varepsilon_0 \\ 6.8eV \text{ for } \varepsilon_\gamma \leq \varepsilon_0 \end{cases}$$

For equation (8), $P_t(x)$ is the distribution of Ore and Powell (1949) with $x = \varepsilon_\gamma^*/\varepsilon_0$, $x_1 = \varepsilon_\gamma/(\varepsilon_0(1+\beta))$, and $x_2 = \min(1, \varepsilon_\gamma/(\gamma\varepsilon_0(1-\beta))$, where γ and β are the Lorentz factor and velocity (divided by c) of the positronium atom formed, corresponding to (E -6.8 eV).

By combining the results of equations (IV-8) and (IV-9), we have plotted in Figure IV-5 photon spectra from thermal positron annihilation via

positronium formed by charge exchange for T = 8000K and 5000K. The FWHM's for these two cases are about 1.5 and 3.2 keV, respectively.

f) Discussion

As we have pointed out in the Introduction, the FWHM of the 0.511 MeV line from the Galactic Center was observed to be less than 3.2 keV (Leventhal et al., 1978a, b). When compared with the line shapes shown in Figure IV-4, this width is narrower than that resulting from annihilation in a cold medium. However, in a partially ionized medium ($X \geq 0.05$), for temperatures less than $\sim 10^5$K the calculated line width is less than the upper limit set by the observations. This result implies that the medium in which the positrons annihilate should be substantially ionized.

If we consider the three component model of the interstellar medium (McKee and Ostriker 1977), then the most acceptable sites of annihilation are the warm neutral and the warm ionized media, whose temperatures are about 8000K and ionization fractions are 0.15 and 0.68, respectively. For this temperature, the width of the line is only ~ 1.5 keV, as can be seen from Figure IV-2, 80% and 98% of the positrons thermalize for these choices of ionization fractions. The bulk of the positrons probably do not annihilate in cold clouds even though most of the interstellar matter is believed to be in them. Since n_e/n_H is very low in clouds ($\lesssim 10^{-5}$, Guelin et al. 1977), the line width would probably be larger than observed. Neither should they annihilate in the hot component whose temperature is about 5×10^5K and density 3×10^{-3}cm^3; however, we do not expect much annihilation in this medium in any case, because the annihilation time is on the order of 3×10^8 years, and in this time the positrons are expected to encounter the denser clouds in which their annihilation time is much shorter.

Other possible annihilation sites are young supernova remnants. For example in the filaments of the Crab Nebula, $n_e \simeq n_H$ and $T_e \leq 10^4$K (Davidson and Tucker 1971). Supernovae are also likely sources of positrons through all the processes mentioned in the Introduction.

The 0.511 MeV line was observed from the direction of the Galactic Center, but because of the wide opening angle of the detector ($\sim 15°$) the field of view included a large portion of the Galactic Center region extending to the expanding arm of 135 km/sec (Mezger 1974). If the positron source, however, is located at the nucleus of the Galaxy, the positrons would thermalize and annihilate in the extended HII region in the nuclear disk, even though most of the diffuse matter is in the 270 pc molecular ring (Scoville 1972) encircling this region (Mezer 1974). The ionized region has an electron density of 15 to 30 cm^{-3} and temperature less than 10^4K. From equations (IV-1) through (IV-4), we expect positrons with initial energies of several hundred keV to traverse a total distance of about 500 pc in about 2000 years before they thermalize. Because of scattering, however, the rectilinear distance could be much smaller, and therefore the positrons would annihilate before reaching the molecular ring. The annihilation time in the ionized medium is about 10^3 years. For the temperature of this medium, the width of the line is less than about 1.5 keV, consistent with the observed upper limit of 3.2 keV.

g) Summary

We have investigated the annihilation of galactic positrons, and the formation of the 0.511 MeV line and the accompanying 3-photon positronium continuum. In a cold and neutral medium, about 95% of the positrons form positronium atoms in flight and these atoms annihilate before undergoing further collisions if the density of the medium is less than $\sim 10^{15} cm^{-3}$.

The shape of the 0.511 MeV line from positron annihilation in a cold neutral medium has a FWHM of about 5 keV (Figure IV-4 panels c and d), and this width appears to be inconsistent with the observed width of the 0.511 MeV line from the Galactic Center (< 3.2 keV), Leventhal et al. 1978a, b).

In a warm, partially ionized gas of temperature less than several times 10^4K, only a fraction of the positrons form positronium in flight and this fraction decreases with increasing n_e/n_H (Figure IV-2). At higher temperatures, essentially all the positrons thermalize before forming positronium or annihilating directly.

The rates for the various processes leading to thermal positron annihilation are shown in Figure IV-3. For temperatures less than $\sim 10^6$K, positronium formation is the dominant annihilation channel, while for higher temperatures free annihilation dominates. The width of the 0.511 MeV line from thermal positron annihilation is about 3 keV for $T \simeq 10^5$K and varies as approximately $T^{\frac{1}{2}}$. The observed width from Galactic Center suggests a temperature less than this value, and a degree of ionization larger than about 5%, for which half the positrons thermalize. For these conditions more than 90% of the positrons annihilate after forming positronium, and this is consistent with the possible evidence for 3-photon continuum found by Leventhal et al. (1978a, b).

Among the various galactic sites, the warm component of the interstellar medium, filaments or knots in supernova remnants, and the extended HII region in the nuclear disk could be sites for forming the 0.511 MeV line from positron annihilation.

V. SUMMARY

This work has been concerned with emission lines and other spectral features in the hard X-ray and soft gamma ray spectra of various astrophysical sites. In this chapter, we summarize the results and attempt to point out the value of future calculations and experiments which could yield information on such sources. Many of the observations could be carried out from the proposed Gamma Ray Observatory (GRO), a satellite which would carry a complement of gamma ray detectors including one of high spectral resolution.

In Chapter II, we have calculated in detail the expected emission of a broad (FWHM $\sim$ 2.4 keV) line at 6.8 keV from the 2p to 1s transition of low energy iron ions. It was shown that this line is sensitive to ions at $\sim$ 10 MeV/amu, an energy at which nuclear interactions leading to gamma ray lines also occur. The processes responsible for the X-ray transition are excitation by ambient gas particles and charge exchange to excited states of the iron ion. Then using nuclear reaction cross sections (for the most recent values see Ramaty, Kozlovsky and Lingenfelter 1979), we calculated the expected ratios of the production of 4.4 MeV line photons from ^{12}C and 0.85 MeV photons from ^{56}Fe to that of the 6.8 keV iron line. The results are shown in Figure II-6.

We applied these results to possible observations of a 4.4 MeV line from the directions of the galactic center and the radio galaxy Centaurus A. For the former, if the line was produced by diffuse fluxes of low energy cosmic rays, the X-ray data can be made consistent with the gamma ray observation, but only if the energy in fast particles is so large that it conflicts with the vertical distribution of gas in the nuclear region. Possible resolutions of this conflict are obtained by confining the energetic particles to regions that are either hotter than $\sim 10^6$K, or dense

enough to be opaque to the X-rays (by photoelectric absorption). Another possibility is time variability on the scale of years; this time scale would be consistent with the existence of a massive black hole at the galactic center. Such an object has been proposed to account for the time variability seen in Cen A. In addition, we find that the X-ray data from Cen A is inconsistent with the reported width of the 4.4 MeV feature there, assuming production by low energy cosmic rays.

Also in Chapter II, we have investigated the possibility of observing very narrow gamma ray emission lines from nuclei excited in interstellar dust grains. The densities of such grains are many orders of magnitude larger than the interstellar gas, so large that excited nuclei can be stopped before emitting the gamma ray. Since the line widths are determined by Doppler broadening, a very narrow component of the line could result. Three conditions should be met: (i) a significant fraction of the element must be condensed in grains, (ii) the lifetime of the nucleus' excited state must be long enough to allow deceleration ($\gtrsim 10^{-13}$s), and (iii) the grains must be large enough that the recoiling nucleus does not pass out of it before being decelerated (linear dimensions $\gtrsim$ few tenths of a micron). Figure II-8 through II-11 show that this effect is important for several elements; thus observations of these very narrow components will yield information on the composition and size distributions of interstellar grains. We point out that this effect can only be observed with high resolution detectors. Future calculations should take better account of the grain composition and deviations from spherical symmetry.

Spectral features in the hard X-ray region resulting from strong magnetic fields were considered in Chapter III. There we confirmed the results of Daugherty and Ventura (1977 and 1978) for the cyclotron line absorption

and emission rates, using a different representation of the electron wave functions, and we also calculated the relativistically correct electron-ion Coulomb cross sections. The momentum transfer in this latter process is quantized by the field, and significant modifications to the non-magnetized case are apparent. Comparing the rates for these processes in the densities assumed to exist in the polar caps of the binary X-ray pulsars led us to conclude that electrons spend most of their time in the magnetic ground state. In other words, cyclotron radiation is so efficient compared to collisional excitation that the perpendicular electron temperature is essentially zero.

Energetic ions accreting onto an X-ray pulsar in a binary system are thought to be channeled into the polar cap with zero pitch angle. We have used the above calculations to determine their energy loss rates and cyclotron line multiplicities, and the rate for production of cyclotron lines in a one-dimensional thermal gas.

These results were applied to recent observations of a possible line feature in the spectrum of Hercules X-1 at about 60 keV. Under either assumption, we found that electron densities are high enough ($n_e \geq 10^{20} cm^{-3}$) to provide large opacity in the line, as calculated from the absorption cross section. These considerations showed that the narrow reported width of the feature implies that the line emission is highly beamed at angles close to 90° with the polar cap field lines (a fan beam). Taken together with the probable existence of an Alfvén shell, our calculations make the interpretation of a cyclotron emission line unlikely. The data are consistent with an absorption feature at lower energies, and we have presented a possible source of absorbing electrons, the knock-ons produced by the infalling ions. Again, we turn to high resolution detectors for discriminating between the possibilities. In addition, further calculations are needed to determine the electron and photon spectra in a self-

consistent manner. We are presently considering the treatment of this problem by means of a Monte Carlo simulation.

Chapter IV treats in detail the annihilation of positrons in the galaxy and the resulting emission of 0.511 MeV gamma rays. By comparing their energy losses to the cross section for forming positronium by charge exchange with neutral hydrogen, we have first evaluated the fraction that annihilate before thermalizing. Since this cross section has a threshold at 6.8 eV, positrons which lose energy fast enough will fall below this threshold and will thermalize before annihilating. Energy losses are faster in an ionized gas, and we have found that the ionization fraction must be less than $\sim 5\%$ for a majority of positrons to annihilate in flight. Then we have determined the rates for the various annihilation channels of thermal positrons. Positronium formation in the triplet state leads to three photon decay, while formation in the singlet state gives the two 0.511 MeV photons upon annihilation, as is the case for direct annihilation.

Next we evaluate the shape of the radiation resulting from all the processes considered in order to compare the calculations with an observed line from the direction of the galactic center. The observed width requires a temperature of $\leqslant 10^5$K, and an ionization fraction $\geqslant 5\%$. Because most of the matter in this region is in cold molecular clouds with practically no ionization, it is difficult to reconcile the observations with our calculations unless the positron source is localized near the center or unless they are somehow excluded from the clouds. We note that the first possibility is consistent with the existence of the massive black hole mentioned in connection with the results of Chapter II. Among the various galactic regions, the warm component of the interstellar medium, filiments or knots in supernova remnants, and the extended HII region in the nuclear disk

could be sites for forming the 0.511 MeV line from positron annihilation. The calculated profiles show again that high resolution detectors can provide valuable information on the annihilation regions. Future calculations to be undertaken include following time variability of the sources and accounting for helium and heavier elements in the charge exchange and energy loss processes.

APPENDIX

In this appendix, we present the details of the calculations of the cross sections and emission rates presented in Chapter III. First we evaluate an integral occurring in all the calculations:

$$I_{n_1, q_1; n_2, q_2}(\vec{k}_\perp) \equiv \int d^2x_\perp \; f^*_{n_1, q_1}(\vec{x}_\perp)\, e^{i\vec{k}_\perp \cdot \vec{x}_\perp}\, f_{n_2, q_2}(x_\perp) \qquad (A\text{-}1)$$

in an operator representation. The argument of the exponential can be written using equations III-8,

$$i\vec{k}_\perp \cdot \vec{x}_\perp = i\left(k^+x^- + k^-x^+\right) = i\,k^+\left(X^- + \frac{i\pi^-}{eB}\right) + i\,k^-\left(X^+ - \frac{i\pi^+}{eB}\right) \qquad (A\text{-}2)$$

where a vector $\vec{V}$ is decomposed according to

$$V^\pm = \frac{1}{\sqrt{2}}\left(V^x \pm i\,V^y\right) \qquad (A\text{-}3)$$

The commutation relations among the various operators are as follows:

$$\begin{aligned} \left[\pi^+, \pi^-\right]_- &= -eB \\ \left[X^+, X^-\right]_- &= \frac{1}{eB} \\ \left[X^\pm, \pi^\pm\right]_- &= 0 \end{aligned} \qquad (A\text{-}4)$$

From Merzbacher, (1970, p. 167) we obtain for this situation:

$$e^{A_1 + A_2} = e^{A_1}\, e^{A_2}\, e^{-\frac{1}{2}\left[A_1, A_2\right]_-} \qquad (A\text{-}5)$$

Applying this relation to the exponential in A-1 gives:

$$e^{i\vec{k}_\perp \cdot \vec{x}_\perp} = e^{ik^+X^-}\, e^{ik^-X^+}\, e^{\frac{k^-\pi^+}{eB}}\, e^{-\frac{k^+\pi^-}{eB}}\, e^{-\xi} \qquad (A\text{-}6)$$

where $\xi = k_\perp^2/(2eB)$. Thus, substituting in A-2 and using the hermicity of the operators, $(X^-)^\dagger = X^+$; $(\pi^-)^\dagger = \pi^+$, yields

$$I_{n_1, q_1; n_2, q_2}(\vec{k}_\perp) = e^{-\xi} \int d^2x_\perp \left(e^{-ik^-X^+}\, e^{\frac{k^+\pi^-}{eB}}\, f_{n_1, q_1}(\vec{x}_\perp)\right)^\dagger e^{ik^-X^+}\, e^{-\frac{k^+\pi^-}{eB}}\, f_{n_2, q_2}(\vec{x}_\perp) \qquad (A\text{-}7)$$

Expanding the exponential and operating on the functions according to (III-9)

and (III-10) gives

$$I_{n_1 q_1 n_2 q_2}(\vec{k}_\perp) = e^{-\xi} \int d^2x_\perp \left[\sum_{\eta_1=0}^{n_1} \sum_{\mu_1=0}^{q_1} \frac{(-ik^-)^{\mu_1}}{\mu_1!} \frac{(k^+)^{\eta_1}}{\eta_1!} \left(\frac{1}{\sqrt{eB}}\right)^{\mu_1+\eta_1} f_{n_1-\eta_1, q_1-\mu_1}(\vec{x}_\perp) \right]^* \tag{A-8}$$

$$\left[\frac{n_1!\, n_2!\, q_1!\, q_2!}{(n_1-\eta_1)!\,(q_1-\mu_1)!\,(n_2-\eta_2)!\,(q_2-\mu_2)!} \right]^{1/2} \sum_{\eta_2=0}^{n_2} \sum_{\mu_2=0}^{q_2} \frac{(ik^-)^{\mu_2}}{\mu_2!} \frac{(-k^+)^{\eta_2}}{\eta_2!} \left(\frac{1}{\sqrt{eB}}\right)^{\mu_2+\eta_2} f_{n_2-\eta_2, q_2-\mu_2}(\vec{x}_\perp).$$

which yields after using the orthogonality property of the f's and $k^\pm = k_1 e^{\pm i\varphi}/\sqrt{2}$, where φ is the azimuth of $\vec{k}$ in the transverse plane,

$$I_{n_1 q_1, n_2 q_2}(\vec{k}_\perp) = e^{-\xi}\, i^{(q_2-q_1)} (-1)^{n_2-n_1} (n_1!\, n_2!\, q_1!\, q_2!)^{1/2} \cdot \sum_{\eta_1=\max(0,\, n_1-n_2)}^{n_1} \sum_{\mu_1=\max(0,\, q_1-q_2)}^{q_1} \frac{(\sqrt{\xi})^{n_2-n_1+q_2-q_1}\, e^{i(n_2-n_1-q_2+q_1)\varphi}}{\mu_1!\,\eta_1!\,(n_2-n_1+\eta_1)!\,(q_2-q_1+\mu_1)!\,(n_1-\eta_1)!\,(q_1-\mu_1)!} \tag{A-9}$$

Substituting $\eta = \eta_1 - \max(0, n_1-n_2)$ and $\mu = \mu_1 - \max(0, q_1-q_2)$ yields

$$I_{n_1 q_1; n_2 q_2}(\vec{k}_\perp) = e^{-\xi}\, i^{(|q_2-q_1|+|n_2-n_1|+n_2-n_1)} (n_1!\, n_2!\, q_1!\, q_2!)^{1/2} (\sqrt{\xi})^{|n_2-n_1|+|q_2-q_1|} \cdot e^{i(n_2-n_1-q_2+q_1)\varphi} \sum_{\eta=0}^{\min(n_1,n_2)} \sum_{\mu=0}^{\min(q_1,q_2)} (-\xi)^{\mu+\eta} \left[\mu!\,(\mu+|q_2-q_1|)!\,\eta!\,(\eta+|n_2-n_1|)!\,(\min(n_1,n_2)-\eta)!\,(\min(q_1,q_2)-\mu)!\right]^{-1} \tag{A-10}$$

From the definition of the Laguerre polynominal:

$$L_s^{(\alpha)}(x) = \sum_{m=0}^{s} \frac{(-x)^m}{m!} \frac{\Gamma(s+\alpha+1)}{(s-m)!\,\Gamma(m+\alpha+1)} \tag{A-11}$$

we see that (A-10) can be written

$$I_{n_1 q_1, n_2 q_2}(\vec{k}_\perp) = e^{-\xi}\, i^{(|q_2-q_1|+|n_2-n_1|+n_2-n_1)} \left[\frac{\min(n_1,n_2)!}{\max(n_1,n_2)!} \frac{\min(q_1,q_2)!}{\max(q_1,q_2)!} \right]^{1/2} (\sqrt{\xi})^{|n_2-n_1|+|q_2-q_1|}\, e^{i(n_2-n_1-q_2+q_1)\varphi}\, L^{|n_1-n_2|}_{\min(n_1,n_2)}(\xi)\, L^{|q_1-q_2|}_{\min(q_1,q_2)}(\xi) \tag{A-12}$$

We can now proceed to the evaluation of the cross sections.

First, we calculate the absorption cross section and emission rate for line photons as prescribed by equations (III-13) and III-14)

$$S_{fi} = ie \left(\frac{2\pi}{\omega V}\right)^{1/2} \int d^4x\, \overline{\psi_f(x)}\, \vec{\gamma}\cdot\hat{\varepsilon}\, e^{-i(\omega t - \vec{k}\cdot\vec{x})}\, \psi_i(x) \tag{A-13}$$

for absorption. Substitution from equation (III-6) for ψ gives

$$S_{fi} = \frac{ie}{2L} \left(\frac{2\pi}{\omega V W_f W_i (W_f+m_e)(W_i+m_e)}\right)^{1/2} \int d^4x \left[(\gamma^\mu \pi_\mu + m_e) f_{j_f-s_f-\frac{1}{2}, q_f}(\vec{x}_\perp) e^{-iW_f t + i p_f z} u_{s_f} \right]^\dagger \cdot \gamma^0 \vec{\gamma}\cdot\hat{\varepsilon}\, e^{-i(\omega t - \vec{k}\cdot\vec{x})} (\gamma^\nu \pi_\nu + m_e) f_{j_i-s_i-\frac{1}{2}, q_i}(\vec{x}_\perp) e^{-iW_i t + i p_i z} u_{s_i} \tag{A-14}$$

which, after using the hermiticity of the Dirac matrices ($\gamma^{\mu\dagger} = \gamma^0\gamma^\mu\gamma^0$), becomes

$$S_{fi} = \frac{ie}{2L}\left(\frac{2\pi}{\omega V W_f W_i (W_f+m_e)(W_i+m_e)}\right)^{1/2}\int d^4x\, f^*_{j_f,-s_f-\frac{1}{2},q_f}(\vec{x}_\perp)e^{iW_f t - ip_f z}\, u^\dagger_{s_f}\gamma^0(\gamma^\mu\pi_\mu+m_e)$$
$$\vec{\gamma}\cdot\hat{\varepsilon}\, e^{-i(\omega t-\vec{k}\cdot\vec{x})}\,(\gamma^\nu\pi_\nu+m_e)\, f_{j_i,-s_i-\frac{1}{2},q_i}(\vec{x}_\perp)e^{-iW_i t+ip_i z}\, u_{s_i} \qquad (A-15)$$

This expression can be reduced to 2x2 from 4x4 by using

$$u_s = \begin{pmatrix}|s\rangle\\ 0\end{pmatrix},\quad \gamma^0 = \begin{pmatrix}1 & 0\\ 0 & -1\end{pmatrix},\ \text{and}\quad \vec{\gamma} = \begin{pmatrix}0 & \vec{\sigma}\\ -\vec{\sigma} & 0\end{pmatrix} \qquad (A-16)$$

where $|s\rangle = \begin{pmatrix}\delta_{s,\frac{1}{2}}\\ \delta_{s,-\frac{1}{2}}\end{pmatrix}$ and $\vec{\sigma}$ are the Pauli matrices. After commuting the exponential factor to the left, we obtain the matrix operator between the states

$$\gamma^0\left[\gamma^\mu(\pi_\mu+k_\mu)+m_e\right]\vec{\gamma}\cdot\hat{\varepsilon}\,(\gamma^\nu\pi_\nu+m_e) \qquad (A-17)$$
$$= \begin{pmatrix}(\varepsilon\pi_0+\omega+m_e)(\hat{\varepsilon}\cdot\vec{\pi}+i\vec{\sigma}\cdot\hat{\varepsilon}\times\vec{\pi})+(\pi^0+m_e)(\hat{\varepsilon}\cdot\vec{\pi}+i\vec{\sigma}\cdot\vec{\pi}\times\hat{\varepsilon}+i\vec{\sigma}\cdot\vec{k}\times\hat{\varepsilon} & u\\ \sim & w\end{pmatrix}$$

where some components are not shown because they are not needed. Then the matrix element A-15 becomes

$$S_{fi} = \frac{ie}{2L}\left(\frac{2\pi}{\omega V W_i W_f (W_i+m_e)(W_f+m_e)}\right)^{1/2}\int d^4x\, f^*_{j_f,-s_f-\frac{1}{2},q_f}(x_\perp)e^{iW_f t-ip_f z}e^{-i\omega t+i\vec{k}\cdot\vec{x}}$$
$$\left\langle s_f\right|\left[(\varepsilon\pi_0+\varepsilon m_e+\omega)\hat{\varepsilon}\cdot\vec{\pi}+i\omega\vec{\sigma}\cdot\hat{\varepsilon}\times\vec{\pi}+i(\pi_0+m_e)\vec{\sigma}\cdot\vec{k}\times\hat{\varepsilon}\right]\left|s_i\right\rangle f_{j_i,-s_i-\frac{1}{2},q_i}(x_\perp)e^{-iW_i t+ip_i z} \qquad (A-18)$$

This equation is valid for all transitions between levels. We simplify by requiring that the initial state be the ground state, by letting $q_i = 0$ without loss of generality, and by evaluating in the center of parallel momentum frame, where $p_f = 0$ and $W_f = W_1 \equiv \sqrt{m^2+2eB}$. Under these conditions, equation A-18 becomes

$$S_{fi} = \frac{ie}{2L}\frac{(2\pi)^{3/2}\delta(W_i+\omega-W_f)\delta(p_f)}{\left[\omega V W_f W_i (W_i+m_e)(W_f+m_e)\right]^{1/2}}\Big\{\delta_{s_f,-\frac{1}{2}}\left[(\varepsilon W_i+\varepsilon m_e+\omega)\varepsilon^z p_i-(W_i+m)(k^-\varepsilon^+-k^+\varepsilon^-)\right]$$
$$I_{1,q_f;0,0}(\vec{k}_\perp)+\delta_{s_f,-\frac{1}{2}}\,\varepsilon(W_i+m_e)\sqrt{eB}\,\varepsilon^- I_{1,q_f;1,0}(\vec{k}_\perp)+\delta_{s_f,\frac{1}{2}}\sqrt{2}\left[(W_i+m_e)(k^z\varepsilon^- -\varepsilon^z k^-)\right.$$
$$\left.-\omega\varepsilon^- p_i\right] I_{0,q_f;0,0}(\vec{k}_\perp)\Big\} \qquad (A-19)$$

We note that if θ is the polar angle of k and φ its azimuth,

$$\varepsilon^3 = -\varepsilon_0 \sin\theta \qquad \varepsilon^{\pm} = \frac{1}{\sqrt{2}} e^{\pm i\varphi}\left(\varepsilon_0 \cos\theta \mp i\varepsilon_x\right) \tag{A-20}$$

where $\varepsilon_o, \varepsilon_x$ are the polarization amplitudes in the ordinary and extra-ordinary modes. Substituting for the I's from A-12 gives

$$S_{fi} = -\frac{ie}{2L}\frac{(2\pi)^{5/2}\,\delta(W_i+\omega-W_f)\,\delta(p_f)}{\left[\omega V W_i W_f (W_i+m_e)(W_f+m_e)\right]^{1/2}} e^{-\xi-i\varphi}\,\frac{(i\sqrt{2}e^{i\varphi})^{\vartheta_f}}{\sqrt{\vartheta_f!}}\left\{\delta_{s_f,-\frac{1}{2}}\sqrt{2eB}\left[(W_i+m_e+\omega)\xi\cos\theta\varepsilon_0 + (W_i+m_e)(\cos\theta\,\varepsilon_0 + i\varepsilon_x)\right] + \delta_{s_f,\frac{1}{2}}\,\omega\left[(W_i+m_e+\omega\cos^2\theta)\varepsilon_0 + (W_i+m_e+\omega)\cos\theta\,\varepsilon_x\right]\right\} \tag{A-21}$$

Carrying out the same analysis for the emission case gives (assuming p_i, $q_i = 0$)

$$S_{fi}^{(emis)} = -\frac{ie}{2L}\frac{(2\pi)^{5/2}\,\delta(W_i-W_f-\omega)\,\delta(p_f+k^3)}{\left[\omega V W_i W_f (W_i+m_e)(W_f+m_e)\right]^{1/2}} e^{-\xi+i\varphi}\,\frac{(-i\sqrt{2}e^{i\varphi})^{\vartheta_f}}{\sqrt{\vartheta_f!}}\left\{\delta_{s_i,-\frac{1}{2}}\sqrt{2eB}\left[(W_f+m_e+\omega)\xi\cos\theta\varepsilon_0 + (W_f+m_e)(\cos\theta\,\varepsilon_0 \mp i\varepsilon_x)\right] + \delta_{s_i,\frac{1}{2}}\,\omega\left[(W_f+m_e+\omega\cos^2\theta)\varepsilon_0 - i(W_f+m_e+\omega)\cos\theta\,\varepsilon_x\right]\right\} \tag{A-22}$$

The absorption cross section is obtained by squaring the magnitude of S_{fi} and summing over electron final states. The square of the δ-functqons are handled heuristically in Bjorken and Drell (1964):

$$|\delta(p)|^2 = \frac{L}{2\pi}\delta(p) \qquad |\delta(W)|^2 = \frac{T}{2\pi}\delta(W) \tag{A-23}$$

where L and T are the (large) normalization length parallel to the field and the normalization time. Then the rate of absorptions is

$$\frac{1}{V}\sigma_a v_{rel} = \frac{1}{T}\int \frac{L\,dp_f}{2\pi}\sum_{\vartheta_f=0}^{\infty}|S_{fi}|^2 \tag{A-24}$$

where V is the electron normalization volume, σ_a is the absorption cross section, and v_{rel} is the relative velocity of the photon and electron. Solving for the absorption cross section yields equ,tion (III-15) in the center of parallel momentum frame.

The emission rate is shown in here in more detail to show the processes involved in arriving at equation III-15. First, the sum over q_f yields

$$\sum_{\vartheta_f=0}^{\infty}\left|e^{-\xi}\frac{(\pm i\sqrt{2}e^{i\varphi})^{\vartheta_f}}{\sqrt{\vartheta_f!}}\right|^2 = e^{-2\xi}\sum_{\vartheta_f=0}^{\infty}\frac{\xi^{\vartheta_f}}{\vartheta_f!} = e^{-\xi} \tag{A-25}$$

The integral over p_f is ignored because of the δ function. Then the emission rate into d^3k centered on k for electrons deexciting from the first excited state can be written as

$$R_{01}(\vec{k})\, d^3k = \frac{V d^3k}{(2\pi)^3} \frac{1}{T} \int \frac{L\, dp_f}{2\pi} \sum_{\beta f=0}^{\infty} \left| S_{fi}^{(emis)} \right|^2 \qquad (A\text{-}26)$$

where $Vd^3k/(2\pi)^3$ expresses the proportionality of the rate to the phase space volume for the emitted photon. Carrying out the operations yields

$$R_{01}(\vec{k}) = \frac{e^2}{8\pi} \frac{\delta(W_f+\omega-W_i)\, e^{-\beta}}{\omega W_f W_i (W_f+m_e)(W_i+m_e)} \left\{ \delta_{S_i,-\frac{1}{2}} \left[(W_i+m_e+\omega)\beta + W_f+m_e \right]^2 \cos^2\theta\, \mathcal{E}_0^2 \right.$$
$$\left. + \delta_{S_i,\frac{1}{2}} (W_f+m_e)^2 \mathcal{E}_x^2 + \delta_{S_i,\frac{1}{2}}\, \omega^2 \left[(W_f+m_e+\omega\cos^2\theta)^2 \mathcal{E}_0^2 + (W_f+m_e+\omega)^2 \cos^2\theta\, \mathcal{E}_x^2 \right] \right\} \qquad (A\text{-}27)$$

When carrying out the integral over d^3k to obtain the inverse of the lifetime τ_1, it must be noted that W_f depends on ω so that the δ function in A-27 should be written

$$\delta(W_f+\omega-W_i) = \delta\left(\sqrt{m_e^2+\omega^2\cos^2\theta}+\omega-W_i\right) = \frac{W_f}{W_f+\omega\cos^2\theta}\, \delta\left(\omega - \frac{W_i-\sqrt{W_i^2\cos^2\theta+m_e^2\sin^2\theta}}{\sin^2\theta}\right) \qquad (A\text{-}28)$$

Then we obtain

$$\tau_1^{-1} = \frac{e^2}{4} \int_{-1}^{1} d\mu \left(\frac{\omega e^{-\beta}}{(W_f+\omega\mu^2) W_i (W_i+m_e)(W_i+m_e)} \right) \left\{ \quad \right\}_{\omega = \frac{W_i-\sqrt{W_i^2\mu^2+m_e^2(1-\mu^2)}}{1-\mu^2}} \qquad (A\text{-}29)$$

where the braces represent the quantity in braces in A-27. This integral was evaluated numerically; the results are shown in Figuee III-1.

Next we consider the scattering of an electron by an ion in an external field, first order approximation, the relativistic extension of the Born approximation. The matrix element involved in the ion's rest frame is given by equation III-20; we Fourier expand the ion potential $Ze/r \cdot e^{-r/r_{sc}}$, where r_{sc} is the screening length:

$$A_0^{(c)}(x) = \int \frac{d^3k}{(2\pi)^3} e^{i\vec{k}\cdot\vec{x}} A_0(\vec{k}) \quad , \quad A_0(\vec{k}) = \frac{4\pi Z e}{k^2 + r_{sc}^{-2}} \qquad (A\text{-}30)$$

Then equation III-20 becomes

$$S_{fi} = -4\pi i Z e^2 \int \frac{d^3k}{(2\pi)^3} \left(k^2+r_{sc}^{-2}\right)^{-1} \int d^4x\, \overline{\psi_f(x)}\, \gamma^0 e^{i\vec{k}\cdot\vec{x}}\, \psi_i(x) \qquad (A\text{-}31)$$

Substituting for ψ from equation III-6 and using hermiticity gives

$$S_{fi} = -\frac{2\pi i Ze^2}{L}\left[W_i W_f (W_i+m_e)(W_f+m_e)\right]^{-\frac{1}{2}} \int \frac{d^3k}{(2\pi)^3}\,(k^2+r_{sc}^{-2})^{-1} \int d^4x\, f^{*}_{j_f-s_f-\frac{1}{2},q_f}(x_\perp)\, e^{iW_f t - ip_f z}$$
$$u^{\dagger}_{s_f}\gamma^0(\gamma^\mu\pi_\mu+m_e)\gamma^0 e^{i\vec{k}\cdot\vec{x}}(\gamma^\nu\pi_\nu+m_e)\,u_{s_i}\, f_{j_i-s_i-\frac{1}{2},q_i}(x_\perp)\, e^{-iW_i t+ip_i z} \qquad (A\text{-}32)$$

After moving $e^{i\vec{k}\cdot\vec{x}}$ to the left, we reduce the inner 4x4 to the 2x2 representation as in A-16 through A-18;

$$u^{\dagger}_{s_f}\gamma^0\left[\gamma^0\pi_0 - \vec{\gamma}\cdot(\vec{\pi}+\vec{k})+m_e\right]\gamma^0(\gamma^\nu\pi_\nu+m_e)\,u_{s_i}$$
$$= \left\langle s_f\right|\left[(\pi_0+m_e)^2 + \vec{\pi}^2 + \vec{k}\cdot\vec{\pi} + i\vec{\sigma}\cdot(\vec{\pi}+\vec{k})\times\vec{\pi}\right]\left|s_i\right\rangle \qquad (A\text{-}33)$$

We note that $\vec{\pi}\times\vec{\pi} = \frac{1}{i}\nabla\times(e\vec{A}) = \frac{e}{i}\vec{B}$. Then substituting this expression into A-32 and assuming the initial state is the ground state gives:

$$S_{fi} = -\frac{2\pi i Ze^2}{L}\left[W_i W_f (W_i+m_e)(W_f+m_e)\right]^{-\frac{1}{2}} \int \frac{d^3k}{(2\pi)^3}\,(k^2+r_{sc}^{-2})^{-1} \int d^4x\, f^{*}_{j_f-s_f-\frac{1}{2},q_f}(x_\perp)\, e^{iW_f t - ip_f z}$$
$$e^{i\vec{k}\cdot\vec{x}}\left\{\delta_{s_f,-\frac{1}{2}}\left[2W_i(W_i+m_e)+k^z p_i\right] - \delta_{s_f,\frac{1}{2}}\sqrt{2}\,k^- p_i\right\} f_{0,q_i}(x_\perp)\, e^{-iW_i t + ip_i z} \qquad (A\text{-}34)$$

The elasticity of the interaction is expressed by the fact that the Coulomb potential had no time varying component. This results in a factor $\delta(W_f-W_i)$ in the above time integration. In evaluating the integral, we put $W_i = W_f = W$ to obtain:

$$S_{fi} = \frac{iZe^2}{L}\,\frac{\delta(W_f-W_i)}{W(W+m_e)}\int \frac{d^3k}{k^2+r_{sc}^{-2}}\,\delta(k^z-p_f+p_i)\, I_{j_f-s_f-\frac{1}{2},q_f;\,0,q_i}(\vec{k}_\perp)$$
$$\left\{\delta_{s_f,-\frac{1}{2}}\left[2W(W+m_e)+p_i(p_f-p_i)\right] - \delta_{s_f,\frac{1}{2}}\sqrt{2eBs}\;p_i e^{-i\varphi}\right\} \qquad (A\text{-}35)$$

Substituting for the I function and carrying out the $k_\perp$ and φ integrations gives (ignoring r_{sc}^{-2}):

$$S_{fi} = \frac{\pi i Ze^2}{L}\,\frac{\delta(W_f-W_i)}{W(W+m_e)}\int_0^\infty \frac{ds\,(\sqrt{s})^{|q_f-q_i|}\,e^{-s}}{s+(p_f-p_i)^2/(2eB)}\; i^{|q_f-q_i|}\left(\frac{\min(q_i,q_f)!}{j!\,\max(q_i,q_f)!}\right)^{\frac{1}{2}}$$
$$\delta_{q_f,q_i+j_f}\,L^{|q_i-q_f|}_{\min(q_i,q_f)}(s)\left\{\delta_{s_f,-\frac{1}{2}}\left[2W(W+m_e)+p_i(p_f-p_i)\right] - \delta_{s_f,\frac{1}{2}}\,p_i\sqrt{2eBj}\right\}.$$

We rewrite the above, noting $q_f = q_i+j_f$ and putting $j = j_f$

$$S_{fi} = \frac{\pi Ze^2}{L}\,\frac{\delta(W_f-W_i)}{W(W+m_e)}\; i^{j+1}\,\delta_{q_f,q_i+j}\left(\frac{q_i!}{j!\,q_f!}\right)^{\frac{1}{2}}\left\{\delta_{s_f,-\frac{1}{2}}\left[2W(W+m_e)+p_i(p_f-p_i)\right]\right.$$
$$\left. - \delta_{s_f,\frac{1}{2}}\,p_i\sqrt{2eBj}\right\}\int_0^\infty \frac{ds\,s^j e^{-s}}{s+x}\,L_{q_i}^{(j)}(s) \qquad (A\text{-}37)$$

where $x = (p_f - p_i)^2/(2eB)$. Next we square this expression, sum over final q and average over initial q according to $1/Q \sum_{q_i=0}^{Q}$ where Q is obtained by noting that the distance from the guiding center to the field line q is given by

$$R^2 f_{nq} = (X^+X^- + X^-X^+) f_{nq} = \frac{2}{eB}\left(q + \tfrac{1}{2}\right) f_{nq} . \qquad (A-38)$$

The maximum q, Q, in a given area $A(= \pi R_{max}^2)$ is given by

$$Q \simeq Q + \tfrac{1}{2} = \tfrac{1}{2} eB R_{max}^2 = \frac{eBA}{2\pi} \qquad (A-39)$$

The rate is obtained from

$$R_j(p_i) = \frac{1}{V}\sigma_j(p_i)\,|v(p_i)| = \frac{1}{T}\frac{1}{Q}\sum_{q_i=0}^{Q}\sum_{q_f=0}^{\infty}\int \frac{L\,dp_f}{2\pi}\,|S_{fi}|^2 \qquad (A-40)$$

In the square, the δ function is handled as in A-23. The δ-function remains, and is used in the p_f integral, after

$$\delta(W_f - W_i) = \delta\left(\sqrt{p_f^2 + m_e^2 + 2eBj} - \sqrt{p_i^2 + m_e^2}\right) = \sum_{\pm}\frac{W_+}{|p_f|}\,\delta\left(p_f \pm \sqrt{p_i^2 - 2eBj}\right) \qquad (A-41)$$

solving (A-40) for σ_j (noting that $v = p/W$) gives

$$\sigma_j(p_i) = \frac{\pi L e^4}{2eBj!\,(W+m_e)^2}\sum_{\pm}\frac{1}{|p_i p_f|}\left\{\delta_{s_f,-\frac{1}{2}}\left[2W(W+m_e) + p_i(p_f - p_i)\right]^2 + \delta_{s_f,\frac{1}{2}}\,p_i^2\,2eBj\right\}$$
$$\cdot \sum_{q_i=0}^{\infty}\left[\int_0^\infty \frac{d\xi\,\xi^j e^{-\xi}}{\xi + x} L_{q_i}^{(j)}(\xi)\right]^2 \frac{q_i!}{(q_i+j)!} \qquad (A-42)$$

The sum can be rewritten by using first of all the Laguerre expansion theorem (Danese, 1965, p. 517):

$$G(\xi) = \sum_{s=0}^{\infty} G_s^{(\alpha)} L_s^{(\alpha)}(\xi)$$
$$G_s^{(\alpha)} = \frac{s!}{\Gamma(s+\alpha+1)}\int_0^\infty d\xi\,\xi^\alpha e^{-\xi} G(\xi) L_s^{(\alpha)}(\xi) \qquad (A-43)$$

Allowing $G(\xi) = (\xi + x)^{-1}$ and $\alpha = j$ gives the expression

$$\sum_{q_i=0}^{\infty}\left[\int_0^\infty \frac{d\xi\,\xi^j e^{-\xi}}{\xi + x} L_{q_i}^{(j)}(\xi)\right]^2 \frac{q_i!}{(q_i+j)!} = \int_0^\infty \frac{d\xi\,\xi^j e^{-\xi}}{\xi + x}\sum_{q_i=0}^{\infty} G_{q_i}^{(j)} L_{q_i}^{(j)}(\xi) \qquad (A-44)$$

But by A-42, we have

$$\int_0^\infty \frac{d\xi\,\xi^j e^{-\xi}}{\xi + x}\sum_{q_i=0}^{\infty} G_{q_i}^{(j)} L_{q_i}^{(j)}(\xi) = \int_0^\infty \frac{d\xi\,\xi^j e^{-\xi}}{(\xi + x)^2} \qquad (A-45)$$

Finally we obtain

$$\sigma_j(p_i) = \frac{\pi Z^2 r_e^2}{|p_i p_f|\,(W+m_e)^2}\,\frac{B_\perp}{2B}\,\frac{1}{j!}\sum_{\pm} \mathcal{E}_j(x_\pm)\left\{\delta_{s_f,-\frac{1}{2}}\left[2W(W+m_e) + p_i(p_f - p_i)\right] + \delta_{s_f,\frac{1}{2}}\,2eBj\,p_i^2\right\} \qquad (A-46)$$

where $r_e = e^2/(mc^2)$ is the classical electron radius, and the ε_j are given by (putting ~~$\xi+x$~~ $= t$ in A-45)

$$\varepsilon_j(x) = \int_x^\infty \frac{dt}{t^2} e^{-(t-x)} (t-x)^j, \qquad x = \frac{(p_f - p_i)^2}{2cB} \qquad (A-47)$$

REFERENCES

Abramowitz, B. and Stegun, I. A. 1965, Handbook of Mathematical Functions (New York: Dover).

Barashenkov, V. S. and Maltsev, V. M. 1961, Fortschritte der Physik, 9, 549.

Barkas, W. H. and Berger, M. J. 1964, Tables of Energy Losses and Ranges of Heavy Charged Particles, NASA SP-3013.

Basko, M. M. and Sunyaev, R. A. 1975, Astron. and Astrophys., 42, 311.

Basko, M. M. and Sunyaev, R. A. 1976, M.N.R.A.S., 175, 395.

Bates, D. R. and Boyd, A. H. 1962, Proc. Phys. Soc., 80, 1301.

Bates, D. R. 1962, Atomic and Molecular Processes (New York: Academic Press), ch. 14.

Becker, R. H., Boldt, E. A., Holt, S. S., Pravdo, S. H., Rothschild, R. E., Serlemitsos, P. J., and Swank, J. H. 1976, Ap. J. Letters, 209, L65.

Bhatia, A. K., Drachman, R. J., and Temkin, A. 1977, Phys. Rev. A, 16, 1719.

Bjorken, J. D. and Drell, S. D. 1964, Relativistic Quantum Mechanics (New York: McGraw-Hill).

Boldt, E. A., Holt, S. S., Rothschild, R. E., and Serlemitsos, P. J. 1976, Astron. and Astrophys. 50, 161.

Book, D. L. and Ali, A. W. 1975, A Collection of Plasma Physics Formulas and Data, NRL Memorandum Report 2898.

Brice, D. K. 1975, Ion Implantation Range and Energy Deposition Distributions, vol. 1, High Incident Ion Energies (New York: Plenum).

Brinkman, H. C. and Kramers, H. A. 1930, Proc. K. Ned. Akad. Wet., 33, 973.

Briscoe, C. V., Choi, S. I., and Stewart, A. T. 1968, Phys. Rev. Letters, 20, 493.

Brisken, A. 1973, Ph. D. thesis, University of Maryland (unpublished).

Brown, R. L. and Lockman, F. J. 1975, Ap. J. Letters, 200, L115.

Burns, D. 1964, J. Chem. Phys., 41, 1521.

Bussard, R. W., Ramaty, R., and Omidvar, K. 1978, Ap. J., 220, 353.

Cameron, A. G. W. 1973, Spa. Sci. Rev., 15, 121.

Canuto, V., Lodenquai, J., and Ruderman, M. 1971, Phys. Rev. D, 3, 2303.

Canuto, V. and Ventura, J. 1977, Fundamentals of Cosmic Physics, 2, 203.

Catura, R. C. and Acton, L. W. 1975, Ap. J. Letters, 202, L5.

Chupp, E. L., Forrest, D. J., Higbie, P. R., Suri, A. N., Tsai, C., and Dunphy, P. P. 1973, Nature 241, 333.

Chupp, E. L., Forrest, D. J., and Suri, A. N. 1975, Proc. IAU/COSPAR Symp. #68, Solar X-, Gamma, and EUV Radiations, ed. by S. Kane, p. 341.

Coe, M. J., Engel, A. R., Quenby, J. J., and Dyer, C. S. 1977, Nature, 268, 508.

Coleman, P. G., Griffith, T. C., and Heyland, G. R. 1974, Appl. Phys., 4, 89.

Crannell, C. J., Joyce, G., Ramaty, R., and Werntz, C. 1976, Ap. J., 210, 582.

Danese, A. E. 1965, Advanced Calculus, Vol. I (Boston: Allyn and Bacon).

Daugherty, J. K. and Ventura, J. 1977, Astron. and Astrophys., 61, 723.

Daugherty, J. K. and Ventura, J. 1978, Phys. Rev. D, 18, 1053.

Davidson, K. and Tucker, W. H. 1971, IAU Symp. #46, The Crab Nebula, ed. by R. D. Davies and F. G. Smith, p. 308.

Davison, P. J. N., Culhane, J. L., and Mitchell, R. J. 1976, Ap. J. Letters, 206, L37.

Drachman, R. J., Omidvar, K., and McGuire, J. H. 1976, Phys. Rev. A, 14, 100.

Elsner, R. F. and Lamb, F. K. 1976, Nature, 262, 356.

Fabian, A. C., Maccagni, D., Rees, M. J., and Stoeger, W. R. 1976, Nature, 260, 683.

Fishman, G. J. and Clayton, D. D. 1972, Ap. J., 178, 337.

Giacconi, R., Gursky, H., Kellogg, E., Levinson, R., Schreier, E., and Tananbaum, H. 1973, Ap. J., 184, 227.

Ginzburg, V. L. and Syrovatskii, S. I. 1964, The Origin of Cosmic Rays (New York: Pergamon), p. 122.

Gnedin, Yu. N. and Sunyaev, R. A. 1973, Zh. Eksp. Teor. Fiz., 65, 102.

Griffiths, R. E. 1972, Astron. and Astrophys., 21, 97.

Guelin, M. 1977, Ap. J. Letters, 217, L165.

Guthrie, P. and Tademaru, E. 1973, Nature Phys. Sci., 241, 77.

Hall, R. D., Meegan, G. A., Walraven, G. D., Djuth, F. T., and Haymes, R. C. 1976, Ap. J., 210, 631.

Hara, S. 1974, J. Phys. B, 7, 1748.

Haymes, R. C., Walraven, G. D., Meegan, C. A.,,Hall, R. D., Djuth, F. T., and Shelton, D. H. 1975, Ap. J. 201, 593.

Herzberg, G. 1950, Spectra of Diatomic Molecules (D. Van Nostrand), p. 340.

Hoffman, W. F., Frederick, C. L., and Emergy, R. J. 1971, Ap. J. Letters, 164, L23.

Holt, S. S., Boldt, E. A., and Serlemitsos, P. J. 1968, Ap. J. Letters, 154, L137.

Holt, S. S., Boldt, E. A., and Serlemitsos, P. J. 1969, Ap. J. Letters, 158, L155.

Humberston, J. W. 1974, J. Phys. B, 7, L286.

Humberston, J. W. and Wallace, J. B. G. 1972, J. Phys. B, 2, 1278.

Jacobson, A. S., Ling, J. C., Mahoney, W. A., and Willett, J. B. 1978, in Gamma Ray Spectroscopy in Astrophysics, ed. by T. L. Cline and R. Ramaty, NASA Technical Memorandum 79619, p. 228.

Johnson, W. N. III, Harnden, F. R., Jr., and Haymes, R. C. 1972, Ap. J. Letters, 172, L1.

Johnson, W. N. III and Haymes, R. C. 1973, Ap. J., 184, 103.

Kauppila, W. E., Stein, T. S., Smart, J. H., and Pol, v. 1977, preprint.

Kellogg, E., Gursky, H., Murray, S., Tananbaum, H., and Giacconi, R., 1971, Ap. J. Letters, 169, L99.

Kestenbaum, H., Angel, J. R. P., and Novick, R. 1971, Ap. J. Letters, 164, L87.

Kieffer, L. J. 1969, Atomic Data, 1, 19 and 120.

Kieffer, L. J. and Dunn, G. H. 1966, Rev. Mod. Phys., 38, 1.

Kozlovsky, B. and Ramaty, R. 1974, Ap. J. Letters, 191, L43.

Leventhal, M. 1973, Ap. J. Letters, 183, L47.

Leventhal, M., McCallum, C. J., and Stang, P. D. 1978a, Ap. J. Letters, 225, L11.

Leventhal, M., McCallum, C. J., and Stang, P. D. 1978b, in Gamma Ray Spectroscopy in Astrophysics, ed. by T. L. Cline and R. Ramaty, NASA Technical Memorandum 79619, p. 169.

Lingenfelter, R. E., Higdon, J. C., and Ramaty, R. 1978, in Gamma Ray Spectroscopy in Astrophysics, ed. by T. L. Cline and R. Ramaty, NASA Technical Memorandum 79619, p. 252.

Lingenfelter, R. E. and Ramaty, R. 1967, in High Energy Nuclear Reactions in Astrophysics, ed. by B. S. P. Shen (New York: Benjamin), p. 99.

Lingenfelter, R. E. and Ramaty, R. 1977a, in The Structure and Content of the Galaxy and Galactic Gamma Rays, NASA CP-002, p. 237.

Lingenfelter, R. E. and Ramaty, R. 1977b, Ap. J. Letters, 211, L19.

Lingenfelter, R. E. and Ramaty, R. 1978, Physics Today, 31, 40.

McCray, R. and Lamb, F. K. 1976, Ap. J. Letters, 204, L115.

McKee, C. G. and Ostriker, J. P. 1977, Ap. J., 218, 148.

Meneguzzi, M. and Reeves, H. 1975, Astron. and Astrophys., 40, 91.

Merzbacher, E. 1970, Quantum Mechanics (New York: Wiley).

Meszaros, P. 1978, preprint.

Meyer, J. P. 1972, Astron. and Astrophys. Suppl., 7, 417.

Meyer, P., Ramaty, R., and Webber, W. 1974, Physics Today, 27, 23.

Mezger, P. G. 1974, Proc. of the ESO/SRC/CERN Conf. on Research Programmes for the New Large Telescope (Geneva), p. 79.

Mitchell, R. J., Culhane, J. L., Davison, P. J. N., and Ives, J. C. 1976, M.N.R.A.S., 176, 29.

Mitchell, R. J., Ives, J. C., and Culhane, J. L. 1977, M.N.R.A.S., 181, 25.

Moiseiwitsch, B. L. and Smith, S. J. 1968, Rev. Mod. Phys., 40, 238.

Nikolaev, V. S. 1967, Soviet Phys. - JETP, 24, 847.

Northcliffe, L. C. and Schilling, R. F. 1970, Nuclear Data (New York: Academic Press) A7, p. 233.

Omidvar, K. 1965, Phys. Rev., 140, 26.

Oppenheimer, J. R. 1928, Phys. Rev., 31, 349.

Ore, A. and Powell, J. A. 1949, Phys. Rev., 75, 1696.

Peimbert, M., Torres-Peimbert, S., and Rayo, J. F. 1978, Ap. J., 220, 516.

Pravdo, S. H. 1976, Ph.D. thesis, University of Maryland (unpublished).

ravdo, S. H., Becker, R. H., Boldt, E. A., Holt, S. S., Rothschild, R. E., Serlemitsos, P. J., and Swank, J. H. 1976, Ap. J. Letters, 206, L41.

ravdo, S. H., Becker, R. H., Boldt, E. A., Holt, S. S., Serlemitsos, P. J. and Swank, J. H. 1977a, Ap. J. Letters, 215, L61.

ravdo, S. H. and Boldt, E. A. 1975, Ap. J., 200, 727.

ravdo, S. H., Boldt, E. A., Holt, S. S. and Serlemitsos, P. J. 1977b, Ap. J. Letters, 216, L23.

Pravdo, S. H., Bussard, R. W., Becker, R. H., Boldt, E. A., Holt, S. S., Serlemitsos, P. J. and Swank, J. H., Ap. J., 225, 988.

Ramaty, R. 1978, Gamma Ray Spectroscopy in Astrophysics, ed. by T. L. Cline and R. Ramaty, NASA Technical Memorandum 79619, p. 6.

Ramaty, R., Borner, G., and Cohen, J. M. 1973, Ap. J., 181, 891.

Ramaty, R., Kozlovsky, B., Lingenfelter, R. E. 1975, Spa. Sci. Rev., 18, 341.

Ramaty, R., Kozlovsky, B., and Lingenfelter, R. E. 1979, Ap. J. Suppl., in press.

Ramaty, R., Kozlovsky, B., and Suri, A. N. 1977, Ap. J., 214, 617.

Ramaty, R. and Lingenfelter, R. E. 1975, in Solar X-, Gamma, and EUV Radiations, ed. by S. Kane, p. 363.

Rule, D. W. 1977, Phys. Rev. A, 16, 19.

Sanders, R. H. and Wrixon, G. T. 1973, Astron. and Astrophys., 26, 365.

Schiff, H. 1954, Canad. J. Phys., 32, 393.

Schulman, S., Friedman, H., Fritz, G., Henry, R. C., and Yentis, D. J. 1975, Ap. J. Letters, 119, L101.

Scoville, N. Z. 1972, Ap. J. Letters, 175, L127.

Scoville, N. Z., Solomon, P. M., and Jefferts, K. B. 1974, Ap. J. Letters, 187, L63.

Seaton, M. J. 1959, M.N.R.A.S., 119, 81.

Serlemitsos, P. J., Boldt, E. A. , Holt, S. S., Ramaty, R., and Brisken, A. F. 1973, Ap. J. Letters, 184, L1.

Serlemitsos, P. J., Boldt, E. A. , Holt, S. S., Rothschild, R. E., and Robinson-Saba, J. L. 1975, Ap. J. Letters, 201, L9.

Serlemitsos, P. J., Smith, B. W., Boldt, E. A., Holt, S. S., and Swank, J. H. 1977, Ap. J. Letters, 211, L63.

Spitzer, L. 1962, Physics of Fully Ionized Gases (New York: Wiley).

Stecker, F. W. 1969, Astrophys. and Spa. Sci., 3, 479.

Steigman, G. 1968, Ph.D. thesis, unpublished,

Sural, D. P. and Mukherjee, S. C. 1970, Physica, 49, 249.

Trumper, J., Pietsch, W., Teppin, C., Voges, W., Staubert, R., and Kendziorra, E. 1978, Ap. J. Letters, 219, L105.

Trumper, J., Pietsch, W., Reppin, C., Sacco, B., Kendziorra, E., and Staubert, R. 1977, Texas Symp. on Relativistic Astrophys. (Boston, 1976), Ann. N.Y. Acad. Sci., in press.

Ventura, J. 1973, Phys. Rev. A, 8, 3021.

Watson, W. D. 1976, Ap. J., 206, 842.

Winterbon, K. B. 1975, Ion Implementation Range and Energy Deposition Distributions, v. 2, Low Incident Ion Energies (New York: Plenum).

TABLE II-1

Element	Abundance	Final State	E = 5 MeV/amu	10	13	20	30
H	1.	1s	2.73-21	8.16-23	2.24-23	2.41-24	3.08-25
		2p	2.25-21	6.64-23	2.00-23	1.55-24	1.58-25
		2s	7.92-23	3.58-24	1.00-24	1.12-25	2.25-26
		1s	4.94-21	1.53-22	4.21-23	4.57-24	5.89-25
He	0.085	2p	4.08-21	1.24-22	3.11-23	2.94-24	3.02-25
	(0.1)	2s	1.46-22	6.72-24	1.90-24	2.14-25	4.29-26
	3.71-4	1s	4.54-21	2.15-22	6.48-23	8.14-24	1.15-24
C	(2.1-3)	2p	3.68-21	1.72-22	4.79-23	5.11-24	5.73-25
		2s	1.78-22	1.00-23	3.05-24	3.91-25	8.63-26
	1.18-4	1s	1.81-21	1.01-22	3.12-23	4.11-24	5.97-25
N	(1.3-3)	2p	1.48-21	7.89-23	2.27-23	2.56-24	4.57-26
		2s	7.86-23	4.72-24	1.49-24	2.01-25	4.57-26
	6.76-4	1s	1.91-20	1.22-21	3.93-22	3.52-23	8.30-24
O	(3.5-3)	2p	1.56-20	9.59-22	2.86-22	3.40-23	4.08-24
		2s	9.15-22	5.84-23	1.91-23	2.74-24	6.46-25
	1.08-4	1s	3.59-21	3.00-22	1.05-22	1.67-23	2.73-24
Ne	(1.9-4)	2p	2.90-21	2.30-22	7.47-23	1.00-23	1.29-24
		2s	2.11-22	1.45-23	5.19-24	8.64-25	2.20-25
	3.34-5	1s	1.46-21	1.50-22	5.63-23	1.01-23	1.82-24
Mg	(2.0-4)	2p	1.17-21	1.13-22	3.93-23	5.92-24	8.79-25
		2s	9.67-23	7.03-24	2.80-24	5.59-25	1.54-25
	3.14-5	1s	2.25-21	2.55-22	1.03-22	2.07-23	4.09-24
Si	(2.3-4)	2p	1.77-22	1.80-22	6.96-23	1.16-23	1.80-24
		2s	1.40-22	1.12-23	5.05-24	1.23-24	3.61-25
	1.57-5	1s	1.35-21	1.51-22	6.42-23	1.42-23	3.08-24
S	(8.0-5)	2p	1.06-21	1.07-22	4.12-23	7.60-24	1.28-24
		2s	6.76-23	7.03-24	3.38-24	9.15-25	2.83-25
	2.61-5	1s	6.75-21	6.62-22	2.85-22	6.51-23	1.75-23
Fe	(1.6-4)	2p	4.72-21	4.55-22	1.61-22	2.82-23	5.52-24
		2s	3.89-22	3.59-23	1.74-23	4.78-24	1.72-24
		1s	4.85-20	3.29-21	1.19-21	2.01-22	4.02-23
TOTALS		2p	3.87-20	2.49-21	7.94-22	1.09-22	1.62-23
		2s	2.30-21	1.59-22	6.22-23	1.20-23	3.58-24

TABLE II-2

Multiplicities

E(MeV/amu)	Neutral Medium (Photons)	Ionized Medium (Photons)
2	2.0×10^{-4}	2.4×10^{-5}
4	.0296	.00414
6	.281	.0413
8	1.031	.156
10	2.32	.361
12	3.92	.620
14	5.48	.877
16	6.77	1.09
18	7.75	1.26
20	8.46	1.38
22	8.98	1.47
24	9.38	1.54
26	9.68	1.60
28	9.92	1.64
30	10.11	1.67
32	10.26	1.70
34	10.38	1.72
36	10.48	1.74
38	10.56	1.76
40	10.63	1.77

Table II-3

Photon Energy (MeV)	Emission Mechanism	Production Processes	Mean Life (sec)
0.092	$^{55}Fe^{*}1.408\rightarrow^{55}Fe^{*}1\ 316$	$^{56}Fe(p,pn)^{55}Fe^{*}$	--
0 110	$^{19}F^{*}0.110\rightarrow g.s$	$^{20}Ne(p,2p)^{19}F^{*}$	$8.5x10^{-10}$
0 159	$^{56}Co^{*}0.158\rightarrow g.s$	$^{56}Fe(p,n)^{56}Co^{*}$	$<10^{-10}$
0 197	$^{19}F^{*}0\ 197\rightarrow g\ s$	$^{20}Ne(p,2p)^{19}F^{*}$	$1.3x10^{-7}$
0.238	$^{19}Ne^{*}0.238\rightarrow g.s.$	$^{20}Ne(p,pn)^{19}Ne^{*}$	$2\ 6x10^{-8}$
0.275	$^{19}Ne^{*}0.275\rightarrow g.s.$	$^{20}Ne(p,pn)^{19}Ne^{*}$	$6.1x10^{-11}$
0.412	$^{55}Fe^{*}0.412\rightarrow g\ s.$	$^{56}Fe(p,pn)^{55}Fe^{*}$	--
0.431	$^{7}Be^{*}0.431\rightarrow g.s.$	$^{4}He(\alpha,n)^{7}Be^{*}$	$2.7x10^{-13}$
0.440	$^{23}Na^{*}0.440\rightarrow g\ s.$	$^{24}Mg(p,2p)^{23}Na^{*}$	$1.6x10^{-12}$
0.451	$^{23}Mg^{*}0.451\rightarrow g.s.$	$^{24}Mg(p,pn)^{23}Mg^{*}$	$1.8x10^{-12}$
0 477	$^{55}Fe^{*}1.408\rightarrow^{55}Fe^{*}0.931$	$^{56}Fe(p,pn)^{55}Fe^{*}$	--
		$^{56}Fe(p,2n)^{55}Co(e^{+};\varepsilon)^{55}Fe^{*}(16\%)$	$9.5x10^{4}$
0.478	$^{7}Li^{*}0.478\rightarrow g.s.$	$^{4}He(\alpha,p)^{7}Li^{*}$	10^{-16}
		$^{4}He(\alpha,n)^{7}Be(\varepsilon)^{7}Li^{*}(10\%)$	$6.6x10^{6}$
0.717	$^{10}B^{*}0.717\rightarrow g.s.$	$^{12}C(p,x)^{10}B^{*}$	$1.0x10^{-9}$
		$^{16}O(p,x)^{10}B^{*}$	$1.0x10^{-9}$
		$^{12}C(p,x)^{10}C^{*}(e^{+})^{10}B^{*}(100\%)$	28
		$^{16}O(p,x)^{10}C^{*}(e^{+})^{10}B^{*}(100\%)$	28
0.744	$^{52}Cr^{*}3.114\rightarrow^{52}Cr^{*}2.370$	$^{56}Fe(p,x)^{52}Cr^{*}$	--
		$^{56}Fe(p,x)^{52}Mn(e^{+};\varepsilon)^{52}Cr^{*}(88\%)$	$7.1x10^{5}$
0.780	$^{27}Si^{*}0.780\rightarrow g\ s.$	$^{28}Si(p,pn)^{27}Si^{*}$	$5x10^{-11}$
0.812	$^{56}Co^{*}0.970\rightarrow^{56}Co^{*}0.158$	$^{56}Fe(p,n)^{56}Co^{*}$	$<10^{-10}$
0.835	$^{54}Cr^{*}0\ 835\rightarrow g\ s.$	$^{56}Fe(p,x)^{54}Mn(\varepsilon)^{54}Cr(100\%)$	$3.9x10^{7}$
0.844	$^{27}Al^{*}0\ 844\rightarrow g\ s.$	$^{28}Si(p,2p)^{27}Al^{*}$	$5.3x10^{-11}$
0.847	$^{56}Fe^{*}0.847\rightarrow g.s.$	$^{56}Fe(p,p')^{56}Fe^{*}$	$9\ 7x10^{-12}$
		$^{56}Fe(p,n)^{56}Co(e^{+};\varepsilon)^{56}Fe^{*}(100\%)$	$9.6x10^{6}$
0.891	$^{22}Na^{*}0.891\rightarrow g.s.$	$^{24}Mg(p,x)^{22}Na^{*}$	$1.4x10^{-11}$
0.931	$^{55}Fe^{*}0.931\rightarrow g.s.$	$^{56}Fe(p,pn)^{55}Fe^{*}$	--
		$^{56}Fe(p,2n)^{55}Co\ (e^{+};\varepsilon)^{55}Fe^{*}(73\%)$	$9\ 5x10^{4}$
0.936	$^{52}Cr^{*}2.370\rightarrow^{52}Cr^{*}1.434$	$^{56}Fe(p,x)^{52}Mn(e^{+};\varepsilon)^{52}Cr^{*}(94\%)$	$7.1x10^{5}$
0.957	$^{27}Si^{*}0.957\rightarrow g\ s.$	$^{28}Si(p,pn)^{27}Si^{*}$	$1.0x10^{-12}$
1.014	$^{27}Al^{*}1.014\rightarrow g.s.$	$^{27}Al(p,p')^{27}Al^{*}$	$1.9x10^{-12}$
		$^{28}Si(p,2p)^{27}Al^{*}$	$1\ 9x10^{-12}$
1.023	$^{10}B^{*}1.740\rightarrow^{10}B^{*}0.717$	$^{12}C(p,x)^{10}B^{*}$	$1.5x10^{-13}$
		$^{16}O(p,x)^{10}B^{*}$	$1.5x10^{-13}$
1.038	$^{56}Fe^{*}3.123\rightarrow^{56}Fe^{*}2.085$	$^{56}Fe(p,n)^{56}Co(e^{+};\varepsilon)^{56}Fe^{*}(14\%)$	$9.6x10^{6}$
1.238	$^{56}Fe^{*}2.085\rightarrow^{56}Fe^{*}0.847$	$^{56}Fe(p,p')^{56}Fe^{*}$	$1.0x10^{-12}$
		$^{56}Fe(p,n)^{56}Co(e^{+};\varepsilon)^{56}Fe^{*}(67\%)$	$9.6x10^{6}$
1.249	$^{31}S^{*}1\ 249\rightarrow g.s.$	$^{32}S(p,pn)^{31}S^{*}$	$7\ 2x10^{-13}$
1.266	$^{31}P^{*}1.266\rightarrow g.s.$	$^{32}S(p,2p)^{31}P^{*}$	$7.4x10^{-13}$
1.275	$^{22}Ne^{*}1.275\rightarrow g.s.$	$^{22}Ne(p,p')^{22}Ne^{*}$	$4.9x10^{-12}$
		$^{22}Ne(\alpha,\alpha')^{22}Ne^{*}$	$4.9x10^{-12}$
		$^{22}Ne(p,n)^{22}Na(e^{+};\varepsilon)^{22}Ne^{*}(100\%)$	$1.2x10^{8}$
		$^{25}Mg(p,x)^{22}Na(e^{+},\varepsilon)^{22}Ne^{*}(100\%)$	$1.2x10^{8}$
		$^{24}Mg(p,x)^{22}Na(e^{+};\varepsilon)^{22}Ne^{*}(100\%)$	$1.2x10^{8}$
		$^{28}Si(p,x)^{22}Na(e^{+};\varepsilon)^{22}Ne^{*}(100\%)$	$1.2x10^{8}$

Photon Energy (MeV)	Emission Mechanism	Production Processes	Mean Life (sec)
1.334	$^{52}Cr^{*}2.763\rightarrow^{52}Cr^{*}1\ 434$	$^{56}Fe(p,x)^{52}Cr^{*}$	--
1.369	$^{24}Mg^{*}1.369\rightarrow g.s.$	$^{24}Mg(p,p')^{24}Mg^{*}$	$1.75x10^{-12}$
		$^{24}Mg(\alpha,\alpha')^{24}Mg^{*}$	$1.75x10^{-12}$
		$^{28}Si(p,x)^{24}Mg^{*}$	$1.75x10^{-12}$
1.370	$^{55}Fe^{*}2.301\rightarrow^{55}Fe^{*}0\ 931$	$^{56}Fe(p,pn)^{55}Fe^{*}$	--
1.408	$^{54}Fe^{*}1.408\rightarrow g.s.$	$^{56}Fe(p,x)^{54}Fe^{*}$	$1.3x10^{-12}$
1.408	$^{55}Fe^{*}1.408\rightarrow g.s.$	$^{56}Fe(p,pn)^{55}Fe^{*}$	--
		$^{56}Fe(p,2n)^{55}Co(e^{+};\varepsilon)^{55}Fe^{*}(18\%)$	$9.5x10^{4}$
1.434	$^{52}Cr^{*}1.434\rightarrow g.s.$	$^{56}Fe(p,x)^{52}Cr^{*}$	$1.3x10^{-12}$
		$^{56}Fe(p,x)^{52}Mn^{*}(e^{+};\varepsilon)^{52}Cr^{*}(100\%)$	$1.8x10^{3}$
		$^{56}Fe(p,x)^{52}Mn(e^{+};\varepsilon)^{52}Cr^{*}(100\%)$	$7.1x10^{5}$
1.600	$^{23}Ng^{*}2.051\rightarrow^{23}Mg^{*}0.451$	$^{24}Mg(p,pn)^{23}Mg^{*}$	$8x10^{-14}$
1.632	$^{14}N^{*}3.945\rightarrow^{14}N^{*}2\ 313$	$^{14}N(p,p')^{14}N^{*}$	$4.5x10^{-15}$
		$^{14}N(\alpha,\alpha')^{14}N^{*}$	$4.5x10^{-15}$
		$^{16}O(p,x)^{14}N^{*}$	$4.5x10^{-15}$
1.634	$^{20}Ne^{*}1.634\rightarrow g.s.$	$^{20}Ne(p,p')^{20}Ne^{*}$	$1\ 2x10^{-12}$
		$^{20}Ne(\alpha,\alpha')^{20}Ne^{*}$	$1.2x10^{-12}$
		$^{20}Ne(p,n)^{20}Na(e^{+})^{20}Ne^{*}(80\%)$	$6.4x10^{-1}$
		$^{24}Mg(p,x)^{20}Ne^{*}$	$1.2x10^{-12}$
		$^{28}Si(p,x)^{20}Ne^{*}$	$1.2x10^{-12}$
1.636	$^{23}Na^{*}2.076\rightarrow^{23}Na^{*}0.440$	$^{24}Mg(p,2p)^{23}Na^{*}$	$4x10^{-14}$
1 772	$^{56}Fe^{*}3.857\rightarrow^{56}Fe^{*}2.085$	$^{56}Fe(p,p')^{56}Fe^{*}$	$3.3x10^{-14}$
		$^{56}Fe(p,n)^{56}Co(e^{+};\varepsilon)^{56}Fe^{*}(16\%)$	$9.6x10^{6}$
1.779	$^{28}Si^{*}1.779\rightarrow g.s.$	$^{28}Si(p,p')^{28}Si^{*}$	$6\ 8x10^{-13}$
		$^{28}Si(\alpha,\alpha')^{28}Si^{*}$	$6.8x10^{-13}$
		$^{32}S(p,x)^{28}Si^{*}$	$6.8x10^{-13}$
1.809	$^{26}Mg^{*}1.809\rightarrow g.s.$	$^{26}Mg(p,p')^{26}Mg^{*}$	$4x10^{-13}$
		$^{26}Mg(\alpha,\alpha')^{26}Mg^{*}$	$4x10^{-13}$
		$^{26}Mg(p,n)^{26}Al(e^{+};\varepsilon)^{26}Mg^{*}(100\%)$	$3.4x10^{13}$
		$^{27}Al(p,pn)^{26}Al(e^{+};\varepsilon)^{26}Mg^{*}(100\%)$	$3.4x10^{13}$
		$^{28}Si(p,x)^{26}Al(e^{+};\varepsilon)^{26}Mg^{*}(100\%)$	$3.4x10^{13}$
1.811	$^{56}Fe^{*}2.658\rightarrow^{56}Fe^{*}0.847$	$^{56}Fe(p,p')^{56}Fe^{*}$	$4x10^{-14}$
1.995	$^{11}C^{*}1.995\rightarrow g.s.$	$^{12}C(p,pn)^{11}C^{*}$	--
2 029	$^{31}P^{*}3.295\rightarrow^{31}P^{*}1.266$	$^{32}S(p,2p)^{31}P^{*}$	$1.4x10^{-13}$
2.034	$^{31}S^{*}3\ 283\rightarrow^{31}S^{*}1.249$	$^{32}S(p,pn)^{31}S^{*}$	--
2.094	$^{56}Fe^{*}2.941\rightarrow^{56}Fe^{*}0\ 847$	$^{56}Fe(p,p')^{56}Fe^{*}$	$2.2x10^{-13}$
2.113	$^{56}Fe^{*}2.960\rightarrow^{56}Fe^{*}0.847$	$^{56}Fe(p,p')^{56}Fe^{*}$	$3\ 9x10^{-14}$
2.124	$^{11}B^{*}2.124\rightarrow g.s$	$^{12}C(p,2p)^{11}B^{*}$	$5.4x10^{-15}$
2.230	$^{32}S^{*}2.230\rightarrow g.s.$	$^{32}S(p,p')^{32}S^{*}$	$2.4x10^{-13}$
		$^{32}S(\alpha,\alpha')^{32}S^{*}$	$2.4x10^{-13}$
2.232	$^{31}S^{*}2.23Z\rightarrow g.s.$	$^{32}S(p,pn)^{31}S^{*}$	$3.2x10^{-13}$
2.234	$^{31}P^{*}2.234\rightarrow g.s$	$^{32}S(p,2p)^{31}P^{*}$	$4\ 0x10^{-13}$
2.313	$^{14}N^{*}2\ 313\rightarrow g.s.$	$^{14}N(p,p')^{14}N^{*}$	$8.5x10^{-14}$
		$^{14}N(\alpha,\alpha')^{14}N^{*}$	$8\ 5x10^{-14}$
		$^{14}N(p,n)^{14}O(e^{+})^{14}N^{*}(100\%)$	102
		$^{16}O(p,x)^{14}N^{*}$	$8.5x10^{-14}$
		$^{16}O(p,x)^{14}O(e^{+})^{14}N^{*}(100\%)$	102

Table II-3 (cont.)

Photon Energy (Mev)	Emission Mechanism	Production Processes	Mean Life (sec)
2.599	$^{56}Fe^{*3.446}\rightarrow^{56}Fe^{*0.847}$	$^{56}Fe(p,n)^{56}Co(e^+;c)^{56}Fe(17\%)$	9.6×10^{6}
2.613	$^{20}Ne^{*4.247}\rightarrow^{20}Ne^{*1.634}$	$^{20}Ne(p,p')^{20}Ne^{*}$	9.3×10^{-14}
		$^{20}Ne(\alpha,\alpha')^{20}Ne^{*}$	9.3×10^{-14}
		$^{24}Mg(p,x)^{20}Ne^{*}$	9.3×10^{-14}
		$^{28}Si(p,x)^{20}Ne^{*}$	9.3×10^{-14}
2.640	$^{23}Na^{*2.640}\rightarrow g.s.$	$^{24}Mg(p,2p)^{23}Na^{*}$	1.1×10^{-13}
2.741	$^{16}O^{*8.872}\rightarrow^{16}O^{*6.131}$	$^{16}O(p,p')^{16}O^{*}$	1.8×10^{-13}
2.754	$^{24}Mg^{*4.123}\rightarrow^{24}Mg^{*1.369}$	$^{24}Mg(p,p')^{24}Mg^{*}$	5.4×10^{-14}
		$^{24}Mg(\alpha,\alpha')^{24}Mg^{*}$	5.4×10^{-14}
3.334	$^{20}Ne^{*4.968}\rightarrow^{20}Ne^{*1.634}$	$^{20}Ne(p,p')^{20}Ne^{*}$	4.8×10^{-12}
		$^{20}Ne(\alpha,\alpha')^{20}Ne^{*}$	4.8×10^{-12}
3.561	$^{6}Li^{*3.562}\rightarrow g.s.$	$^{4}He(\alpha,pn)^{6}Li^{*}$	$>1.3\times10^{-19}$
3.684	$^{13}C^{*3.684}\rightarrow g.s.$	$^{13}C(p,p')^{13}C^{*}$	1.5×10^{-15}
		$^{13}C(\alpha,\alpha')^{13}C^{*}$	1.5×10^{-15}
		$^{16}O(p,x)^{13}C^{*}$	1.5×10^{-15}
3.736	$^{40}Ca^{*3.736}\rightarrow g.s.$	$^{40}Ca(p,p')^{40}Ca^{*}$	6.1×10^{-11}
		$^{40}Ca(\alpha,\alpha')^{40}Ca^{*}$	6.1×10^{-11}
3.853	$^{13}C^{*3.684}\rightarrow g.s.$	$^{13}C(p,p')^{13}C^{*}$	1.1×10^{-11}
		$^{13}C(\alpha,\alpha')^{13}C^{*}$	1.1×10^{-11}
		$^{16}O(p,x)^{13}C^{*}$	1.1×10^{-11}
4.438	$^{12}C^{*4.439}\rightarrow g.s.$	$^{12}C(p,p')^{12}C^{*}$	5.62×10^{-14}
		$^{12}C(\alpha,\alpha')^{12}C^{*}$	5.62×10^{-14}
		$^{14}N(p,x)^{12}C^{*}$	5.62×10^{-14}
		$^{14}N(\alpha,x)^{12}C^{*}$	5.62×10^{-14}
		$^{16}O(p,x)^{12}C^{*}$	5.62×10^{-14}
		$^{16}O(\alpha,x)^{12}C^{*}$	5.62×10^{-14}
4.443	$^{11}B^{*4.444}\rightarrow g.s.$	$^{12}C(p,2p)^{11}B^{*}$	1.2×10^{-15}
		$^{12}C(\alpha,x)^{11}B^{*}$	1.2×10^{-15}
5.099	$^{28}Si^{*6.879}\rightarrow^{28}Si^{*1.779}$	$^{28}Si(p,p')^{28}Si^{*}$	2.5×10^{-12}
		$^{28}Si(\alpha,\alpha')^{28}Si^{*}$	2.5×10^{-12}

Photon Energy (MeV)	Emission Mechanism	Production Processes	Mean Life (sec)
5.105	$^{14}N^{*5.106}\rightarrow g.s.$	$^{14}N(p,p')^{14}N^{*}$	1.2×10^{-11}
		$^{14}N(\alpha,\alpha')^{14}N^{*}$	1.2×10^{-11}
		$^{16}O(p,x)^{14}N^{*}$	1.2×10^{-11}
		$^{16}O(\alpha,x)^{14}N^{*}$	1.2×10^{-11}
5.180	$^{15}O^{*5.181}\rightarrow g.s.$	$^{16}O(p,pn)^{15}O^{*}$	$<10^{-13}$
		$^{16}O(\alpha,x)^{15}O^{*}$	$<10^{-13}$
5.241	$^{15}O^{*5.242}\rightarrow g.s.$	$^{16}O(p,pn)^{15}O^{*}$	3.2×10^{-12}
		$^{16}O(\alpha,x)^{15}O^{*}$	3.2×10^{-12}
5.270	$^{15}N^{*5.271}\rightarrow g.s.$	$^{16}O(p,2p)^{15}N^{*}$	2.9×10^{-12}
		$^{16}O(\alpha,x)^{15}N^{*}$	2.9×10^{-12}
5.298	$^{15}N^{*5.299}\rightarrow g.s.$	$^{16}O(p,2p)^{15}N^{*}$	$<10^{-14}$
		$^{16}O(\alpha,x)^{15}N^{*}$	$<10^{-14}$
6.129	$^{16}O^{*6.131}\rightarrow g.s.$	$^{16}O(p,p')^{16}O^{*}$	2.4×10^{-11}
		$^{16}O(\alpha,\alpha')^{16}O^{*}$	2.4×10^{-11}
		$^{20}Ne(p,x)^{16}O^{*}$	2.4×10^{-11}
6.176	$^{15}O^{*6.177}\rightarrow g.s.$	$^{16}O(p,pn)^{15}O^{*}$	$<4.7\times10^{-14}$
		$^{16}O(\alpha,x)^{15}O^{*}$	$<4.7\times10^{-14}$
6.322	$^{15}N^{*6.324}\rightarrow g.s.$	$^{16}O(p,2p)^{15}N^{*}$	$<4\times10^{-14}$
		$^{16}O(\alpha,x)^{15}N^{*}$	$<4\times10^{-14}$
6.337	$^{11}C^{*6.339}\rightarrow g.s.$	$^{12}C(p,pn)^{11}C^{*}$	$<1.1\times10^{-13}$
6.478	$^{11}C^{*6.480}\rightarrow g.s.$	$^{12}C(p,pn)^{11}C^{*}$	$<2.5\times10^{-13}$
6.741	$^{11}B^{*6.743}\rightarrow g.s.$	$^{12}C(p,2p)^{11}B^{*}$	$<3\times10^{-13}$
6.791	$^{11}B^{*6.793}\rightarrow g.s.$	$^{12}C(p,2p)^{11}B^{*}$	$<5\times10^{-14}$
6.878	$^{28}Si^{*6.879}\rightarrow g.s.$	$^{28}Si(p,p')^{28}Si^{*}$	2.5×10^{-12}
		$^{28}Si(\alpha,\alpha')^{28}Si^{*}$	2.5×10^{-12}
6.917	$^{16}O^{*6.919}\rightarrow g.s.$	$^{16}O(p,p')^{16}O^{*}$	6.8×10^{-15}
		$^{16}O(\alpha,\alpha')^{16}O^{*}$	6.8×10^{-15}
7.117	$^{16}O^{*7.119}\rightarrow g.s.$	$^{16}O(p,p')^{16}O^{*}$	1.1×10^{-14}
		$^{16}O(\alpha,\alpha')^{16}O^{*}$	1.1×10^{-14}
7.299	$^{15}N^{*7.301}\rightarrow g.s.$	$^{16}O(p,2p)^{15}N^{*}$	$<2.5\times10^{-14}$

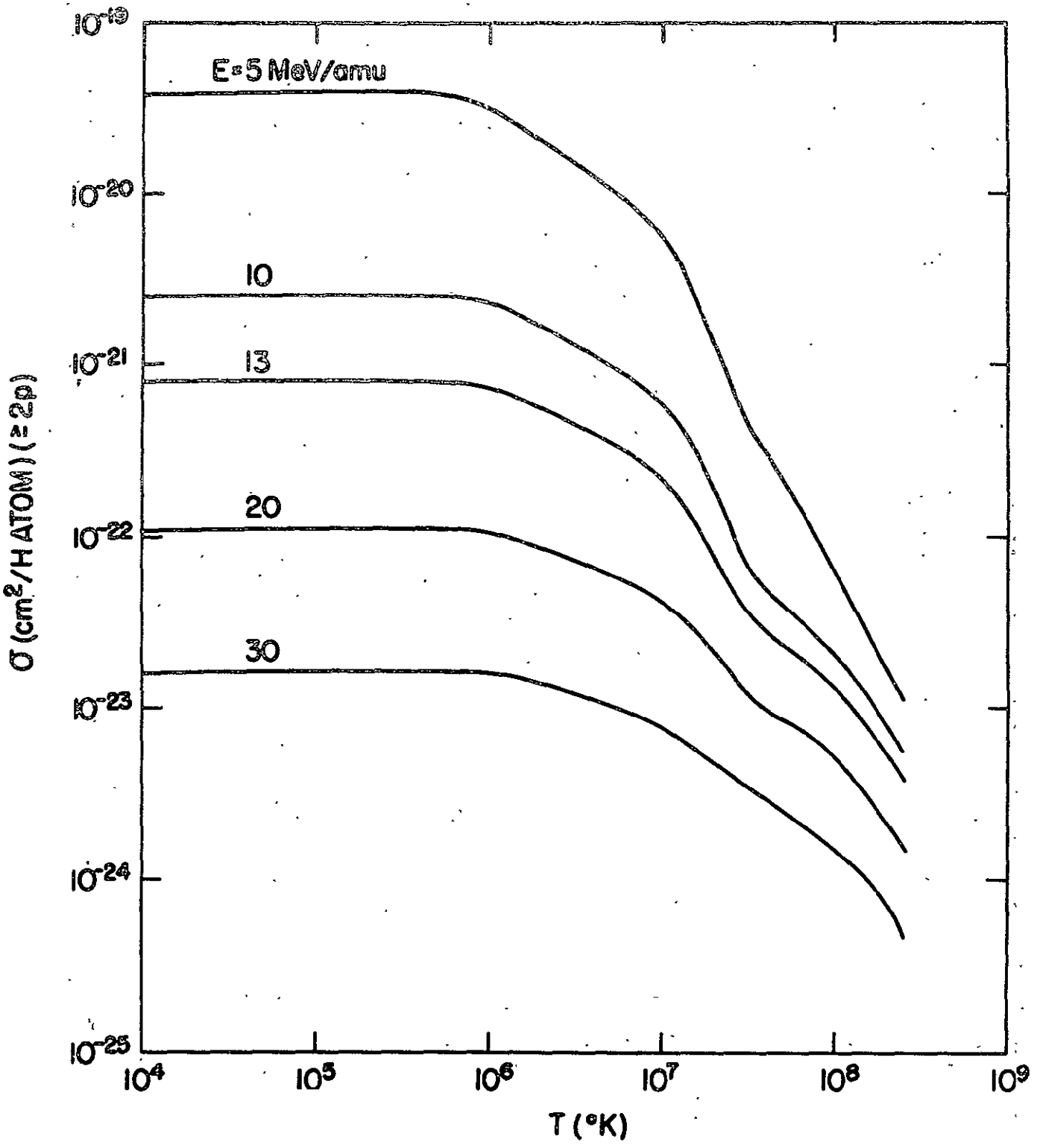
E=5 MeV/amu
10
13
20
30
σ (cm²/H ATOM) (≥2p)
T (°K)
10⁻¹⁹
10⁻²⁰
10⁻²¹
10⁻²²
10⁻²³
10⁻²⁴
10⁻²⁵
10⁴
10⁵
10⁶
10⁷
10⁸
10⁹

Figure II-1

Table III-1

ΔE (keV) for $B = 6 \times 10^{12}$ G

T = 35 keV

θ	N_e = 10^{22} cm^{-2}	10^{23} cm^{-2}	10^{24} cm^{-2}	10^{25} cm^{-2}
10°	106.2	136.5	162.2	182.3
30°	78.9	93.5	102.4	106.6
50°	47.0	52.7	56.7	59.8
70°	25.9	31.7	35.9	39.3
80°	19.0	24.7	29.1	32.6
90°	15.2	20.3	24.5	28.0

T = 20 keV

10°	80.6	102.2	120.3	136.6
30°	63.2	76.2	85.7	92.9
50°	41.3	46.1	49.8	52.7
70°	20.6	25.1	28.7	31.7
80°	14.0	18.2	21.7	24.7
90°	10.1	13.6	16.8	19.6

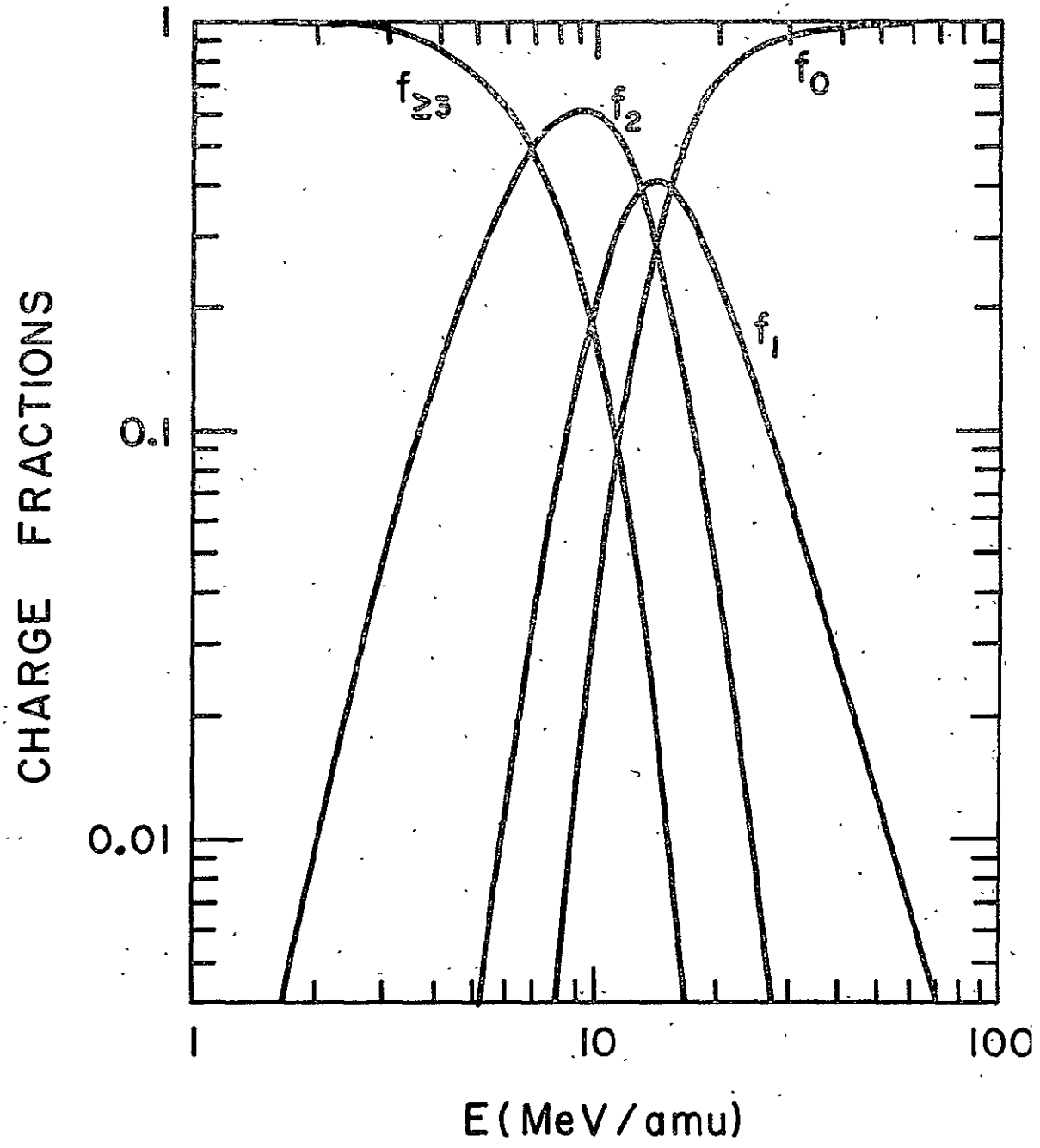

Figure II-3

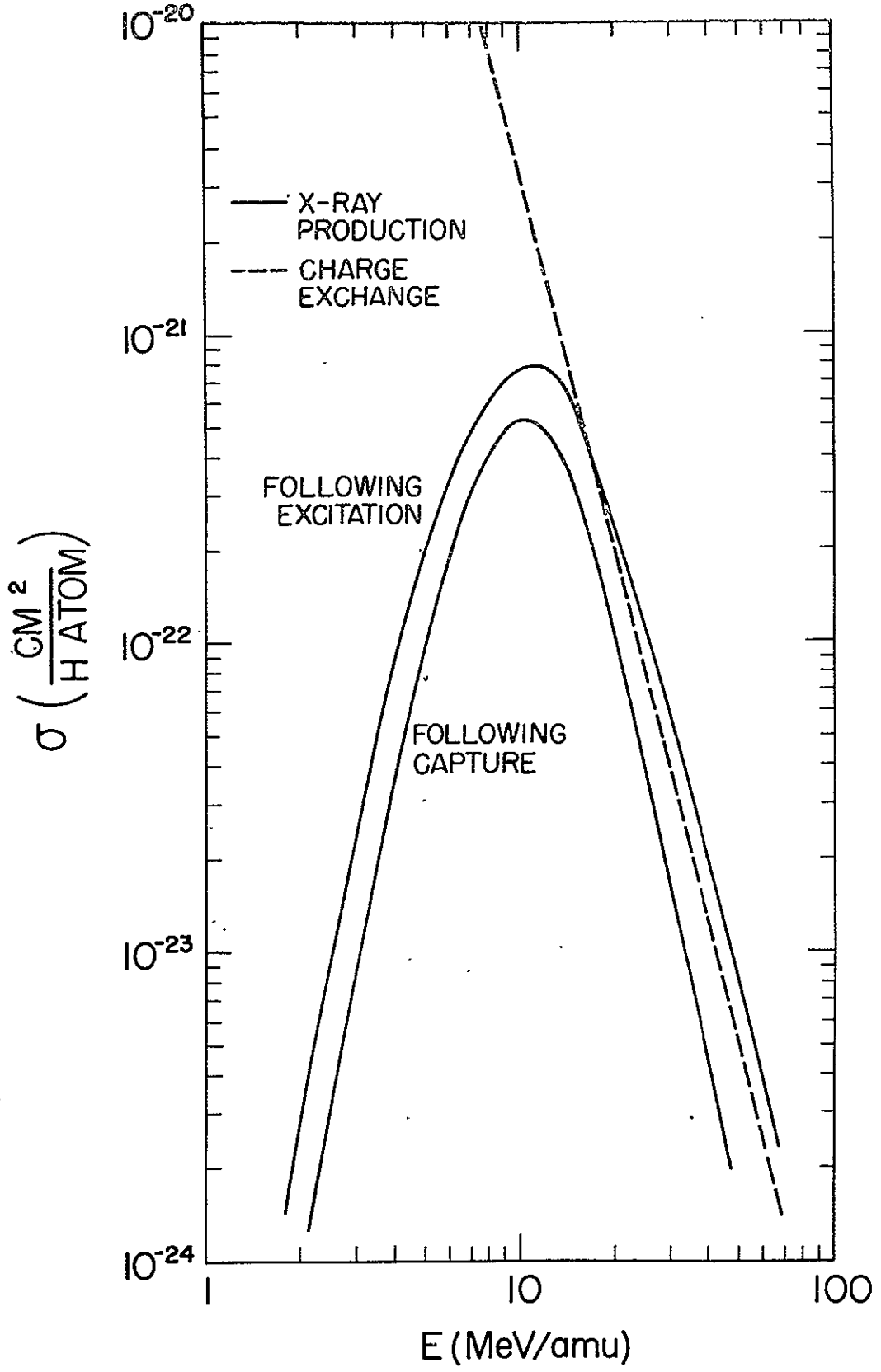
10^{-20}
10^{-21}
10^{-22}
10^{-23}
10^{-24}
X-RAY PRODUCTION
CHARGE EXCHANGE
FOLLOWING EXCITATION
FOLLOWING CAPTURE
$\sigma\left(\frac{CM^2}{H\ ATOM}\right)$
1
10
100
E (MeV/amu)

Figure II-2

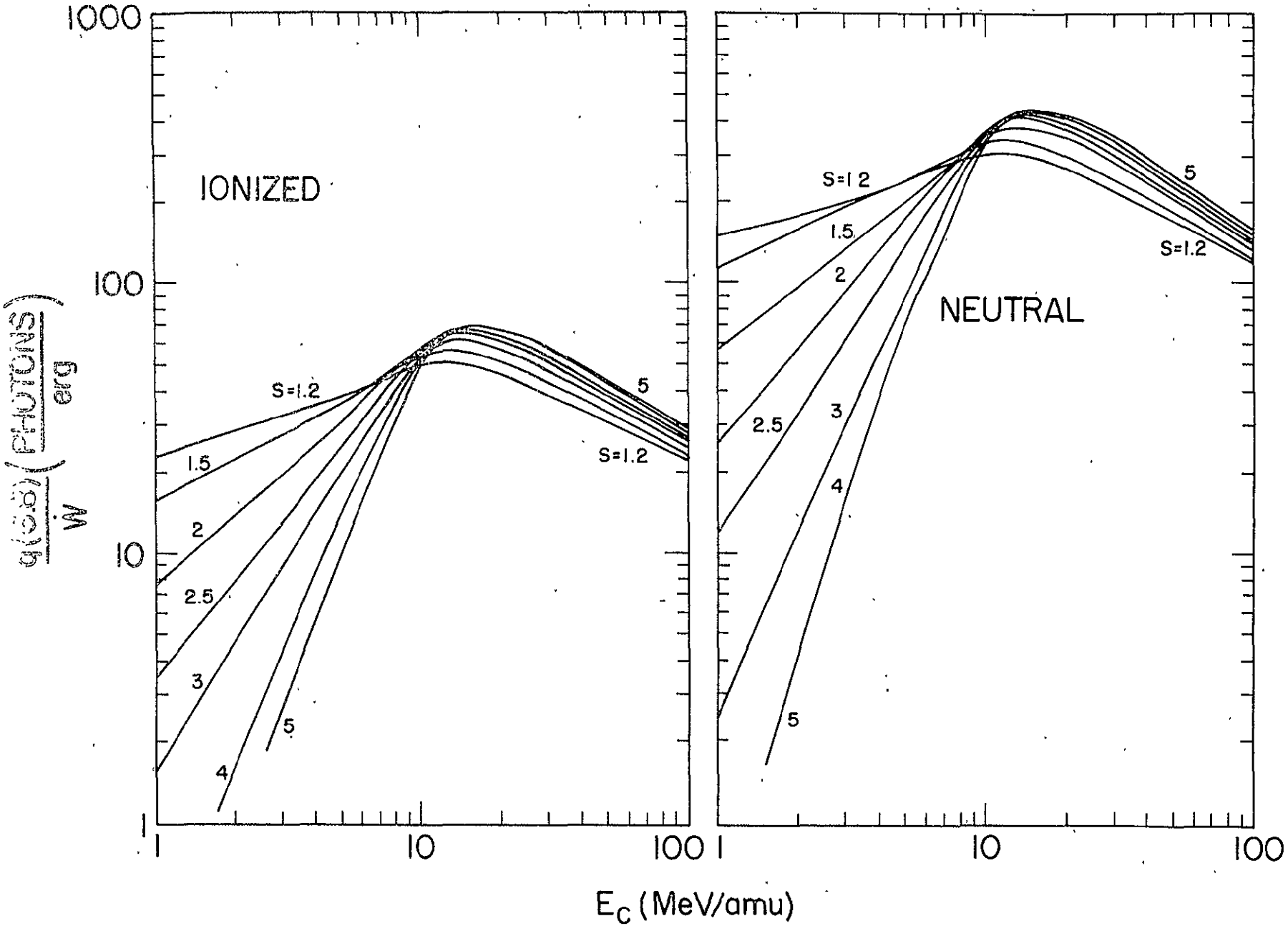
1000
100
10
1
IONIZED
NEUTRAL
S=1.2
1.5
2
2.5
3
4
5
1
10
100
$\frac{q(e,\theta)}{W}\left(\frac{\text{PHOTONS}}{\text{erg}}\right)$
E_C (MeV/amu)

Figure II-5

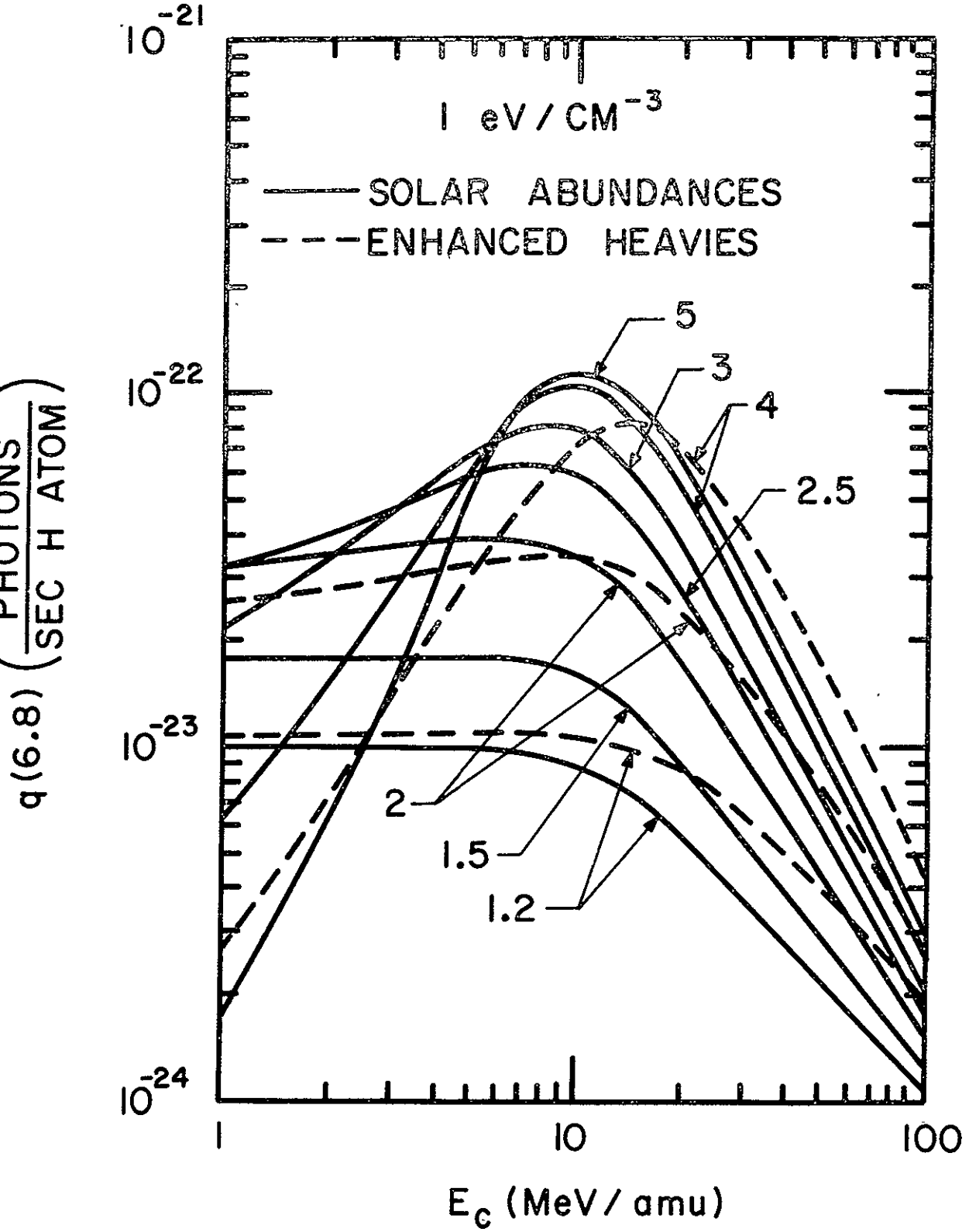
10^{-21}
10^{-22}
10^{-23}
10^{-24}
1 eV / CM^{-3}
SOLAR ABUNDANCES
ENHANCED HEAVIES
5
3
4
2.5
2
1.5
1.2
q(6.8) (PHOTONS / SEC H ATOM)
1
10
100
E_c (MeV / amu)

Figure II-4

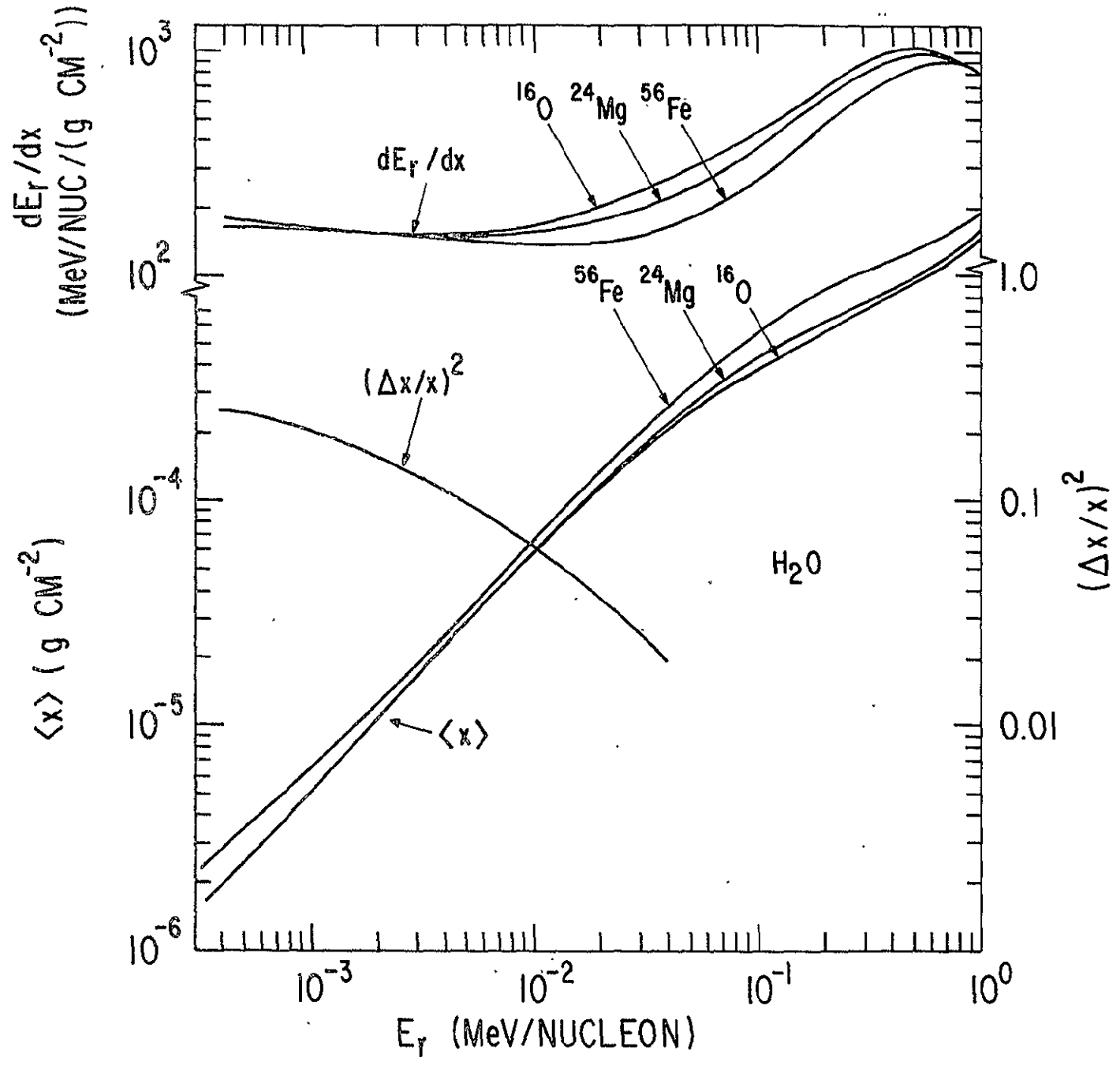
dE_r/dx (MeV/NUC/(g CM^-2))
10^3
10^2
10^-4
10^-5
10^-6
16O 24Mg 56Fe
dE_r/dx
56Fe 24Mg 16O
(Δx/x)^2
H2O
⟨x⟩
⟨x⟩ (g CM^-2)
1.0
0.1
0.01
(Δx/x)^2
10^-3
10^-2
10^-1
10^0
E_r (MeV/NUCLEON)

Figure II-7

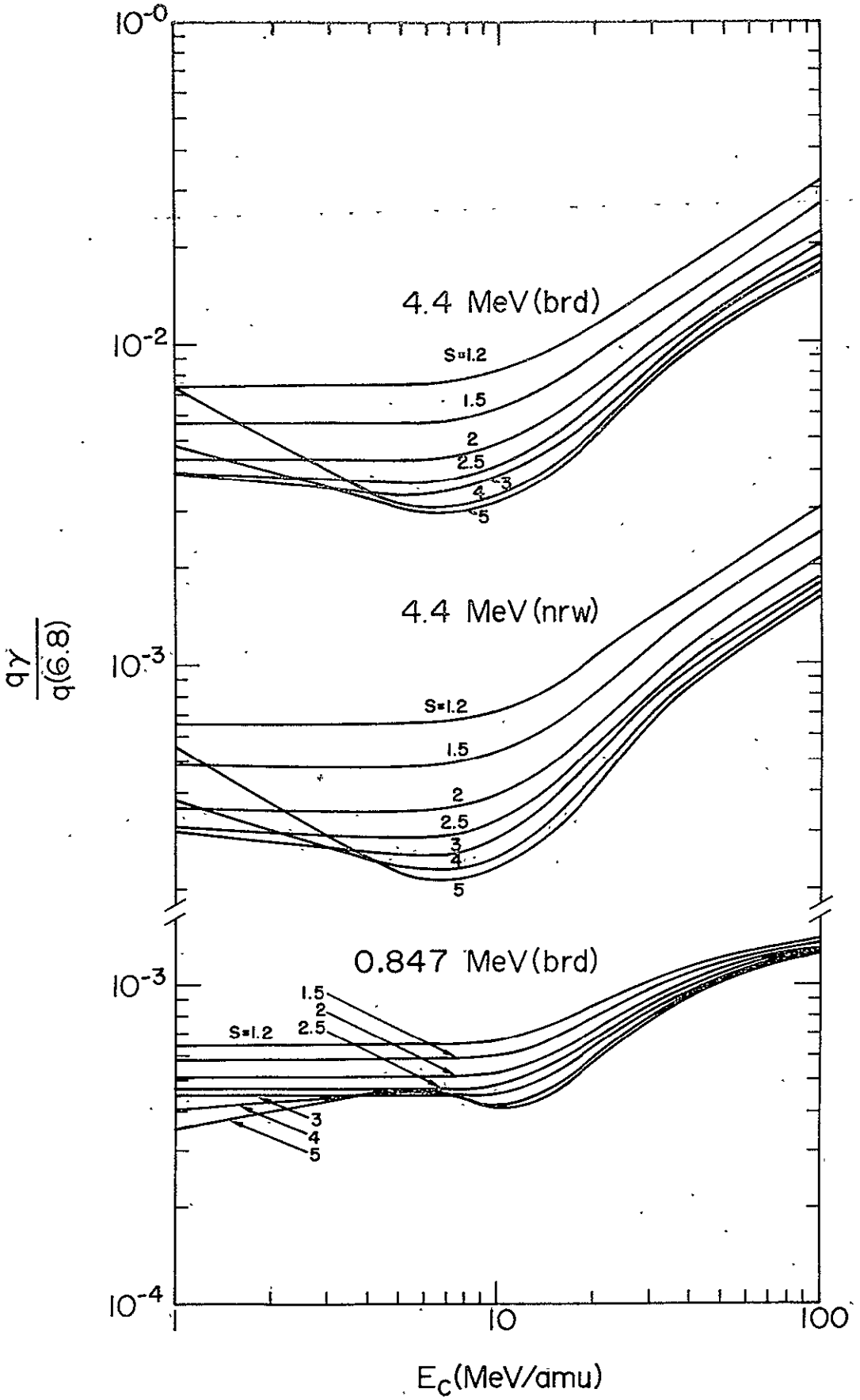
10^{-0}
10^{-2}
10^{-3}
10^{-3}
10^{-4}
4.4 MeV(brd)
S=1.2
1.5
2
2.5
3
4
5
4.4 MeV(nrw)
S=1.2
1.5
2
2.5
3
4
5
0.847 MeV(brd)
S=1.2
1.5
2
2.5
3
4
5
10
100
E_c(MeV/amu)
$\frac{q\gamma}{q(8.8)}$

Figure II-6

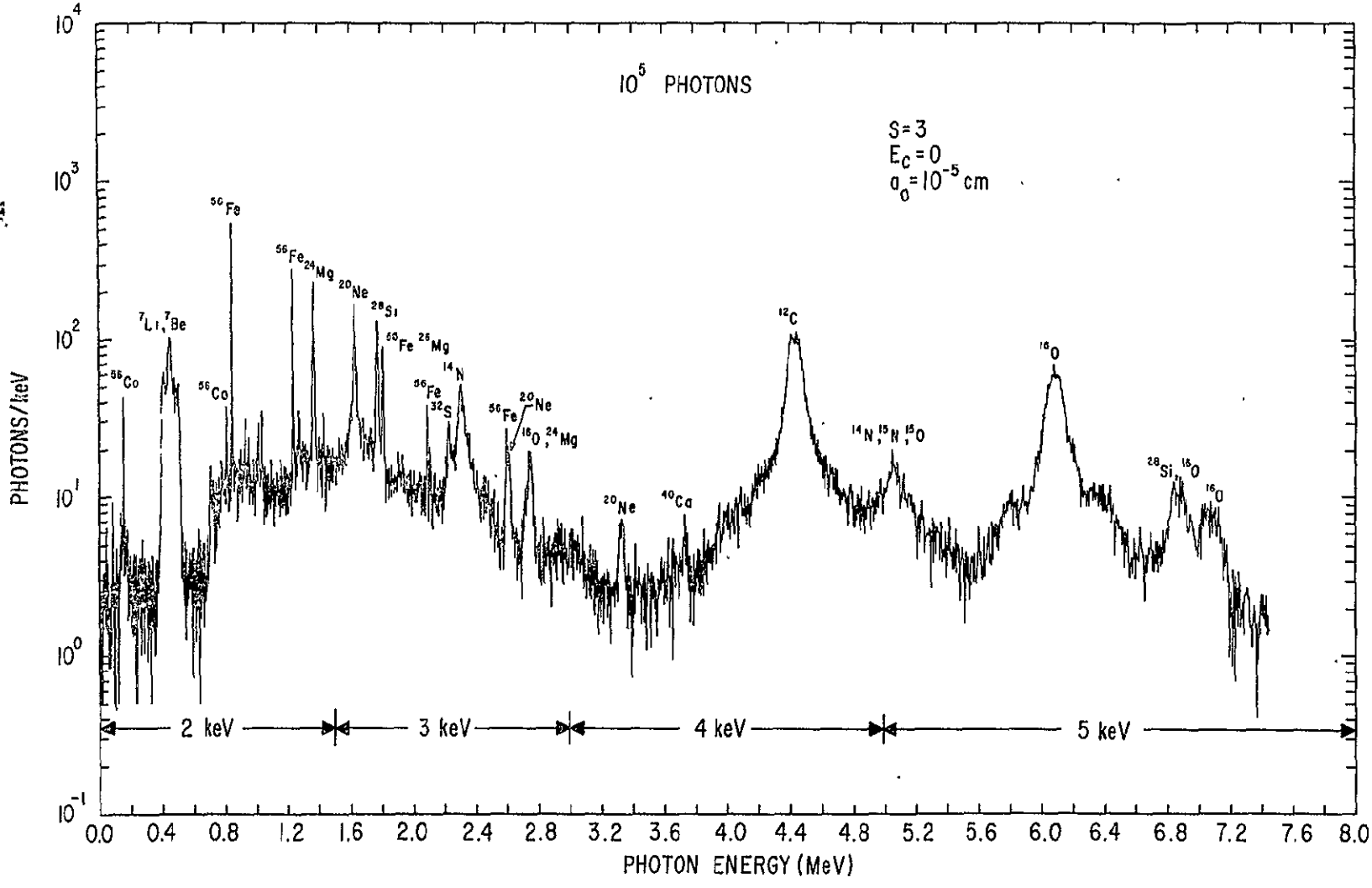

Figure II-9

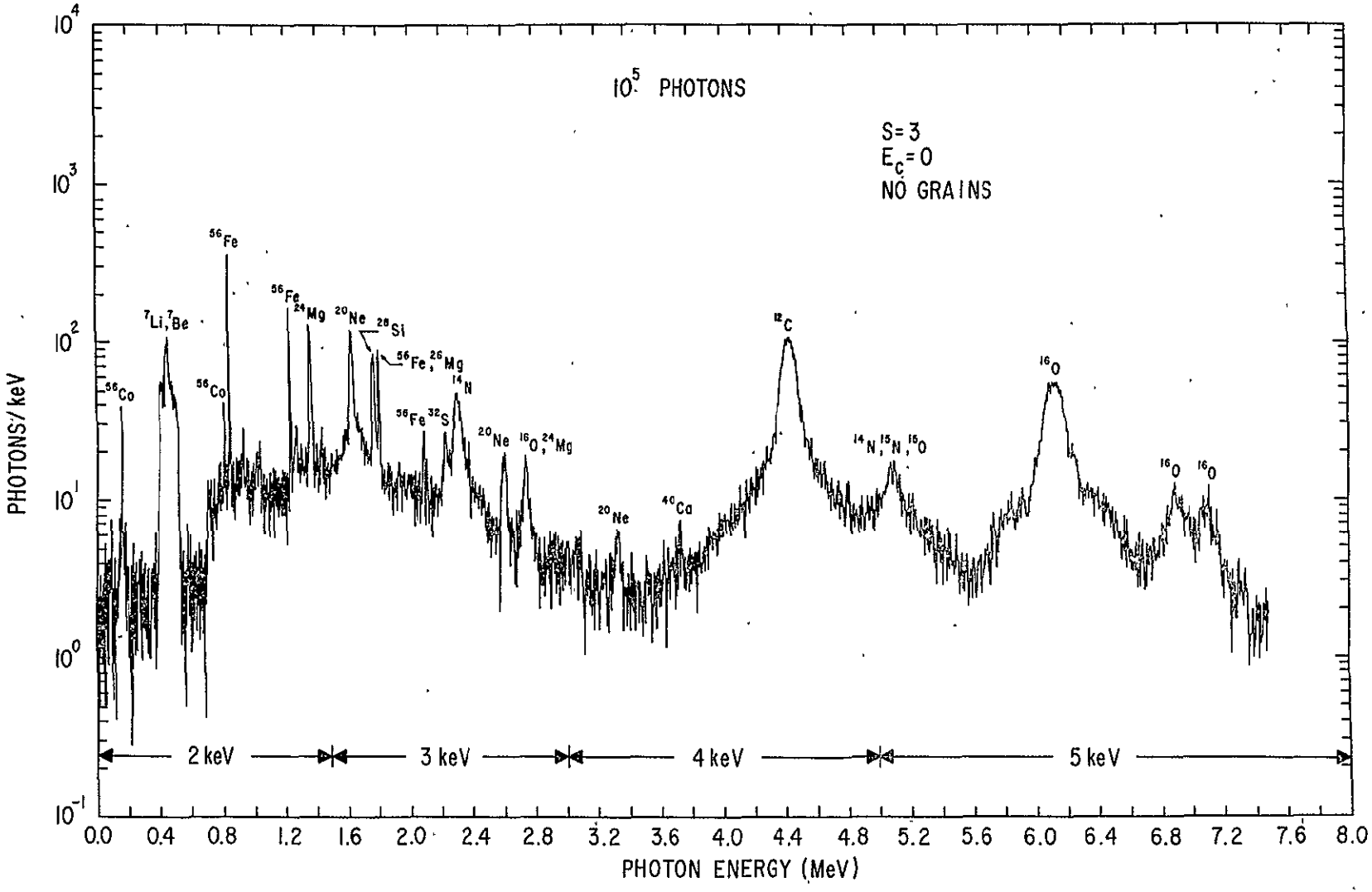
10^5 PHOTONS
S=3
E_c=0
NO GRAINS
PHOTONS/keV
PHOTON ENERGY (MeV)
^{56}Co
^{7}Li,^{7}Be
^{56}Co
^{56}Fe
^{56}Fe
^{24}Mg
^{20}Ne
^{28}Si
^{56}Fe,^{26}Mg
^{14}N
^{56}Fe
^{32}S
^{20}Ne
^{16}O,^{24}Mg
^{20}Ne
^{40}Ca
^{12}C
^{14}N,^{15}N,^{15}O
^{16}O
^{16}O
^{16}O
2 keV
3 keV
4 keV
5 keV

Figure II-8

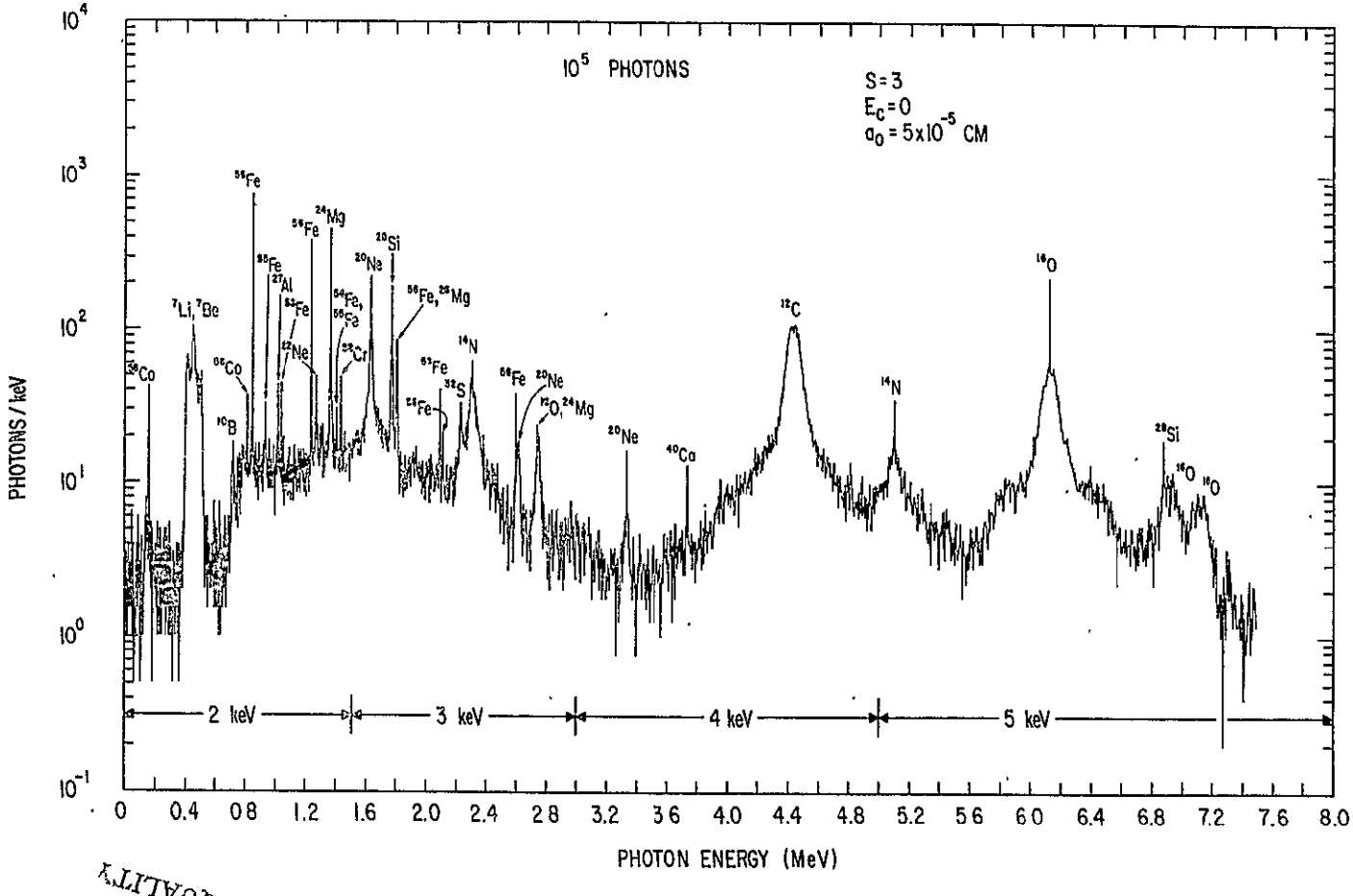

Figure II-11

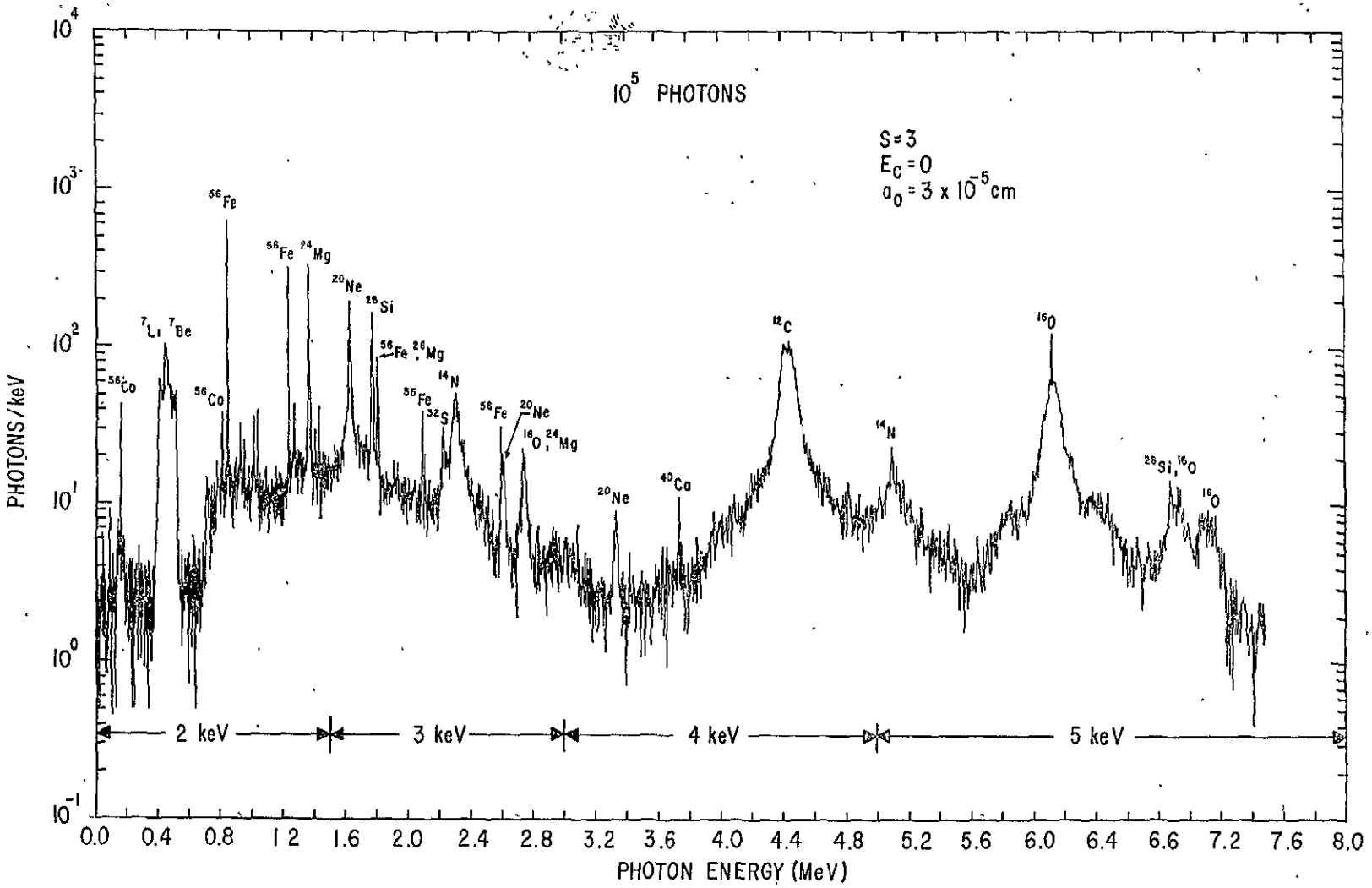
10^5 PHOTONS
S=3
E_C=0
a_0=3 x 10^{-5}cm
PHOTONS/keV
PHOTON ENERGY (MeV)
2 keV
3 keV
4 keV
5 keV
^{56}Co
^{7}Li, ^{7}Be
^{56}Co
^{56}Fe
^{56}Fe ^{24}Mg
^{20}Ne
^{28}Si
^{56}Fe, ^{26}Mg
^{14}N
^{56}Fe
^{32}S
^{56}Fe
^{20}Ne
^{16}O, ^{24}Mg
^{20}Ne
^{40}Ca
^{12}C
^{14}N
^{16}O
^{28}Si, ^{16}O
^{16}O

Figure II-10

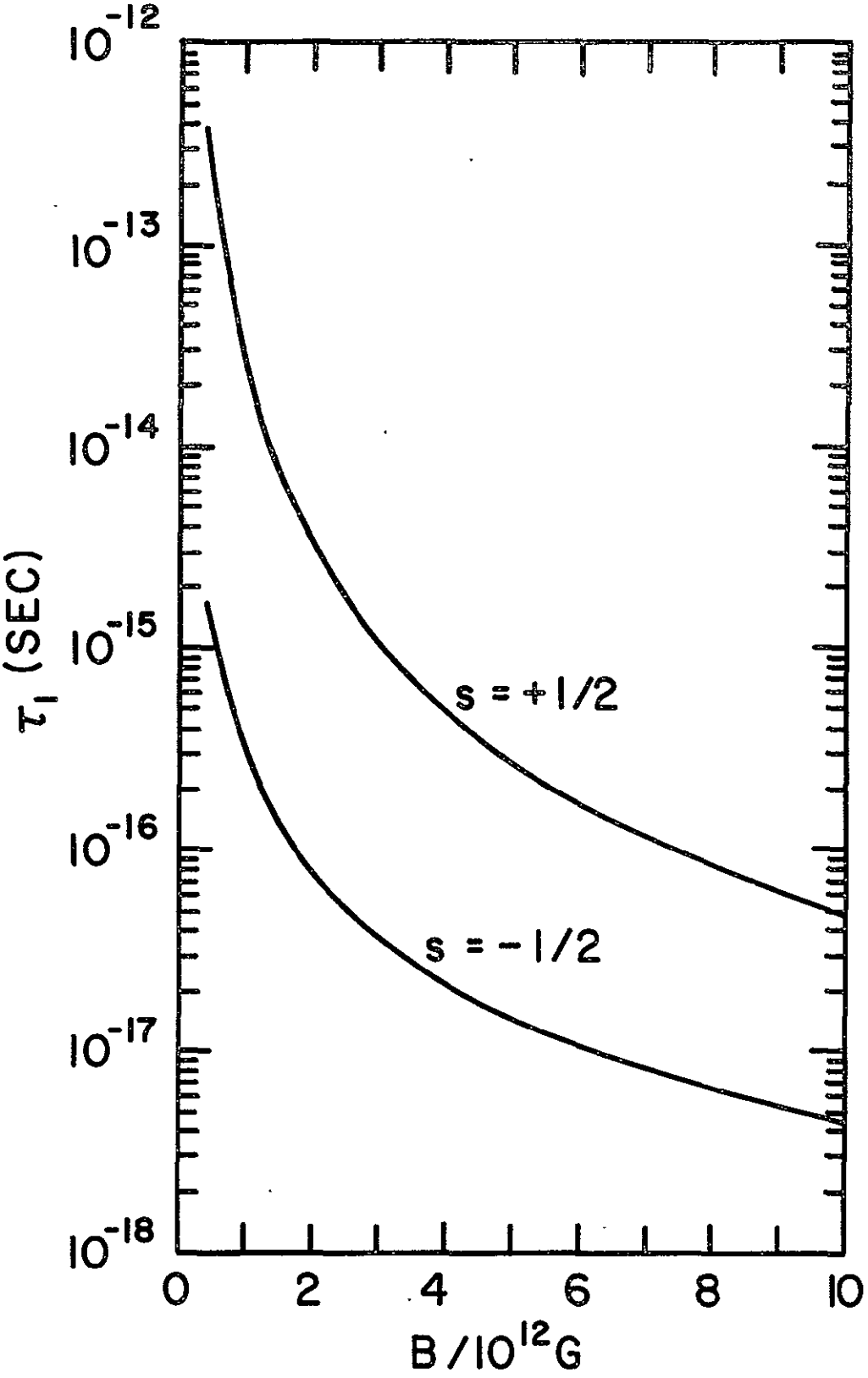
10^{-12}
10^{-13}
10^{-14}
10^{-15}
10^{-16}
10^{-17}
10^{-18}
τ_1 (SEC)
s = +1/2
s = −1/2
0
2
4
6
8
10
$B/10^{12}G$

Figure III-1

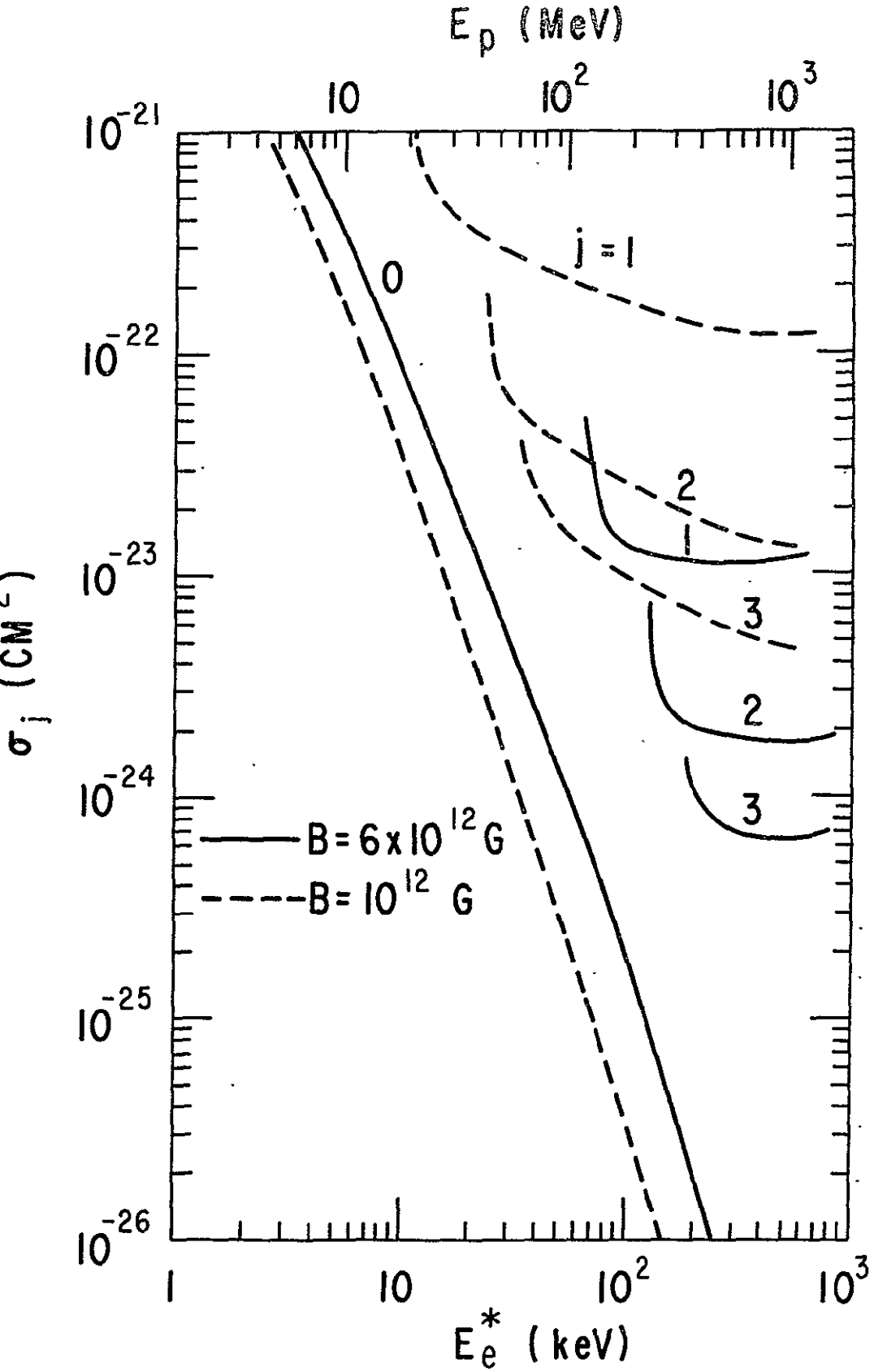
E_p (MeV)
10
10^2
10^3
10^{-21}
10^{-22}
10^{-23}
10^{-24}
10^{-25}
10^{-26}
σ_j (CM^2)
j = 1
0
2
3
2
3
B = 6×10^{12} G
B = 10^{12} G
1
10
10^2
10^3
E_e^* (keV)

Figure III-2

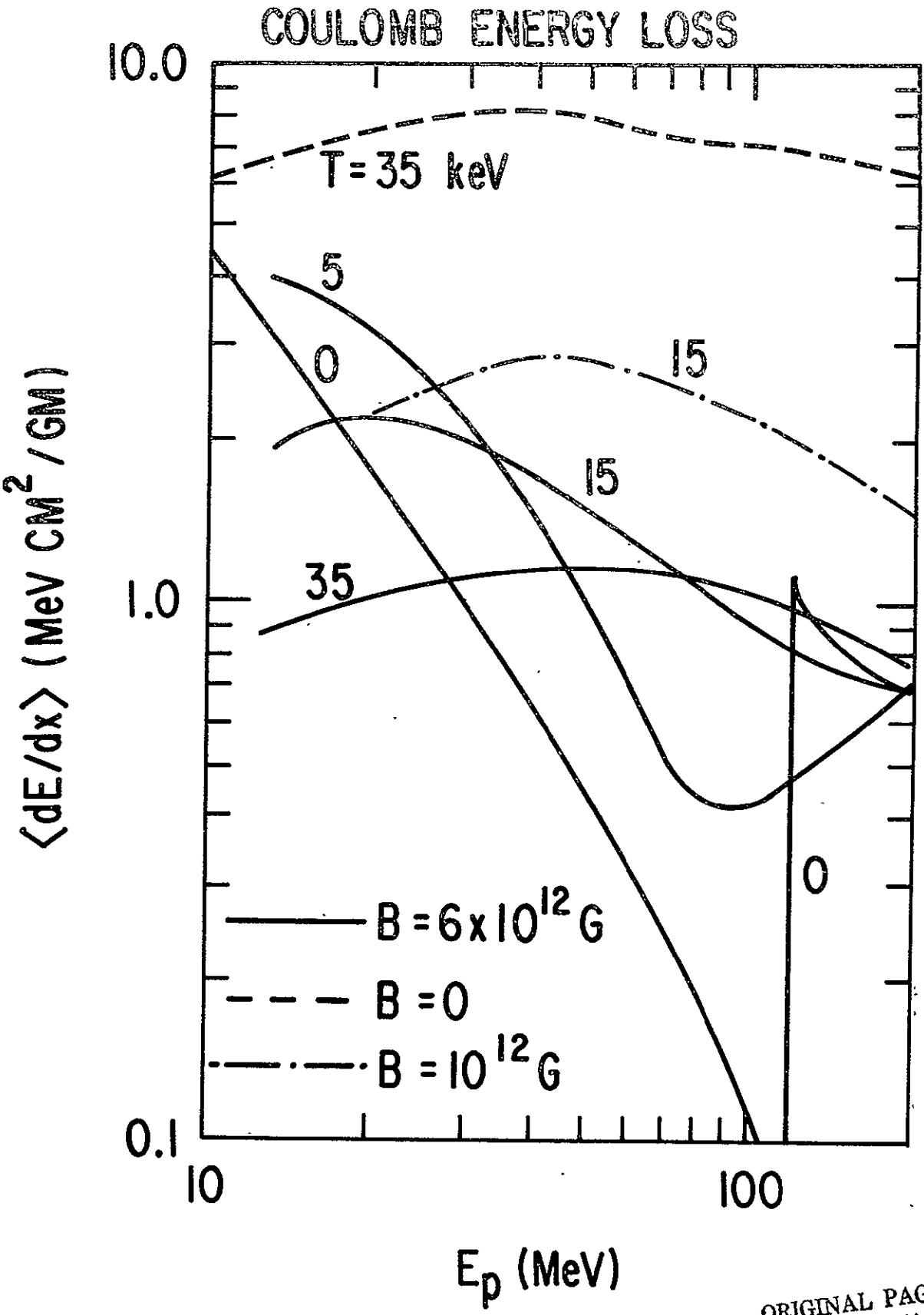

Figure III-3

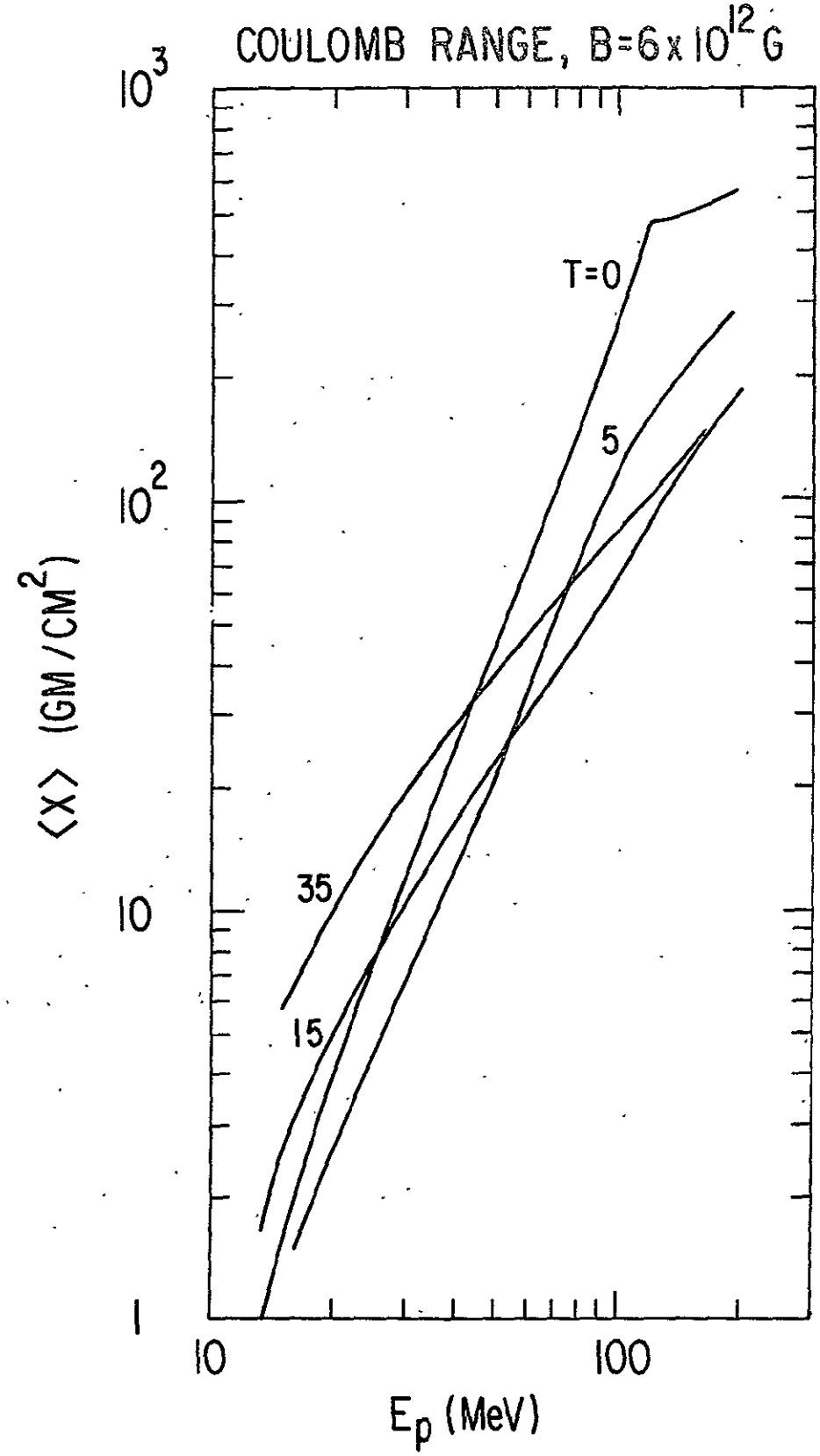
COULOMB RANGE, B=6x10^12 G
10^3
10^2
10
1
<X> (GM/CM^2)
T=0
5
35
15
10
100
Ep (MeV)

Figure III-4

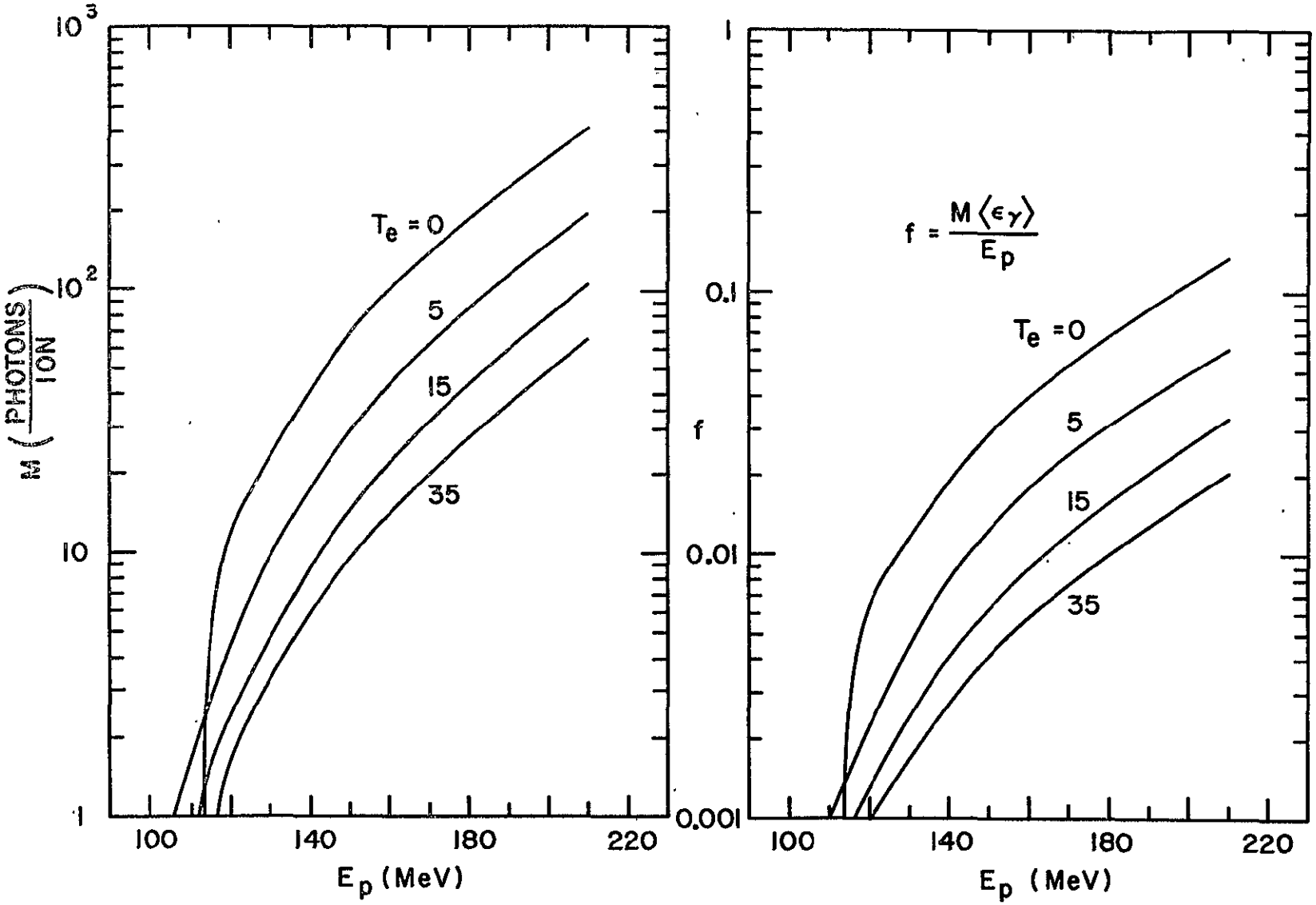
10^3
10^2
10
1
$M\left(\frac{\text{PHOTONS}}{\text{ION}}\right)$
$T_e = 0$
5
15
35
100
140
180
220
E_p (MeV)
1
0.1
0.01
0.001
f
$f = \frac{M\langle\epsilon_\gamma\rangle}{E_p}$
$T_e = 0$
5
15
35
100
140
180
220
E_p (MeV)

Figure III-5

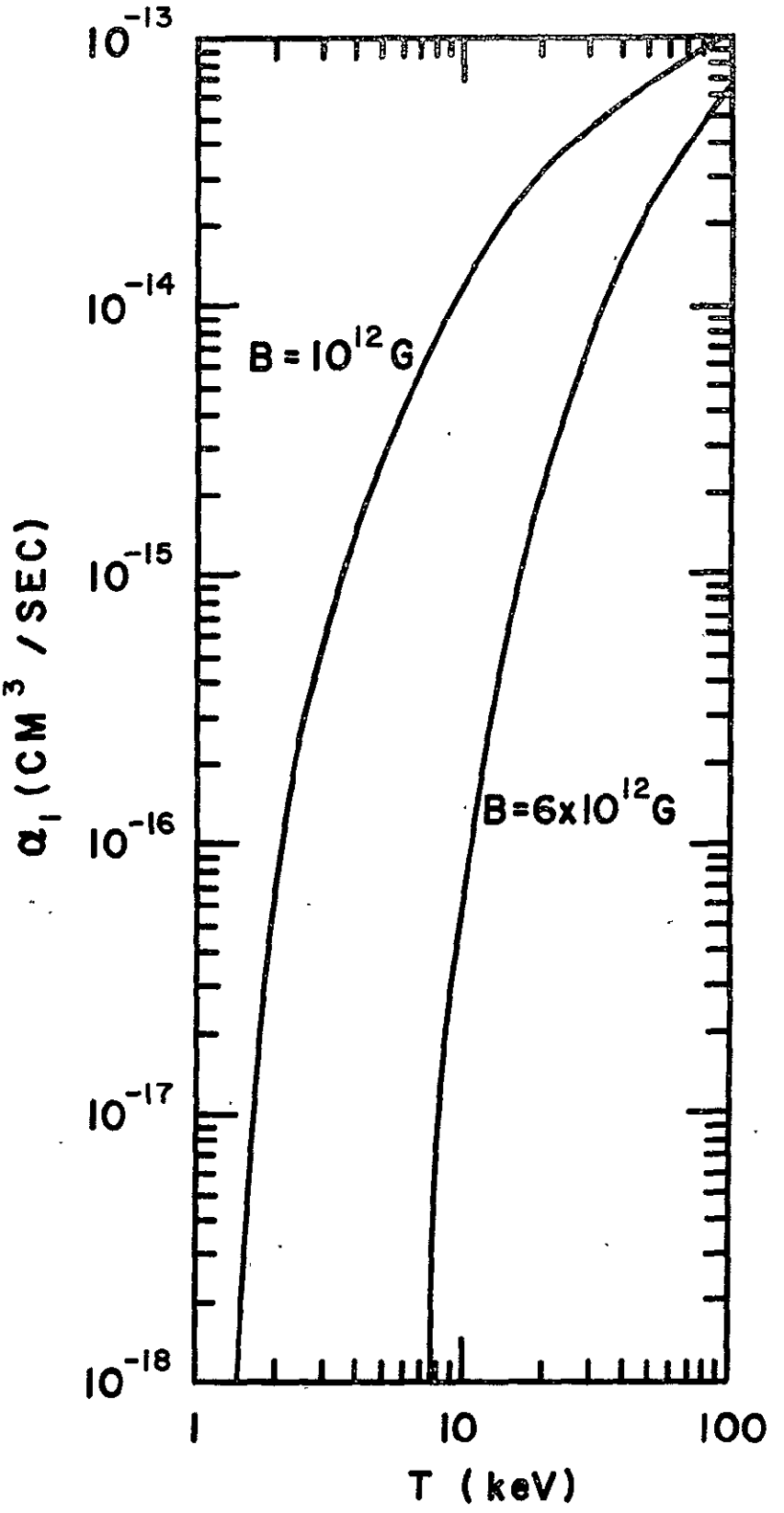
10^{-13}
10^{-14}
10^{-15}
10^{-16}
10^{-17}
10^{-18}
α_1 (CM^3 / SEC)
B = 10^{12} G
B = 6x10^{12} G
1
10
100
T (keV)

Figure III-6

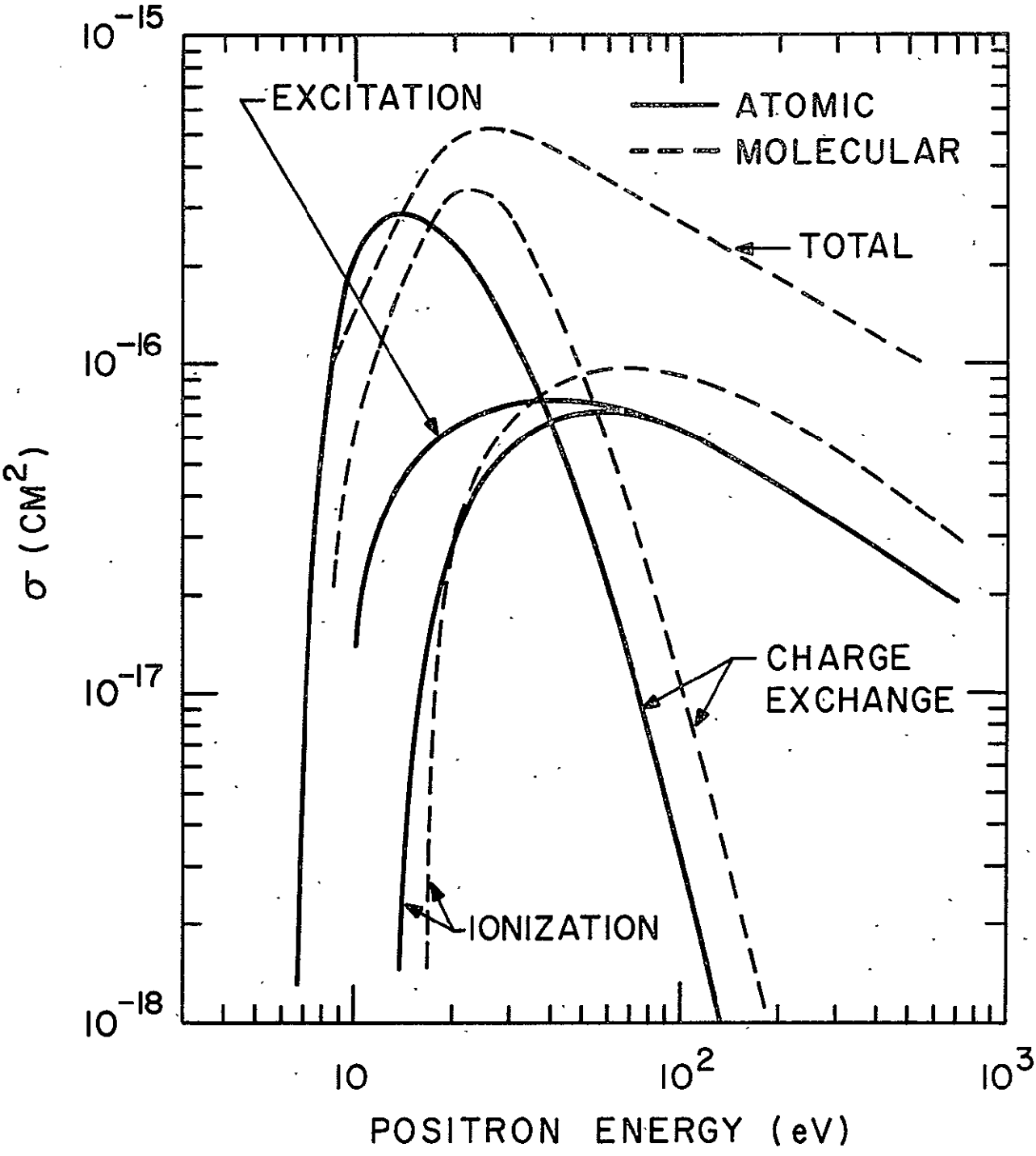
10^{-15}
10^{-16}
10^{-17}
10^{-18}
σ (CM^2)
EXCITATION
ATOMIC
MOLECULAR
TOTAL
CHARGE
EXCHANGE
IONIZATION
10
10^2
10^3
POSITRON ENERGY (eV)

Figure IV-1

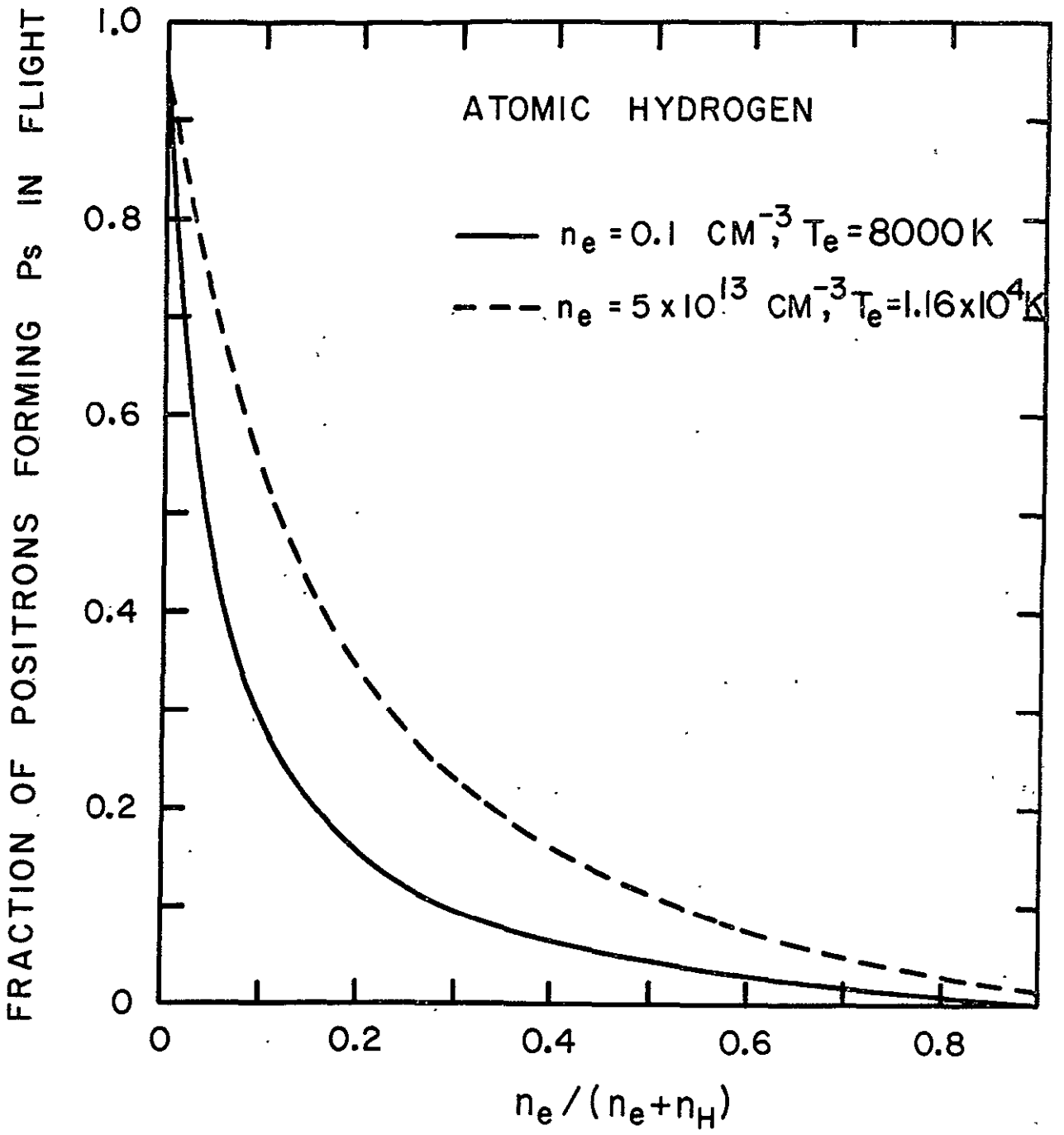
FRACTION OF POSITRONS FORMING Ps IN FLIGHT
1.0
0.8
0.6
0.4
0.2
0
0
0.2
0.4
0.6
0.8
ATOMIC HYDROGEN
$n_e = 0.1$ CM^{-3}, $T_e = 8000$ K
$n_e = 5 \times 10^{13}$ CM^{-3}, $T_e = 1.16 \times 10^4$ K
$n_e / (n_e + n_H)$

Figure IV-2

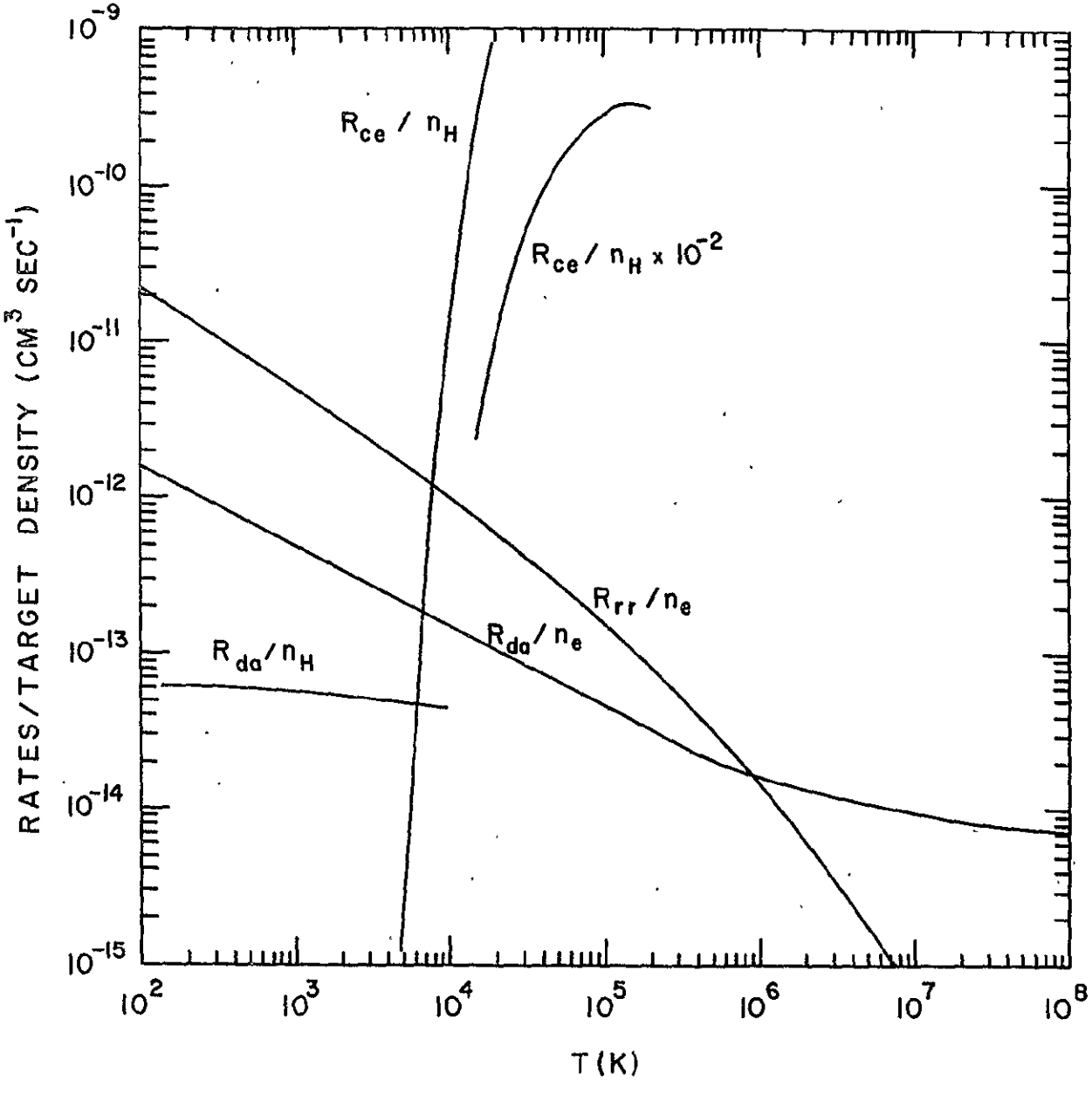

Figure IV-3

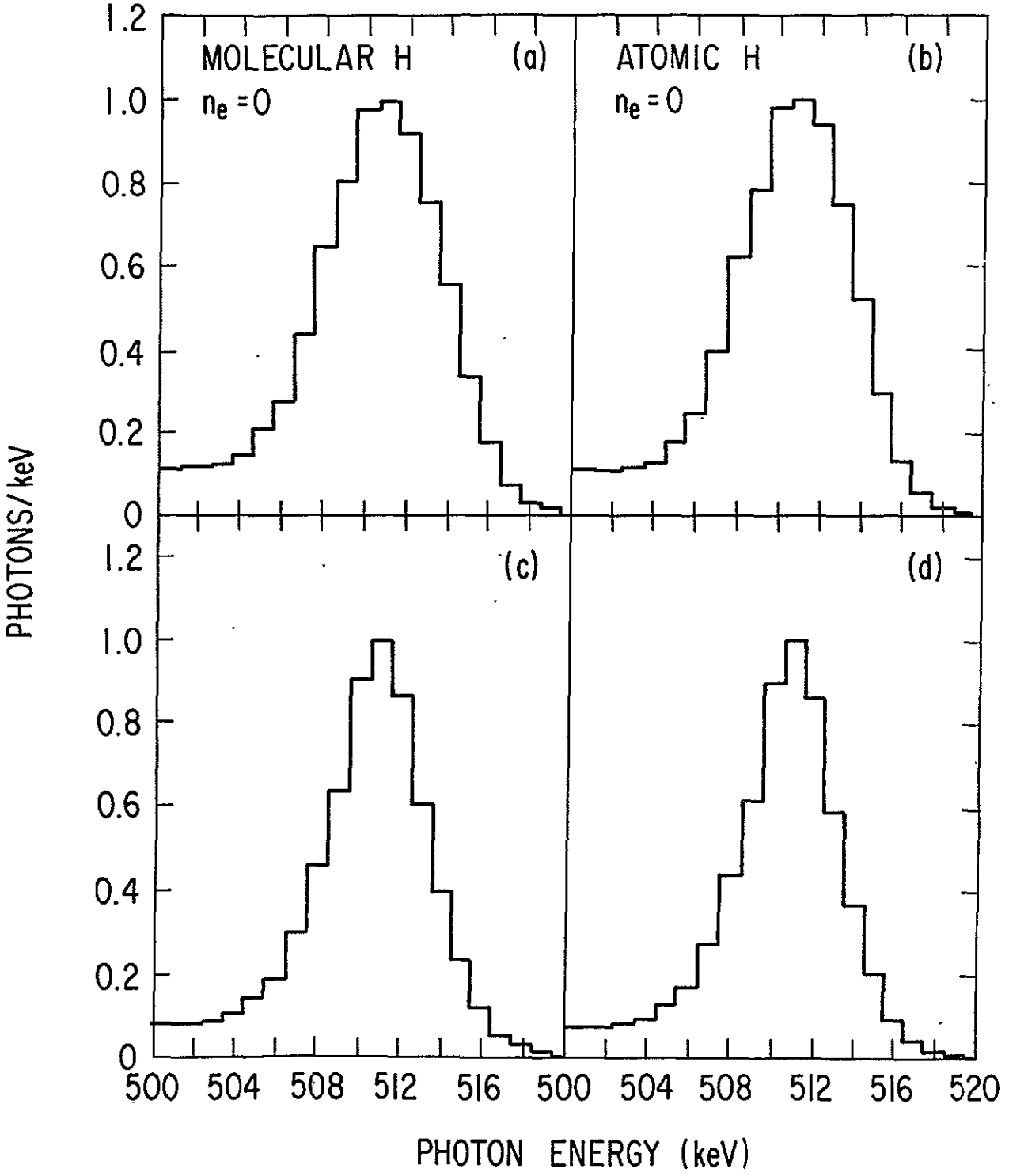
MOLECULAR H
(a)
$n_e = 0$
ATOMIC H
(b)
$n_e = 0$
(c)
(d)
PHOTONS/keV
PHOTON ENERGY (keV)
0
0.2
0.4
0.6
0.8
1.0
1.2
500
504
508
512
516
520

Figure IV-4

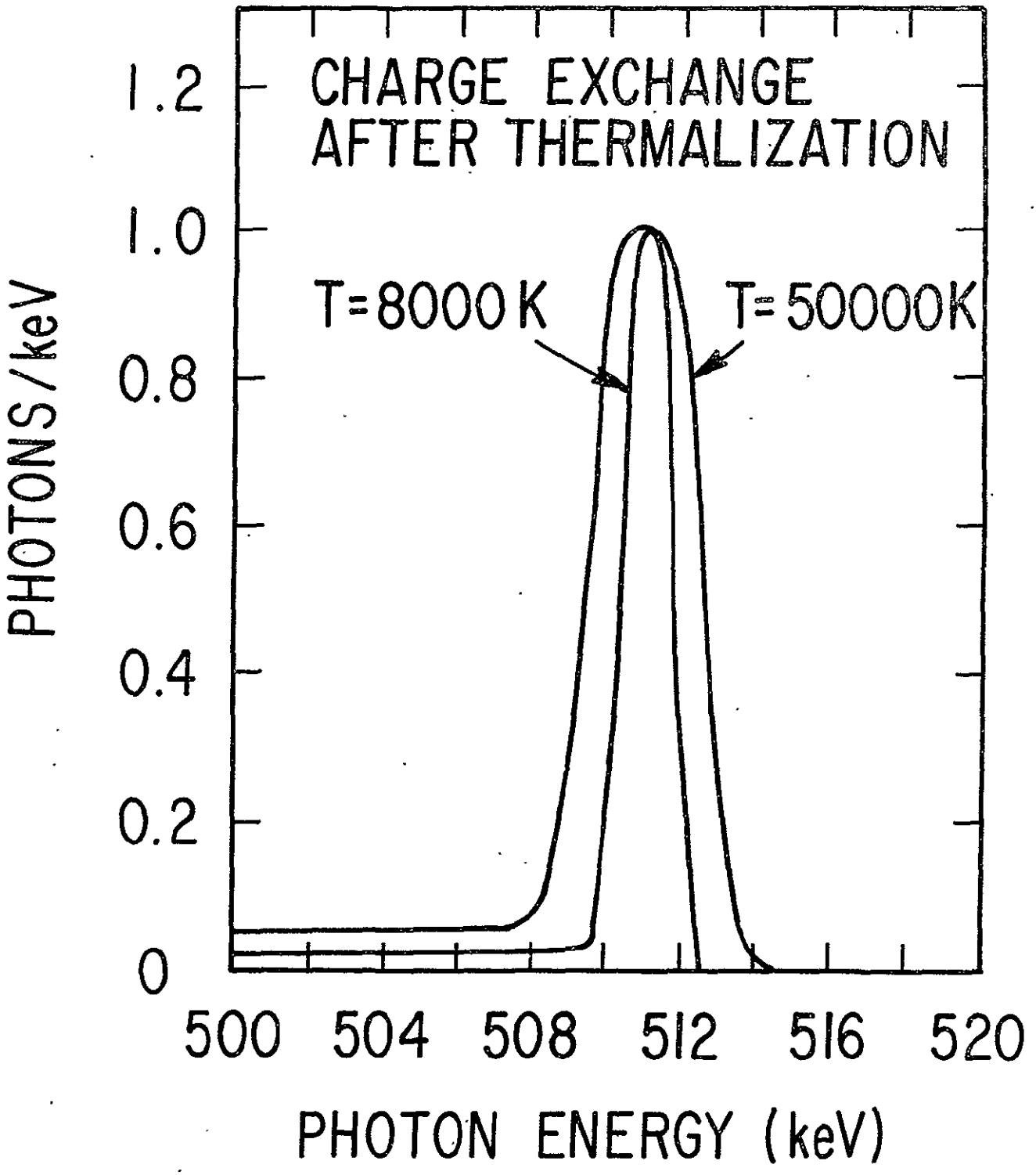
CHARGE EXCHANGE
AFTER THERMALIZATION
T=8000 K
T=50000K
PHOTONS/keV
1.2
1.0
0.8
0.6
0.4
0.2
0
500
504
508
512
516
520
PHOTON ENERGY (keV)

Figure IV-5

BIBLIOGRAPHIC DATA SHEET

1. Report No.	2. Government Accession No.	3. Recipient's Catalog No.
TM79690		

4. Title and Subtitle	5. Report Date
Topics in Astrophysical X-ray and Gamma Ray Spectroscopy	November 1978
	6. Performing Organization Code: 660
7. Author(s): Roger W. Bussard	8. Performing Organization Report No.
9. Performing Organization Name and Address: Laboratory for High Energy Astrophysics Theoretical Group	10. Work Unit No.
	11. Contract or Grant No.
	13. Type of Report and Period Covered: TM
12. Sponsoring Agency Name and Address	14. Sponsoring Agency Code

15. Supplementary Notes

16. Abstract

We have investigated a number of topics concerning observations already made or currently planned of spectral features in the X-ray and gamma ray regimes. First, we have compared the production of the iron Kα line to that of selected strong γ-ray lines from nuclear excitation, assuming both result from fluxes of ions with energies from 1 to 300 MeV/nucleon. Limits placed by X-ray observations generally fall below γ-ray observations reported in the literature. We also show the effect of interstellar dust on narrowing certain gamma ray line profiles. Second, we have considered the effect of strong magnetic fields on X-ray pulsar spectra. We find that recent observations of Hercules X-1 are more likely to be consistent with an abosrption feature than an emission line. Finally, we have calculated the line shape at 0.5 MeV resulting from positron annihilation in the galaxy, and find that a recent observation from the galactic center direction implies annihilation in a medium with greater than 5% ionization, but cooler than $\sim 10^5$K.

17. Key Words (Selected by Author(s))	18. Distribution Statement
X-ray lines, gamma ray lines, X-ray pulsars, cyclotron lines, positron annihilation, interstellar medium, galactic center	

19. Security Classif. (of this report)	20. Security Classif. (of this page)	21. No. of Pages	22. Price*
UN	UN		

*For sale by the National Technical Information Service, Springfield, Virginia 22151.

GSFC 25-44 (10/77)